INFORMATION TO USERS

This manuscript has been reproduced from the microfilm master. UMI films the text directly from the original or copy submitted. Thus, some thesis and dissertation copies are in typewriter face, while others may be from any type of computer printer.

The quality of this reproduction is dependent upon the quality of the copy submitted. Broken or indistinct print, colored or poor quality illustrations and photographs, print bleedthrough, substandard margins, and improper alignment can adversely affect reproduction.

In the unlikely event that the author did not send UMI a complete manuscript and there are missing pages, these will be noted. Also, if unauthorized copyright material had to be removed, a note will indicate the deletion.

Oversize materials (e.g., maps, drawings, charts) are reproduced by sectioning the original, beginning at the upper left-hand corner and continuing from left to right in equal sections with small overlaps.

ProQuest Information and Learning
300 North Zeeb Road, Ann Arbor, MI 48106-1346 USA
800-521-0600



Downloaded from SHAREOK. Persistent Handle URL: https://hdl.handle.net/11244/498

UNIVERSITY OF OKLAHOMA

GRADUATE COLLEGE

SYNTHESIS AND SPECTROSCOPIC STUDIES OF POLYMER ELECTROLYTE HOSTS: LINEAR POLY(ETHYLENIMINE), LINEAR POLY(*N*-METHYLETHYLENIMINE) AND LINEAR POLY(*N*-2-(2-METHOXYETHOXY)ETHYLETHYLENIMINE)

A Dissertation

SUBMITTED TO THE GRADUATE FACULTY

in partial fulfillment of the requirements for the

degree of

Doctor of Philosophy

By

ALBERT G. SNOW

Norman, Oklahoma

2002

UMI Number: 3059898

UMI®

UMI Microform 3059898
Copyright 2002 by ProQuest Information and Learning Company.
All rights reserved. This microform edition is protected against
unauthorized copying under Title 17, United States Code.

ProQuest Information and Learning Company
300 North Zeeb Road
P.O. Box 1346
Ann Arbor, MI 48106-1346

© COPYRIGHT ALBERT G. SNOW 2002

All Rights Reserved

SYNTHESIS AND SPECTROSCOPIC STUDIES OF POLYMER ELECTROLYTE HOSTS: LINEAR POLY(ETHYLENIMINE), LINEAR POLY(*N*-METHYLETHYLENIMINE) AND LINEAR POLY(2-(2-METHOXYETHOXY)ETHYLETHYLENIMINE)

A Dissertation APPROVED FOR THE
DEPARTMENT OF CHEMISTRY AND BIOCHEMISTRY

BY

Daniel T. Glatzhofer

Roger Fresh

K. M. Nicholas

James J. Sluss, Jr.

Robert White

Ralph A. Wheeler

ACKNOWLEDGMENTS

The past five years of schooling have been part of a long journey and I am thankful to many people. It was 1996 when I first stepped into Dr. D. T. Glatzhofer's lab as a inexperienced undergrad for a summer internship and that summer left a lasting impression on me that helped bring me back to OU for my graduate work in 1997. I want to thank Dr. Glatzhofer for the opportunity to work in his lab and to be a part of such exciting work and a positive work environment. I also want to thank both Dr. Glatzhofer and Dr. R. Frech and for their insight and their success in talking me into switching research projects. The switch could not have been any better for me. I would also like to thank the other members of my committee. I owe Dr. R. White, Dr. J. J. Sluss, Dr. K. Nicholas, Dr. R. Wheeler, and Dr. R. Lehr a debt of gratitude for keeping their doors open for great discussions and taking the time to help me along the way. I would also like to thank the many graduate students that I have had the pleasure working with. Both Doug Masterson and Warren Dinges kept on me on my toes in my first two years at OU and they both taught me a lot. I want to thank other members of Dr. Glatzhofer's research group, past and present for their help. I would also like to thank Dr. Shawna York, Nathan Hesse, and Rebecca Sanders; without your input, training, and help I would not have been able to accomplish as much as I have.

My family has played the most significant role in my academic success and to that end, I owe my family an undying dept of gratitude. I was taught at an early age what a great work ethic can provide you. My father, Andy, taught me that by working hard

anyone can accomplish anything. My mother, Ellen, instilled into me the desire to learn and the value of education. These traits have provided the foundation for the success that I now share with my family and friends. Lastly, I want to thank the two people that mean the most to me. Rosa and AJ have been with me during my greatest accomplishments and worst flops. However, their unwavering love and support for me was always there whenever I needed it. For this I will always be grateful and their love and support has helped make this possible.

TABLE OF CONTENTS

ACKNOWLEDGMENT		IV
ABSTRACT		VIII
CHAPTER		
I.	INTRODUCTION	1
	1. BACKGROUND	1
	2. POLY(ETHYLENE OXIDE)	12
	3. SUMMARY OF INTRODUCTION	27
	4. PROJECT GOALS	27
II.	POLY(ETHYLENIMINE)	31
	1. INTRODUCTION	31
	2. RESULTS AND DISCUSSION	35
	3. CONCLUSIONS AND FUTURE DIRECTIONS	48
	4. EXPERIMENTAL	51
III.	LINEAR POLY(*N*-METHYLETHYLENIMINE)	56
	1. INTRODUCTION	56
	2. RESULTS AND DISCUSSION	58
	3. CONCLUSIONS AND FUTURE DIRECTIONS	71
	4. EXPERIMENTAL	73
IV.	LINEAR POLY(*N*-2-(2-METHOXYETHOXY)ETHYL)ETHYLENIMINE)	78

1. INTRODUCTION 78

2. RESULTS AND DISCUSSION 79

3. CONCLUSIONS AND FUTURE DIRECTIONS 109

4. EXPERIMENTAL 111

5. OVERALL CONCLUSIONS 117

BIBLIOGRAPHY 118

APPENDIX OF SPECTRA 125

ABSTRACT

Polymer electrolytes are materials that contain dissolved salts in heteroatom-containing polymer hosts. The ion-ion and polymer-ion interactions have been extensively studied using poly(ethylene oxide) (PEO) as the polymer electrolyte host with many different dissolved metal salts. PEO-salt systems, however, like to form crystalline polymer-salt complexes which drastically reduces ionic conductivity. Changing the heteroatom from oxygen to a softer heteroatom such as nitrogen, may suppress the formation of polymer-salt crystalline complexes.

Synthesis of linear poly(ethylenimine) (LPEI) was accomplished by hydrolysis of commercially available poly(2-ethyl-2-oxazoline). Linear poly(*N*-methylethylenimine) (LPMEI) was made from LPEI using the Eschweiler-Clarke reductive methylation. Linear poly(*N*-2-methoxyethylethylenimine) (LPEI-G1), linear poly(*N*-2-(2-methoxyethoxy)ethylethylenimine) (LPEI-G2), linear poly(*N*-2-(2-(2-methoxyethoxy)ethoxy)ethylethylenimine) (LPEI-G3), and (3,6-dioxaheptyl)diethyl amine (DEA-G2) were all synthesized by a reductive alkylation using the corresponding carboxylic acid.

Three topics that are of interest to scientists in polymer electrolytes are: 1) ion-ion interactions; 2) ion-polymer interactions; and 3) how these interactions correlate to ionic conductivity. A spectroscopic study of LPEI and LPEI:MTf (M = Li^+or Na^+, Tf is triflate, $CF_3SO_3^-$) was undertaken using infrared spectroscopy, Raman spectroscopy,

differential scanning calorimetry, and AC complex impedance measurements. LPEI is a highly crystalline polymer with extensive hydrogen bonding interactions. Ionic speciation in LPEI:LiTf decreases from 25% "free" ion at a N:Li ratio of 20:1 to 13% at a 10:1 N:Li ratio. LPEI-NaTf systems, however, did not follow the same trends seen for the LPEI-LiTf systems. The ionic speciation of LPEI-NaTf consisted of mainly ion pairs for all salt concentrations investigated. The highest conductivity obtained was 3×10^{-6} S/cm at 60°C for 20:1 LPEI-LiTf. The ionic speciation of LPMEI:MTf decreases from 36% "free" ion at a N:Li ratio of 20:1 to 24% at a 5:1 N:Li ratio. LPMEI-NaTf systems however, did not follow the same trends seen for the LPEI-LiTf systems. The ionic speciation of LPMEI-NaTf actually showed an increase of "free" ions, 27% to 52% for the 20:1 and 5:1 sample compositions, respectively. The highest conductivity that was obtained was 2×10^{-5} S/cm at 50°C for the 20:1 LPMEI-LiTf. The ionic speciation of LPEI-G2:LiTf samples changes from 50% "free" ion at a N:Li ratio of 20:1 to 26% at a 5:1 N:Li ratio. The highest conductivity that was obtained was 7×10^{-5} S/cm at 60°C for the 20:1 O:Li sample.

Future investigations using LPEI-G1, LPEI-G3, and their respective model compounds will be carried out to evaluate their potential as polymer electrolyte hosts. All polymer systems discussed in this thesis can be crosslinked to form elastomeric networks. These elastomeric networks have better physical and mechanical properties than the parent polymers and may be used to improve the mechanical stability of the polymer electrolyte hosts.

Chapter I

Introduction:

The use of batteries has grown tremendously over the past century. The growth has been extraordinary since Alessandro Volta introduced the electrochemical cell in 1800. The first high current battery, introduced in 1840, began to define a general consumer market in the 1870's. The flashlight, which uses household batteries, was first used at the turn of the century, some twenty years after the invention of the light bulb.[1] Almost one hundred years later in 1998, more than three billion industrial and household batteries were bought in the United States alone and demand for batteries in the U.S. is projected to increase 5.8% every year through 2002.[2] It is this growing industry that continues to spur research into new materials for use in batteries to find those that are safer, better, and environmentally friendly.

One area of interest for scientist is the electrolyte layer that separates the cathode from the anode in a battery system. There are different types of electrolyte layers. Solid polymer electrolytes are one specific type of electrolyte layer that is being studied. The research discussed in this thesis is broken into two main areas: 1) polymer synthesis, and 2) polymer electrolyte spectroscopy and ionic conductivity. These two area are repeated for three polymer systems.

Background:[1-17]

In 1789, Galvani discovered an electrochemical source of current with his "frog leg" experiment. However, it was Volta who first designed a practical and useful current

source or battery, Volta's pile.[10] In 1803 and 1805, Ritter showed that current passed between two like electrodes (contained in an electrolyte) could be polarized; with the removal of the current, the stored current flowed in the opposite direction. Ritter's pile was the beginning of storage batteries. It was discovered in 1853-5 that lead electrodes could be polarized and an effective storage battery could be made. The development of storage battery technology changed dramatically over the next one hundred years and the grid designs for batteries, overall, evolved into those that are being used today, see **Figure I-1**.[1]

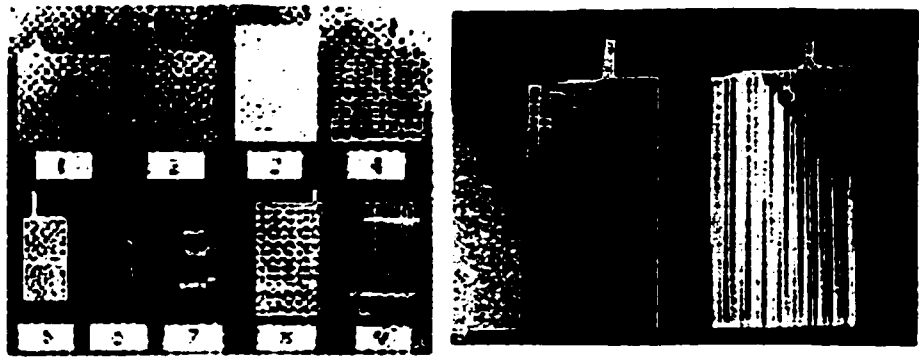

Figure I-1 Left-Old Grid Designs Right-Newer Grid Designs

A battery contains galvanic cells that are connected in series or in parallel. A galvanic cell, see **Figure I-2**,[15] contains four components: an anode, cathode, electrolyte and some type of an electrical load. The anode (the negative electrode) is the part of the battery where oxidation occurs. The anode releases electrons to the electrical load and metal cations into the electrolyte. The cathode (the positive electrode) accepts electrons and is formally reduced. The anode and cathode together are considered the electrodes.

Lead and lithium, to name a few materials, are both used as electrodes.

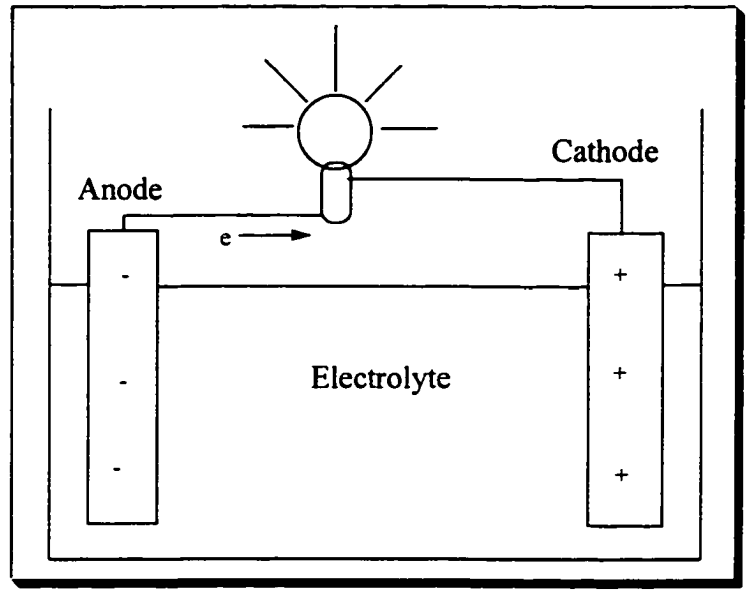

Figure I-2 Generic Galvanic Cell

Both liquid and solid electrolytes have advantages and disadvantages for a given battery design. These advantages and disadvantages are related to each other in a complex fashion. The output of a battery depends on how the cells within the battery are connected. Cells that are connected in series will have a higher voltage, V, than the cell by itself. Cells connected in parallel have voltage equal to the single cell, but the current, *i*, is twice the amount (assuming a two-cell system), see **Equation I-1**, where V is voltage in volts, *i* is current in amps and R is resistance in ohms. Batteries can be

$$V = iR$$

Equation I-1 Ohm's Law

designed for almost any current and voltage using combinations of series and parallel circuits.

Batteries can be classified by how they are used. Primary batteries are discharged fully and secondary batteries are rechargeable. The liquid electrolyte that a battery contains is generally either acidic or alkaline in nature. The acid electrolyte in a liquid battery is strongly or moderately acidic. The battery used in automobiles contains a liquid electrolyte and is a secondary battery. Sulfuric acid is normally the main component in the electrolyte liquid used in a automobile battery. The lead-acid battery in automobiles is the most widely used battery in the world. The cathode is lead dioxide and the anode is lead. The chemical reaction that occurs in a lead acid battery is shown in **Figure I-3**. The electrolyte in an alkaline battery contains sodium or potassium hydroxide as the main component in the battery electrolyte. An example of an alkaline

$$PbO_2 + Pb + 2H_2SO_4 \underset{\text{discharge}}{\overset{\text{charge}}{\rightleftharpoons}} 2PbSO_4 + 2H_2O$$

Figure I-3 Chemical Reaction for Lead Acid Battery

electrolyte battery system is a zinc manganese dioxide battery. Alkaline household batteries use a gel or paste electrolyte and are considered "dry" batteries. Strongly acidic electrolytes are used in batteries that can be found in automobiles; whereas moderately acidic electrolytes are used in batteries that can be found in household items like a flashlight. Alkaline electrolyte-containing batteries are used for cell phones, pagers, and portable CD players.

A few disadvantages of liquid electrolytes are: a necessary battery spatial orientation, high cost, short life cycle, toxicity, and complexity. Battery orientation is a problem since the liquid electrolyte can flow and gas pockets can form. If a gas pocket forms around the electrode the battery will not produce current. High maintenance for some liquid batteries is a problem, but lead acid batteries are now typically sealed and are maintenance free. The life time of the lead acid battery is about 500 cycles. The performance of the lead acid battery is also poor in very cold temperatures.

The advantages of liquid batteries are: an established industry, low cost, and a long life cycle for specific liquid batteries.[12] However, the lead acid battery technology is more than one hundred years old, and has reached some limitations. The advantages and disadvantages that battery types have are related depending on which electrolyte is used to make the battery.[12] Dry electrolyte-containing batteries[1] use solid or powdery electrolytes. The use of the term "dry" electrolyte battery should not be equated with true solid electrolytes or solid state cells. Dry electrolyte-containing batteries that use solid or powdery electrolytes often have to use the moisture in the air to complete the chemical reaction that generates current. A specific class of dry batteries actually uses a liquid electrolyte that is suspended in a gel or some other absorbent substance. The use of gelling material allows for any battery orientation and helps minimize leaks when the battery has been punctured. The components of dry electrolyte batteries are the same as the liquid electrolyte containing batteries. A common "dry" electrolyte containing battery is the zinc-MnO_2 cell battery, the Leclanché cell.

The first important dry battery was the Leclanché cell developed in 1866. The chemical reaction for the Leclanché cell is shown in **Figure I-4**. In 1886, Carl Geissner

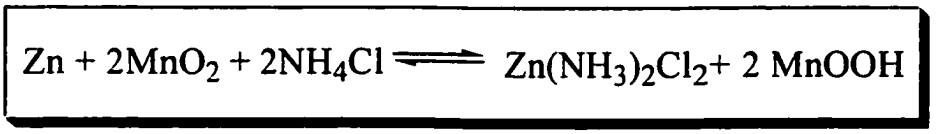

Figure I-4 Chemical Reaction for the Leclanché Cell

changed the initial design. Geissner incorporated the zinc anode in the form of a cup and had it encased in plaster of Paris and a carbon rod was used as collector. To make the Leclanché cell truly a dry cell the container, the cathode, and the electrolyte composition were changed. The electrolyte was immobilized with cereal paste. A main problem with the Leclanché cell was its propensity to leak (due to byproduct formation after heavy discharge). When the battery is heavily discharged, there is formation of insoluble zinc complexes. The insoluble zinc complexes cause the pH to fall rapidly in the electrolyte and zinc corrosion occurs. The corrosion produces hydrogen gas, which builds pressure that forces gas byproducts past the battery seals. Better designed seals and other advances have addressed the leakage problem.

A few sizes of the "dry" battery are D size, 9 volt and the "paper" battery. The paper battery, made by Matsushita, is a slim Leclanché cell and has a voltage output of 1.5 volts. The paper battery has a maximum thickness of 0.8 mm, a diameter of 38 mm, and weighs 1.5 g, see **Figure I-5.**[1] A few advantages of the dry battery have already been mentioned: battery orientation and size. The ability to place the battery in any position

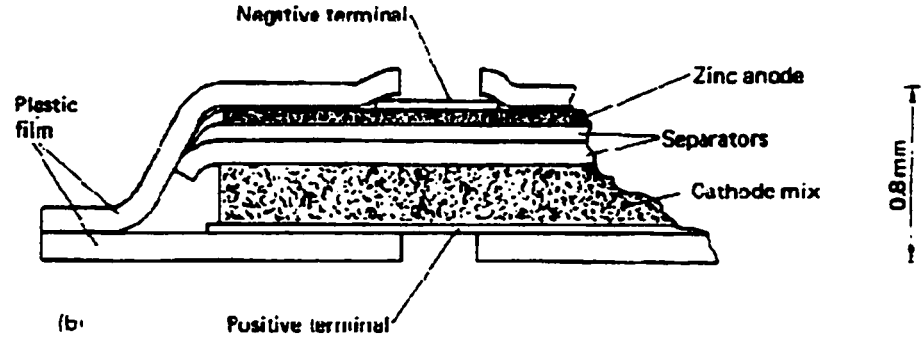

Figure I-5 Paper Size Battery

has many applications in the home. Portable electronic equipment, radios, CD players, and toys are just a few applications for which battery orientation can be a concern. The materials used in making Leclanché batteries are of low cost and readily available. Processing and manufacturing of the batteries is straightforward and simple.

The two main disadvantages of the Leclanché battery are the propensity to leak (due to byproduct formation) and poor discharge rates. In the US and Europe, these disadvantages have caused the replacement of Leclanché technology by other closely related technologies, specifically zinc chloride cells. Dry cells are useful and have many applications in the battery market. However, solid state batteries[1,4] are attractive since a solid does not flow and therefore would not leak. The temperature range of a solid battery could be much wider than a liquid batter since a battery containing a liquid electrolyte could freeze and become a "dead" battery. A solid battery could also have a longer shelf life. A solid can be packaged more efficiently than a liquid, and light weight containers could be used to hold the battery materials. Miniaturization of batteries has been demonstrated with the "dry" batteries, and solid state batteries can take

miniaturization a step further.

Two requirements need to be fulfilled before a "true" solid state cell can be of value. The first requirement is high voltage and the second is a low internal resistance. The solid electrolyte must have high ionic conductivity, so that the internal resistance is low. In addition, the solid electrolyte should have negligible electronic conductivity but must conduct appropriate ions. The negligible electronic conductivity controls self-discharge by shorting and contributes to long shelf life.

Two types of solid electrolytes[1] are polymer electrolytes and ceramic crystalline or vitreous phases. Conductivity in ceramic solid electrolytes occurs due to a combination of several factors. The first is a high concentration of mobile ions and the second is low activation energy for ionic motion. A problem with ceramic electrolytes is the electrode interface. The interfacial resistance must be accounted for and depending on how the electrodes contract and expand during charge and discharge cycles, the contact between the electrode and the solid electrolyte can become poor.

Polymer electrolytes are polymers that have metal salts dissolved in them. The metal salts can be dissolved in different forms of polymers like polymer gels and polymer films. Good polymer electrolytes have at least three key features.[1,4,18-20] The first is the polymer should have a good electron donating ability, which allows coordinative interactions to occur with metal cations. The second is that the energy for bond rotation should be low to allow polymer segmental motion to occur readily. Lastly, the polymer coordination sites should be appropriately spaced for optimum interactions with metal

cations. Polymer electrolytes have several advantages over liquid electrolytes. Polymer electrolytes can often be cast or formed into very thin films that increase the energy density by lowering the resistance. The inert porous separator is no longer needed since the polymer electrolyte can act as the spacer. The polymer electrolyte may act as a binder that facilitates good electrical contact with the electrodes. An example of a polymer electrolyte host is poly(ethylene oxide) (PEO). PEO is a polyether that has been widely studied for battery applications.

Candidates for electrode materials are numerous. Browsing a standard reduction potential table will provide information on half cell voltages. For example, the lithium

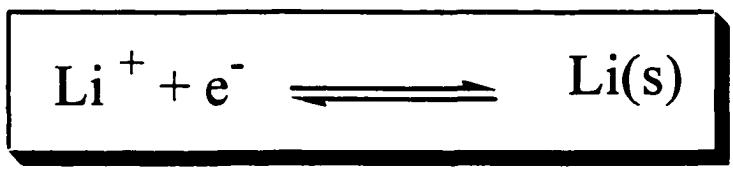

Figure I-6 Lithium Half Cell Reaction

half cell reaction, shown in **Figure I-6**, has a cell potential of -3.045 V. The lead half cell reaction from **Figure I-1** has a half cell potential of only -1.455 V. Other elements that have been used as electrodes are nickel, iron, cadmium, zinc, and sodium.

Lithium has a very high half cell potential. Research using lithium as an electrode in polymer electrolytes has been extensive and many specific lithium ion battery studies have been conducted over the last three decades.[12] Lithium primary batteries use a lithium salt and an organic liquid for the electrolyte. A few solvents[6,12]

used for this purpose are propylene carbonate (PC), methyl formate, dioxolane, acetonitrile, and sulfoxides. All of these solvents are aprotic. Some commonly used salts are $LiN(CF_3SO_2)_2$, $LiPF_6$, $LiBF_4$, and $LiClO_4$. Salt/organic solvent solutions are generally not as efficient at conducting as aqueous electrolytes. Cathodic materials have been widely studied, and some common materials used are MnO_2, CF_x, CuO, and Ag_2CrO_4, although the most widely used systems are CF_x and MnO_2.

Lithium primary batteries, like button cells and cylindrical cells (up to D size), have been used for applications like watch batteries, heart pacemakers, and hearing aids. These applications have one thing in common and that is a low discharge rate. Primary lithium batteries have been made that have high discharge rates. In the 1970s, the primary lithium battery became successful and research turned towards developing rechargeable lithium batteries. A large step was taken in developing rechargeable lithium batteries when Whittingham[12] discovered that an inorganic material, i.e., TiS_2, would react with lithium by an intercalation mechanism and allow lithium ions to incorporate into the crystalline lattice without changing the crystal lattice structure. The incorporation into the lattice is reversible and fast.

Moli Energy Limited commercialized the first rechargeable lithium battery in the late 1980s, the Molicel™. The rechargeable battery came in AA and C sizes and could be recycled 200-300 times. A common problem with the Molicel™ battery was electroplating of lithium metal in organic solvents or electrolytes. The electroplating of lithium on the electrode is not as efficient because the lithium surface is altered when

lithium has reacted with the organic liquid. Lithium, when freshly formed, reacts with or decomposes organic solutions , see **Figure I-7**, until the lithium is covered by a

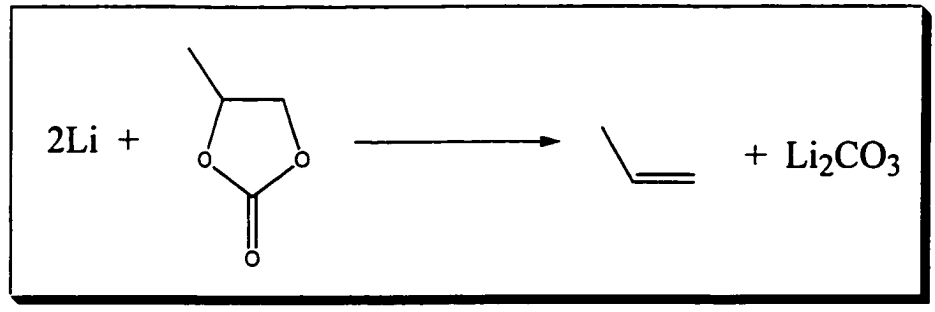

Figure I-7 Decomposition of Organic Molecule by Lithium Metal

protective film. The electroplating problem is common to many lithium batteries. The protective film does make the cycling of the battery poor. However, if the protective film can act like a solid electrolyte and contribute to a long shelf life for the battery, it is not always a complete loss. To combat this problems, researchers have turned to development of a "lithium ion battery". The electrodes in a lithium ion battery are both lithium intercalation electrodes. These electrodes must have a large difference in free energy. An example of two materials used as intercalation electrodes are carbon (graphite) with a composition of C_6Li and metal oxides such as $LiCoO_2$ or $Li_xMn_2O_4$.

Other names for lithium ion batteries are 'swing' or 'rocking-chair' batteries. The lithium ions move back and forth, swing, or rock between electrodes. Lithium ion batteries can also use a solid polymer electrolyte, as mentioned before. The lithium cations move through the polymer electrolyte host, see **Figure I-8**.[18] Armand[21,22], in the

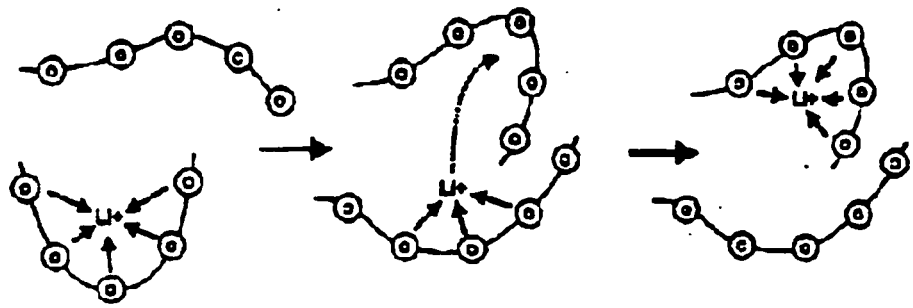

Figure I-8 Movement of Lithium Cation in Polymer Electrolyte Host

1970s, studied salts dissolved in polymers. Polymers that contain heteroatoms, for example sulfur, nitrogen, and oxygen, can have large dielectric constants. Heteroatom-containing polymers can dissolve metal salts in reasonable concentrations. A few commonly used lithium salts are lithium trifluoromethanesulfonate ($LiCF_3SO_3$, "lithium triflate", LiTf) and lithium perchlorate ($LiClO_4$). Poly(ethylene oxide) (PEO), see **Figure I-9**, is a widely studied polymer electrolyte host.[18-20,23-32] Extensive research has been

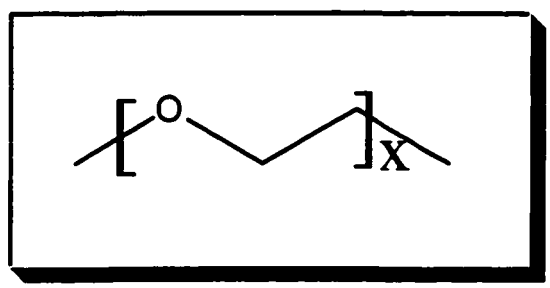

Figure I-9 PEO

done on PEO systems using different techniques: infrared (IR) spectroscopy, Raman spectroscopy, nuclear magnetic resonance (NMR) spectroscopy, X-ray diffraction, and computational methods, to name just a few.

The repeat unit of PEO is a simple ether unit, ROR where R is alkyl or aryl

groups. A basic understanding of PEO is desirable. Model compound studies have been done on glycols and glymes and are still ongoing in many groups. Matsuura[33,34] has studied polyethylene glycol systems using infrared and Raman spectroscopy and split the results of these studies into two categories: 1) terminal group or end group vibrations, and 2) internal chain or backbone vibrations. Their results showed that the terminal vibrations are set apart by two characteristics. The first characteristic is the relative intensities of the absorption bands and the second characteristics is the consistency of the frequencies with respect to chain length. **Table I-1** shows the terminal group frequency assignments from the IR and Raman spectroscopy experiments. These vibrational modes will become important when chain conformation is dependent upon salt concentration, as will be discussed later.

Table I-1 Terminal Group Frequencies(cm^{-1})[33,34]

Infrared (cm^{-1})	Raman (cm^{-1})	Assignments
2985-2975	2985-2978	CH_3 asymmetric stretching
2930-2920 2825-2815	2940-2937 2825-2821	CH_3 symmetric stretching + 1450 X 2
- - - - -	1452-1450	CH_3 asymmetric deformation
1200-1193	1199-1198	CH_3 symmetric deformation CH_3 out-of-plane rocking
1032-1027	1030-1026	CH_3 out of plane rocking

Data taken from reference[33,34]

Their results also showed that three types of internal vibrations are characteristic. The first of the types is the internal vibrations of the methylene unit,

which include the CH_2 symmetric stretch, CH_2 anti-symmetric stretch, and CH_2 bending vibrations. The second type includes the external vibrations of the methylene unit; the CH_2 wagging, twisting, and rocking. The final type includes backbone chain stretching, deformation, and internal rotation, see **Table I-2.**

An important conclusion that Matsuura reached in his study of polyethylene glycols was that "*the internal rotation conformations along the series of bonds O-CH_2 CH_2O- are perhaps trans, gauche, and trans (tgt), just as in the case of high molecular weight Carbowax*".

Table I-2 Frequency Regions for (-CH_2 CH_2O-)n Chain Vibrations[33,34]

Regions, cm^{-1}	CH_2 internal modes	CH_2 external modes	Skeletal Modes
4000-1400	CH_2 stretching CH_2 bending	-----	-----
1400-1200	-----	CH_2 wagging CH_2 twisting	-----
1200-800	-----	CH_2 rocking	skeletal stretching
800 >	-----	-----	Skeletal Deformation Internal Rotation

Data taken from reference[33,34]

Once again, the frequencies of these rocking modes displayed in **Table I-2** will play an important role defining the interaction of the backbone with dissolved lithium cations. Matsuura[35] has also investigated molten poly(ethylene oxide) (Carbowax) using

IR spectroscopy. **Table I-3** shows IR absorption frequencies for poly(ethylene oxide) in the molten state. The conformations of the $-CH_2CH_2O-$ unit will play an important role in determining how PEO behaves as a polymer electrolyte host.

Table I-3 IR Absorption Frequencies (cm^{-1}) of Molten poly(ethylene oxide)[35]

Frequency, cm^{-1}	Intensity	Frequency, cm^{-1}	Intensity
2930	sh	1249	m
2865	sh	1140	sh
2730	sh	1038	s
1460	m	945	m
1352	w	915	sh
1326	m	855	m
1296	m	810	sh

Data taken from reference[35], vs, very strong; s, strong; m, medium; w, weak; sh, shoulder

The poly(ethylene glycol)s are insulators. However, poly(ethylene glycol)s are better conductors with salt dissolved in them. Poly(ethylene glycol)s that have dissolved salts may be considered polymer electrolytes. An understanding of polymer-salt interactions would also be useful. Papke et al.[36] has carried out a series of studies of PEO-salt systems, which is summarized in **Table I-4**. Papke also looked at the polymer-salt complexes using Raman spectroscopy; the data is reproduced in **Table I-5**. Papke, mainly looking at $LiNO_3$, was able to deduce that ion-pair interactions occur in PEO/$LiNO_3$ complexes, and these interactions are extensive. It is expected that contact ion pair interactions will reduce ionic conductivity in a polymer electrolyte system

compared to a system that does not contain a significant ion pairing.[37] Overall, ion pairs are neutral and should not move in an electric field.

Table I-4 Selected IR Absorption Frequencies (cm^{-1}) of PEO/LiX Complexes[36]

PEO	PEO/ $LiNO_3$	PEO/ LiTf	PEO/ $LiCF_3CO_2$	PEO/ $LiBF_4$	Assignments
1473 sh	1474 m	1477 m	1473 s*	1477 s	$\delta(CH_2)_a$
1466 m	1457 m	1460 mw	1460 mw	1467 sh	$\delta(CH_2)_a$
1453 m	~ 1416 s*	1455 mw	1440 m	1453 mw	$\delta(CH_2)_a$
1283 m	1285	1270 vs*	1282 m	1282 m	$t(CH_2)_a$,$t(CH_2)_s$
1244 m	1248 w	1231 m*	1245 m	1247 s	$t(CH_2)_a$
~1103 vs	1105 vs	1095 vs	~1110 vs	~1090 ws*	$\nu(COC)_a$
958 s	957 m	968 ms	951 s	970 sh	$r(CH_2)_s$
844	839 m	842 m	839 s	842 s	$r(CH_2)_a$
		760 m*		778 m	

Data taken from reference[36] vs, very strong; s, strong; m, medium; mw, medium-weak; sh, shoulder; r, rocking(ρ); t, twist; ν, stretching; w, wagging; τ torsion; δ, bending; Subscript a and s denote asymmetric and symmetric motion.

A commonly used salt for polymer electrolyte systems is lithium triflate, as mentioned earlier. Interactions between the lithium cation and the triflate anion have been investigated using the techniques mentioned earlier, i.e. IR, Raman, and etc. The cation-anion interactions will affect the dissociation constants for cation-anion pairing or complex formation and therefore the conductivity. The assignments in both **Tables 1-4** and **1-5** established the precedent for using LiTf as an experimental marker. The values shown in these two tables indicate the type of shifts one would expect for different

types of ionic speciation in specific salts, i.e., lithium triflate.

Table I-5 Selected Raman Absorption Frequencies (cm^{-1}) of PEO/LiX Complexes[36]

Pure PEO	PEO/LiTf	PEO/$LiBF_4$	PEO/$LiNO_3$	Assignments
1480 s	1473 m	1477 s	1475 s	$\delta(CH_2)_a$
1281 s	1280 m	1280 s	1284 m	$t(CH_2)_a$, $t(CH_2)_a$
1144 m	1143 m	1142 m	1152 w	$\nu(CC)$, $\nu(COC)_a$
1065 m	1056 m	~1065 mw	1062 sh	$\nu(COC)_s$, $\tau(CH_2)_s$
961 mw	859 m	858 m	857 s	$r(CH_2)_s$, $\nu(COC)_s$
846 s	836 m	830 m	841 m	$r(CH_2)_a$

Data taken from reference[36] vs, very strong; s, strong; m, medium; mw, medium-weak; sh, shoulder; r, rocking(ρ); t, twist; ν, stretching; w, wagging; τ torsion; δ, bending; Subscript a and s denote asymmetric and symmetric motion.

The triflate anion has a point group of C_{3v}.[38] The symmetry of the anion is perturbed by interactions with the metal cations that result in spectral differences that can be seen. Huang et al.[38] studied these changes and reported *"the calculated geometries, energies, normal vibrations, and internal force constants of the free triflate anion, lithium triflate ion pairs, and several lithium triflate aggregates"*. The calculated and experimental vibrational frequencies were compared for the $\nu_s(SO_3)$, $\delta_s(CF_3)$, and the $\nu_{as}(SO_3)$.

Table I-6 shows the calculated bond lengths and angles for the "free" triflate anion, lithium-triflate ion pair, and aggregates. Huang, et al. noted that the lithium triflate is in four different types of arrangements, "free" ion, ion pair, and two types of

aggregate. The reporting of two distinctly different aggregates by Huang et al. was the first in the literature.

Table I-6 Optimized Geometries of the Free Triflates Anion, and Its Lithium Ion Pairs and Aggregates[38]

Bond Length/ Angle Å/Degrees	Free Anion[a]	Ion Pair Mono-dentate[a]	Ion Pair Bi-dentate[a]	Aggregate Bidentate Bridge[a]	Aggregate Tridentate Bridge[a]
R(C-S)	1.818	1.805	1.802	1.800	1.802
R(S-O_1)	1.438	1.475	1.463	1.456	1.444
R(C-F_1)	1.371	1.355	1.356	1.353	1.350
R(C-F_2)		1.366	1.368	1.360	
R(Li-O_1)		1.672	1.934	1.737	1.805
∠(C-S-O_1)	102.0	99.3	102.9	102.1	104.3
∠(C-S-O_2)		104.7	105.9	107.0	
∠(S-C-F_1)	112.8	112.0	111.7	110.4	109.4
∠(O_1-S-O_3)	115.8	112.9	105.0	111.9	114.1
∠(O_2-S-O_3)		119.6	119.0	115.8	
∠(F_1-C-F_3)	105.9	107.8	108.4	109.4	109.3
∠(F_2-C-F_3)		106.4	107.5	108.1	
∠(O_1-S-C-F_3)	60.0	59.2			60.0
∠(O_2-S-C-F_1)			60.8	60.5	
∠(F_2-C-S-O_1)			54.5	57.9	0.0

[a]Values derived using 3-21+G* basis set, Data taken from reference[38]

Coordination of the lithium cation to the triflate oxygen can be classified as

monodentate, bidentate and tridentate. The bidentate structure for the ion pair has the lowest calculated total energy. However, the monodentate structure was shown to be most consistent with experimental results. A noticeable difference between the "free"ion, monodentate ion pair, and the bidentate-bridged aggregate is that the C-F_1 bond distance decreases from 1.371 to 1.355 to 1.353 Å, respectively (using the 3-21+G* basis set). In addition, the F_1-C-F_3 bond angle increases from 105.9 to 109.4 degrees while the O_1-S-O_3 decreases from 115.8 to 111.9 degrees as triflate becomes a more ordered species, i.e. from "free" ion to bidentate-bridged aggregate..

Speciation in polymer electrolytes has been studied by many groups and it has been shown by Kakihana et al.[39] that PEO/NaTf systems consist of mixtures of "free" ions and ion pairs. The percentage of "free" ion at room temperature was 78 % and 74 % respectively for a 30:1 and 16:1 O:Na complex. The percentage of "free" ions was different from that found in similar studies of poly(propylene oxide) (PPO)/NaTf systems. Kakihana[39] also saw that with increasing salt concentration the percentage of "free" ion decreased, which was attributed to the distance between ions decreasing as salt concentration increased. Kakihana also studied the temperature dependence of speciation. The experiments indicated that with increasing temperature ion pair concentration goes up. The increase in ion-ion interactions as temperature is increased can be explained as a result of the free volume for the polymer and salt being dissimilar and therefore ion-ion interactions are favored before ion-polymer interactions.[39] Kakihana did not report the ionic conductivity of these samples.

An increase in temperature can also lead to phase separation.[39] Dissanayake and Frech[26] looked at the effects of temperature on pure PEO and a PEO/LiTf complex. They showed that the absorption band intensities gradually decrease with increasing temperature (up to 60°C) and frequency shifts are not significant. The change of intensity was attributed to "*simple growth of the amorphous phase at the expense of the crystalline phase*." No change was seen in the spectra for the amorphous phase from 60 - 120°C. Dissanayake and Frech also studied the temperature dependence of the triflate absorption band in PEO/LiTf complexes, see **Table I-7.** It was indicated that the temperature dependence of the absorption bands for PEO was consistent with its phase diagram.

Table I-7 Temperature Dependence of the $\nu_{as}(SO_3)$, $\nu_s(CF_3)$ and $\nu_{as}(SO_3)$ Band Frequencies (cm^{-1}) in $(PEO)_9LiTf$[26]

Mode	25°C	60°C	135°C	150°C
$\nu_{as}(SO_3)$	1262	1265	1257	1250
$\nu_{as}(SO_3)$	1296	1296	1296	1296
$\nu_s(CF_3)$	1233	1233	1228	1227
$\nu_{as}(CF_3)$	1160	1160	1160	1174

Data taken from reference[26]

Dissanayake and Frech also noted that the comparison of spectra for PEO and PEO/LiTf complexes "*can be viewed as the superposition of the spectra of the pure crystalline phase of PEO and the compound $(PEO)_3LiTf$.*" Model compounds, PEO, dissolved salts within model compounds, and dissolved salts within PEO have been studied using computational chemistry, as shown earlier. Computational chemistry has

yielded a tremendous amount of information that has been used for mode assignments. Matsuura and Miyazawa[40] studied glymes using an intra-chain force field method. **Table I-8** contains a brief listing of the observed and calculated frequencies and potential energy distributions for the A_1 and A_2 vibrations of normal polyethylene glycols that Matsuura and Miyazawa calculated.

Table I-8 Observed and calculated frequencies (cm^{-1}) and potential energy Distributions for the $A_1$and A_2 vibrations of normal polyethylene glycols[40]

	Observed Freq. Infrared	Observed Freq. Raman	Calculated Freq.	Potential-Energy Distributions
A_1		2939	2940	CH_2 antisymmetric-stretch
		1484	1479	CH_2 scissor
		1126	1137	CH_2 rock, CO stretch
		861	866	CO stretch, CH_2 rock
A_2	2890		2883	CH_2 symmetric stretch
	1345		1344	CH_2 wag
	1102		1087	CO stretch
	963		964	CH_2 rock, CH_2 twist

A_1 symmetric and A_2 antisymmetric vibrations. Data take from reference[40]

An important spectroscopic region contains the CO stretch and CH_2 rock, which will be discussed in Chapter IV. The A_1 calculated frequency is 866 cm^{-1}, which is close to the experimental value and is of interest since these modes are sensitive to chain conformation. Hyun et al.[41] has also used computational methods to study amorphous $CH_3O(CH_2CH_2O)_4CH_3$ and $CH_3O(CH_2CH_2O)_4CH_3$/LiTf structures. Hyun used molecular

dynamics simulations to calculate the mean-square radius of gyration $<S^2>$ and the mean-square backbone end-to-end distance, $<R^2>$. The radius of gyration is a measure of the average spatial domain of polymer chains. The mean-square backbone end-to-end distance is a measure of the average distance (in three dimensions) of polymer chain ends. Both of these values can help characterize the local environment of the salt.

Table I-9 contains the calculated values of $<S^2>$ and $<R^2>$ at 300 and 400 K for tetraglyme and tetraglyme/LiTf. The data indicated that the polymer chains packed closer or tighter upon addition of lithium triflate by a decrease in both $<S^2>$ and $<R^2>$. The $<S^2>$ changes from 21.3 to 18.2 $Å^2$ at 300 K. The interactions of the lithium cations with the ether oxygen atoms are due to a strong Coulombic attraction. The data also showed a reversal in the trend of $<S^2>$ between tetraglyme and tetraglyme/LiTf when a change of temperature occurs. The $<S^2>$ decreases for pure tetraglyme from 21.3 to 20.0 $Å^2$ at 300 and 400 K, however the $<S^2>$ increases for tetraglyme:LiTf from 18.2 to 18.6 $Å^2$ at 300 and 400 K, repectively.

Table I-9 Calculated Mean-Square Radius of Gyration and Mean-Square Backbone End-to-End Distance at T = 300 and 400 K[41]

Sample	T(K)	$<S^2>$ ($Å^2$)	$<R^2>$ ($Å^2$)
Tetraglyme	300	21.3± 0.3	142.7 ± 4.3
	400	20.0 ± 0.4	129.5 ± 6.3
Tetraglyme:LiTf	300	18.2 ± 0.5	101.6 ± 6.4
	400	18.6 ± 0.8	110.9 ± 10.3

Data take from reference[41]

Coulombic interactions decrease as the mixture is heated. Knowing that lithium triflate can exist as "free" ion, ion pair, or aggregates, Hyun, et al. calculated the percent contribution of the different triflate species in $CH_3O(CH_2CH_2O)_4CH_3$/LiTf systems. **Table I-10** contains the resulting data.

Hyun showed that molecular dynamics simulations reproduced experimental results closely. For example, the percent contribution of "free" ions at 300 K was 20% by experimental methods and 20% by molecular dynamics simulations. Forsyth et al.[42] also used molecular dynamics to calculate structural and transport properties in polymer electrolytes. The transport properties are of interest since the mobility of the ions in the electrolyte will affect the internal resistance.

Table I-10 Percent Contributions[a] of Triflate Species to the $\delta_s(CF_3)$ Bands from IR and Molecular Dynamics Simulations[41]

Temperature	Experiment	Tf$^-$	LiTf	$[Li_2Tf]^+$	$[Li_3Tf]^{2+}$
300 K	IR[b]	20	51	27	2
	MD	20	46	28	6
400 K	IR	21	44	28	7
	MD	18	44	30	8

Data taken from reference[41] [a]The relative contributions of each component band to the total integrated band intensity in the $\delta_s(CF_3)$ region. [b] This IR experiment was carried out at 295 K.

By integration of the velocity auto correlation function, **Equation I-2**, the self-diffusion coefficient, D, can be obtained. They calculated a series of diffusion coefficients that are partially reproduced in **Table I-11.**

Table I-11 Calculated Diffusion Coefficients[42]

Experiment*	Temperature, K	D_+ (m^2s^{-1}) (10^{-9})	D_- (m^2s^{-1}) (10^{-9})	D_s (m^2s^{-1}) (10^{-9})
A[a]	180	1.27	1.07	1.76
	240	2.77	2.25	3.14
	315	3.68	2.14	3.8
	450	6.37	3.32	6.09
B[a]	180	0.22	0.31	1.81
	270	0.5	0.62	3.42
	360	0.81	0.9	----------
C[a]	270	0.43	0.61	----------
	360	0.44	0.52	4.13
D[a]	360	1.05	1.35	4.82

Data take from Reference[42] [a]Experiments are defined in reference.

$$D = \frac{1}{3}\int_0^\infty < v(t)v(0) > dt$$

Figure I-2

It was concluded that strong ion-ion interactions will be reflected in a decrease in the diffusion coefficient. Johansson et al.[43] also studied diffusion coefficients by looking at the chain mobility of PEO-based polymer electrolytes using NMR. Johansson studied the line widths of peaks in NMR spectra of PEO and concluded that they are a result of two components, the amorphous and crystalline regions in PEO. The spectral lines due to the crystalline regions are broader than the spectral lines due to the amorphous region since the chain mobility is considerably more restricted than the

amorphous region. The line-width increases with decreasing temperature. Distinguishing the two components in the NMR spectral peaks below the Tg is difficult and they cannot be distinguished based on shape. Johansson also investigated PEO with dissolved salts using NMR. The chain mobility should decrease with addition of salt and Johansson concluded "*that the chain mobility in the amorphous complex is reduced compared to that of pure, amorphous PEO.*"

A second group, Ward et al.[44] studied the ionic and molecular mobility using NMR spectroscopy. Ward studied PEO systems using NMR spectroscopy to determine diffusion coefficients. Using **Equation I-3** the self-diffusion coefficient, D, can be

$$R = \exp\{-\gamma^2 \delta^2 G^2 (\Delta - \delta/3) D\}$$

Figure I-3

determined by plotting log R vs. G^2, where δ (1st gradient pulse time duration) = 7 ms, Δ (time at which a 2nd gradient pulse is applied) = τ = 20 ms, γ is the gyromagnetic ratio of the spin and G was varied between 0.2-2 Tm^{-1}. The self-diffusion coefficients decrease as salt concentration is increased. Ward also studied polymer mobility using NMR. Ward's work addressed two issues. The first issue was the influence of dissolved salts and how the salt changed the topology of the polymer network by increasing or decreasing the apparent entanglement molecular weight. The second issue addressed was

how the salt interaction affects the ionic mobility; which is reflected in the ionic conductivity. Ward reported that "*it is clear that the ionic salts do not produce cross-links but only change the molecular dynamics*" and "*Mc is independent of salt concentration,*" where Mc is critical molecular weight.[44]

PEO has been studied extensively, but PEO-based solid polymer electrolytes for battery applications have not been commercialized to any great extent. Problems with PEO polymer electrolyte systems (and others as well) are abundant. PEO forms polymer-salt complexes with different salts and the polymer-salt complexes usually have poor conductivities, physical and mechanical properties. The structure and morphology of the polymer electrolyte depends on different factors: preparation of the sample and the polymer and salt used. The lack of control over the structure and morphology of the polymer electrolyte make it difficult to address problems with polymer electrolytes systems; specifically PEO.

Several problems need to be addressed before a polymer electrolyte system will become commercially viable, issues including transference numbers and polarization. Both need to be addressed since a high cation transference number leads to a high concentration polarization. The degree of dissociation of the salt should be high since more associated systems tend to have a low conductivity. Stability (thermal and electrochemical) of the polymer electrolyte is a major concern since stability will reflect product safety, recycleability, and shelf life. Physical and mechanical properties should be controllable to improve the processability of the polymer electrolyte.

Summary of Introduction

The use of a solid electrolyte in batteries has many advantages, as mentioned earlier. The investigation of PEO and PEO/salt systems over the last few decades has provided copious amounts of data. These studies have provided a limited understanding of polymer electrolyte systems, and investigations are still ongoing. Research on glymes, PEO, and PEO-LiTf systems using IR, Raman, and DSC (just to name a few) has been carried out to help understand how the polymer interacts with the dissolved salt. The understanding of the environment in a polymer electrolyte systems is critical. Monitoring the state of the ions ("free" ion, contact ion pair, or aggregates) can be accomplished using IR spectroscopy and Raman spectroscopy, since the anion (Tf) is sensitive to the ion speciation within the polymer electrolyte, as shown earlier. The aggregate absorption bands are usually shifted to higher wavenumbers, where as ion pair absorption bands have a lower wavenumber than aggregate absorption bands. "Free" ion absorption bands are shifted to lower wavenumbers. For example, in PEO-LiTf systems the $\delta_s(CF_3)$ stretch is seen for aggregates at ~760 cm^{-1}(or higher), ion pairs at ~756 cm^{-1}, and "free" ions are at ~752 cm^{-1},see **Figure I-10**. Crystal structures provide more help in understanding the local structure of the polymer electrolyte system. A thorough understanding of ion speciation, local structure, and physical properties may provide the foundation to make a polymer electrolyte system viable.

Project Goals

Polymer electrolyte systems have been studied by various groups. The research

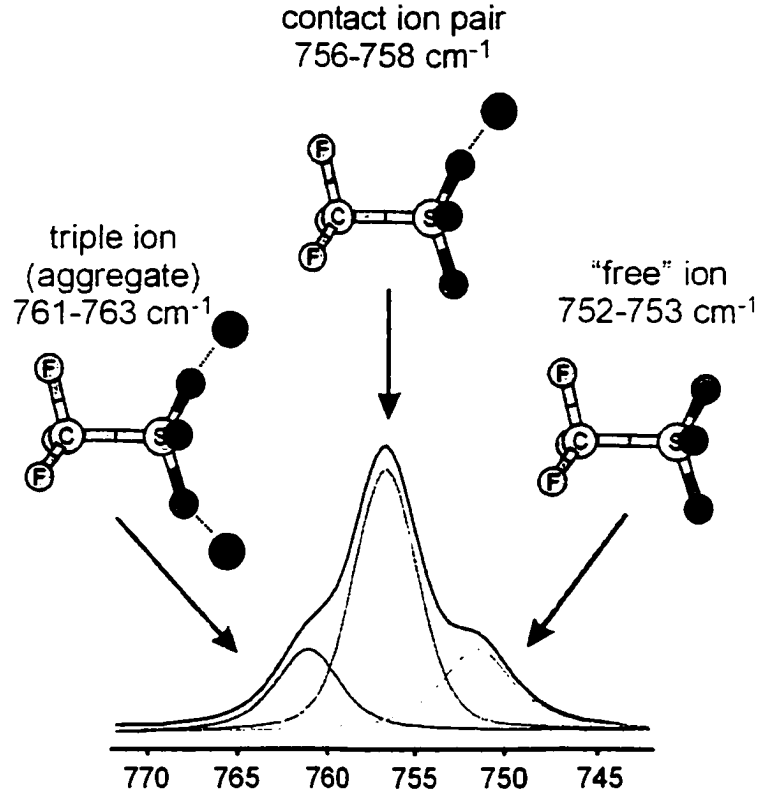

Figure I-10 Ionic Speciation of the $\delta_s(CF_3)$ for LiTf

interests of these groups are very diverse. However, all groups share common goals for polymer electrolytes: high ionic conductivity, a lithium transference number approaching unity, negligible electronic conductivity, high electrochemical and chemical stability, good mechanical and physical properties, low cost, and a benign chemical composition. PEO has average conductivities at reasonable salt concentrations but the physical properties are poor. Physical properties of PEO-salt systems can be improved by crosslinking PEO, however, the crosslinking process is done using extreme measures (gamma radiation for example). The data for PEO systems shows that by optimizing one property (high ionic conductivity) another deteriorates (mechanical and physical

properties) and this is a difficult problem to solve.

Poly(ethylenimine)-(CH_2NHCH_2)-was studied briefly as a polymer electrolyte host but interest was low since it was hard to synthesize and did not show as much initial promise as PEO.[45-71] The conductivity of PEI/LiTf systems is roughly an order of magnitude lower than similar PEO/LiTf systems. However, PEI has many advantages that PEO does not have. PEO, in its simplest form, is a polyether and ethers are fairly unreactive. PEI, in its simplest form, is a polyamine and amines can do many different things. Amines can act as nucleophiles, bases, and solvate metal salts. The synthetic versatility of PEI may overcome the small discrepancy in ionic conductivity between PEO and PEI salt systems. PEI can be synthetically modified and allows the polymer properties to be altered. This in turn, may enhance the ionic conductivity.

Two types of PEI exist, linear PEI (LPEI) and branched PEI (BPEI). The goal of this project is to study PEI and modified PEI systems. The BPEI contains primary, secondary, and tertiary nitrogen. The complex nature of BPEI complicates its fundamental study. However, once fundamental studies have been completed using LPEI, deconvolution of data for BPEI can be accomplished. The systematic study of LPEI will provide a foundation for future study of BPEI and PEI derivatives. Derivatives of LPEI can be synthesized using known synthetic routes. The LPEI derivatives that are synthesized may have enhanced properties, such as ionic conductivity. The understanding of data from PEO systems will drive fundamental research on PEI. The techniques that helped deconvolute PEO data will also be used to

understand PEI, for example the use of model compounds. The study of PEI systems and model compounds will provide further insight into polymers used as polymer electrolyte hosts. The goal of this project are to synthesize and investigate new polymers for potential use as polymer electrolyte hosts. The effects of hydrogen bonding interactions and tethered side-chains will be investigated to determine the effects on these new polymer electrolyte hosts.

The research presented here is the result of a collaboration between Dr. Shawna York, Rebecca Sanders, and myself. Dr. York was responsible for the IR and Raman spectroscopy on linear poly(ethylenimine) (LPEI). R. Sanders and I were both responsible for the IR spectroscopy for the linear poly(*N*-methylethylenimine) (LPMEI). Dr. York and R. Sanders were both responsible for the DSC and ionic conductivity measurements for all polymer systems (York-LPEI, Sanders-LPMEI and linear poly(*N*-2-(2-methoxyethoxy)ethylethylenimine) (LPEI-G2)). I carried out all synthesis of polymer systems and I was able to synthesize a new polymer system, LPEI-G2.

The data showed that hydrogen bonding does change how the polymer system behaves as a polymer electrolyte host. The data also showed that two of the polymer systems (LPMEI and LPEI-G2) contained a significant relative concentration of "free" ions at high salt concentrations. Lastly, the ionic conductivity of LPMEI and LPEI-G2 were higher than LPEI.

Chapter II

POLY(ETHYLENIMINE), PEI

Introduction:

PEO is synthetically hard to modify, however, PEI is not. PEI, linear (LPEI) and branched (BPEI), have been studied as polymer electrolyte hosts using IR spectroscopy, Raman spectroscopy, and other techniques.[45-60,62-64,66,67,72-75] PEI can be commercially bought and is highly branched. The first reported synthesis of LPEI was by Saegusa et al.[56,72,75] in 1972, and is shown in **Figure II-1**. Saegusa et al.[56,72,75] cationically

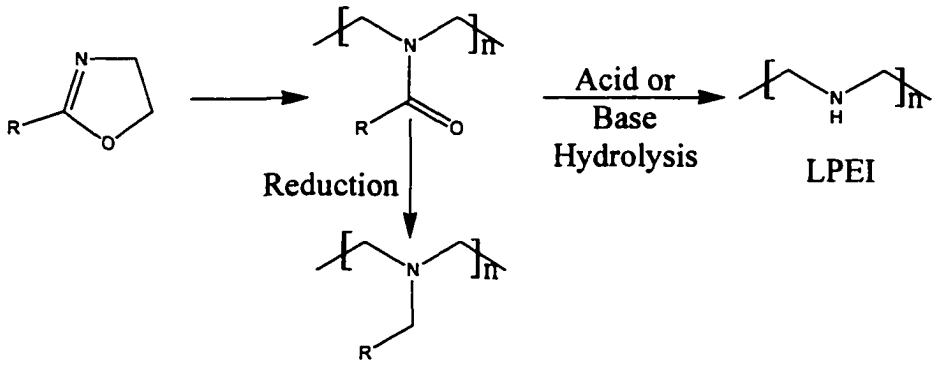

Figure II-1 Reactions of R Substituted Oxazolines

polymerized 2-alkyloxazolines to get the parent poly(oxazoline), a polyamide. The parent polyamide polymer was also identified by alkaline hydrolysis. The alkaline hydrolysis provided the corresponding linear polyamine, LPEI. The resulting LPEI was characterized by NMR spectroscopy, melting point, and elemental analysis. LPEI has a melting temperature of 58.5 °C and its ^{1}H NMR spectrum showed a single peak at 2.75 ppm. Saegusa et al. later reported that LPEI has a Tg of -23.5°C. LPEI was shown to be

a highly crystalline polymer. Saegusa obtained relatively low molecular weight (2800 g/mol) LPEI. The molecular weight plays a critical role in the properties of the polymer, as will be discussed later.

Tanaka[68]reported modification of LPEI using the Eschweiler-Clarke variation of the Leuckart reaction, and this will be discussed in chapter three. Saegusa[54] also reported, in 1978, synthesis of various alkylated LPEIs. Poly(*N*-alkylethylenimine)s were hydrolyzed or reduced using either lithium aluminum hydride ($LiAlH_4$, LAH) or alane (AlH_3), see **Figure II-1**. Saegusa polymerized various substituted 2-oxazolines and the resulting polymers were hydrolyzed or reduced to provide the corresponding polymer. The polymers had molecular weights ranging from 1820 to 5500 g/mol in yields from 25 to 98 percent. Solvent was a problem that Saegusa had to address since poly(*N*-acylethylenimine)s are not soluble in normal solvents for metal hydrides, i.e. diethyl ether or THF. A mixture of methylene chloride and diethyl ether (or THF) was used. LAH and alane both reduced the respective polymers with high yields, but did not completely reduce the poly(2-phenyloxazoline). The reduction gave a mixture of products. One of the products was attributed to LAH cleaving the $N\text{-}C(O)C_6H_5$ bond.

The reduction using alane was not attempted since poly(oxazoline) is not soluble in CH_2Cl_2 and THF. Saegusa synthesized linear poly(*N*-methylethylenimine) (LPMEI) by synthetically modifying the corresponding poly(*N*-formylethylenimine) by an in situ acid hydrolysis followed by an Eschweiler-Clarke methylation. LPMEI is an important analogue of LPEI. LPMEI will be discussed in **Chapter III**.

LPEI was shown to form two different hydrates by Chatani.[52,53] Chatani studied the hydrates and determined that both a sesquihdratate and a dihydrate exist. He also looked at the LPEI anhydrate. The hydrates are both monoclinic and the polymer chains are planar zigzag. Chatani showed that the anhydrate forms a [5.1] double stranded helix. The two LPEI chains are bound by extensive N-H---N hydrogen bonding. **Figure II-2** shows two LPEI chains forming a double-stranded helix. The N-H---N bonding is

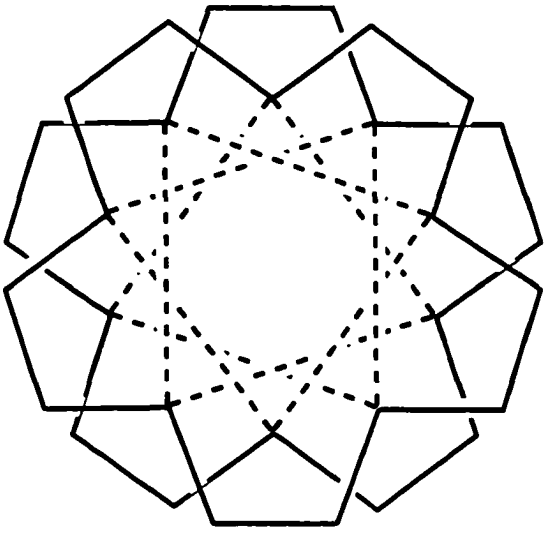

Figure II-2 Two LPEI Chains in a Double Stranded Helix

clearly shown down the channel by dashed lines. In 1982, Chatani reported a new hydrate of LPEI. A hemihydrate was shown to be monoclinic and have the same planar zigzag chain conformation as the other two hydrates. Comparing the four forms of these LPEI systems it is easy to see how the systems differ, see **Figure II-3**.

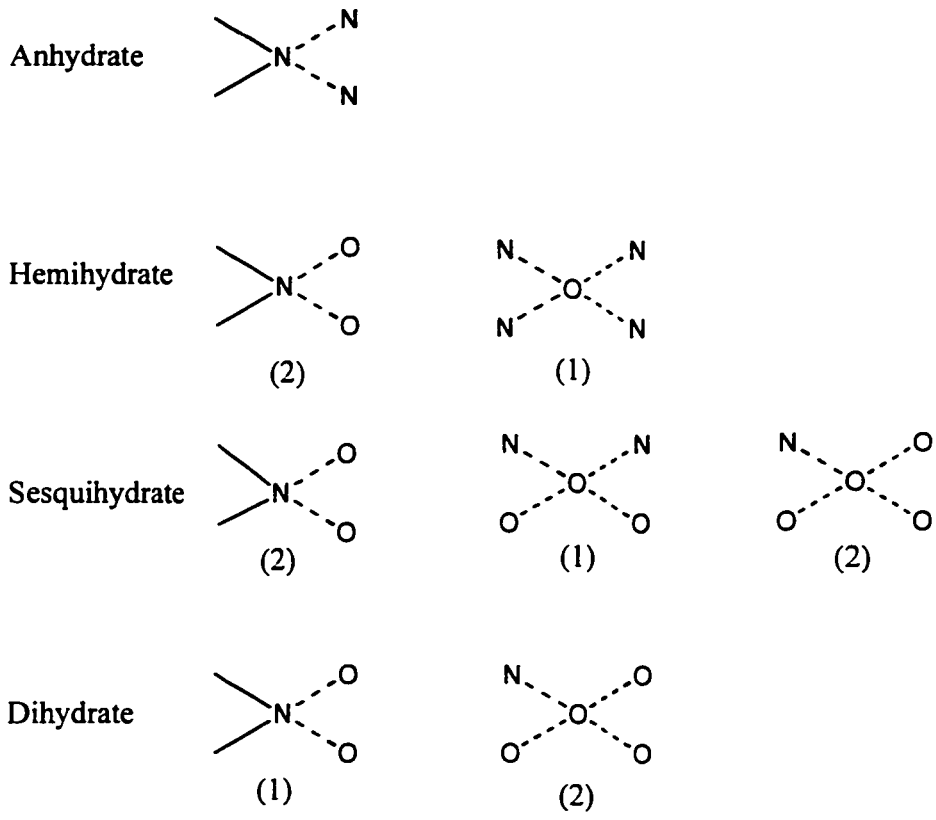

Figure II-3 Hydrogen Bonding Interactions of LPEI and LPEI-Hydrates, hydrogen atoms have been left out for clarity.

The hydrogen bonding schemes are different in the three hydrates. The relative appearance of components or hydrogen bonding interactions are different and the sesquihydrate contains three types of interactions whereas the other two hydrates only have two interactions. The anhydrate is different than the hydrates; it contains only one hydrogen bonding interaction and is highly ordered as discussed earlier.

Tanaka[51] used a different approach to synthesize LPEI. Instead of using the corresponding methyl or hydrogen oxazoline he used 2-phenyloxazoline to provide the corresponding poly(*N*-phenyloxazoline) (PPOz). He was able to obtain molecular

weights up to 350 $X10^3$ g/mol. He was also the first to report that basic hydrolysis of poly(2-phenyloxazoline) (PPOz) did not work. Poly(*N*-acetylethylenimine) and poly(*N*-formylethylenimine)both are hydrolyzed to LPEI using either basic or acidic hydrolysis. PPOz however, remained intact after two days of basic hydrolysis (30 % NaOH). Acid hydrolysis was used to cleave the carbonyl-nitrogen bond in the polyamide. The acid hydrolysis went cleanly, and Tanaka reported that ten hours was sufficient to remove 98 % of the benzoyl groups. The acid hydrolysis was allowed to proceed for an additional 4.5 days, which did not improve the overall hydrolysis. The resulting LPEI hydrochloride salt was neutralized and washed. The anhydrous LPEI had a melting temperature of 59-60 °C which agreed with previous literature values. Hashida[67] has also investigated the hydrates of LPEI. Hashida has studied the hydration process using time-resolved infrared spectroscopy.

Initial studies of LPEI and LPEI-salt systems for potential use as a polymer electrolyte host have been carried out.[45-50,57,58,62,63,76] A fundamental analysis of LPEI and LPEI-salt systems was undertaken by our research group and was guided by the background literature on LPEI and PEO.

Results and Discussion:

Synthesis of LPEI for our studies was accomplished using two different methods. The starting materials for each method were slightly different and the final LPEI products were of two different molecular weight ranges. Generally, high molecular weight (86,000 g/mol) LPEI was synthesized from commercially available

poly(2-ethyl-2-oxazoline), PEOz (MW=200,000, Aldrich). A five day acid hydrolysis using hydrochloric acid converted the poly(2-ethyloxazoline) to LPEI•HCl. The resulting polymer salt was neutralized with sodium hydroxide and washed with distilled water to provide the resulting high molecular weight LPEI. Since low molecular weight LPEI or PEOz was not readily available, a second batch of LPEI was synthesized from poly(2-methyl-2-oxazoline). 2-methyl-2-oxazoline was cationically polymerized in our lab to provide the corresponding polymer that was base hydrolyzed to yield low molecular weight LPEI.

The resulting low molecular weight LPEI had a molecular weight of ~1200 g/mol. The polymer products were characterized by ^{1}H NMR and ^{13}C NMR spectroscopy and their spectra were consistent with literature values. The high molecular weight polymer was only soluble in methanol, ethanol, isopropanol, and water (above ~65°C). It was not soluble in other solvents that were listed in the literature, specifically $CHCl_3$. There are at least two explanations for this difference: first, the molecular weight of the LPEI we used is much higher than that generally found in the literature and second, the LPEI used for our experiments was anhydrous.

It is possible that the solubility of LPEI-hydrates is greater than the anhydrous polymer. However, this has not been proved. Infrared analysis by our group was performed on LPEI samples, with and without dissolved salts.[66] Assignment of the absorption bands was difficult since the spectrum of LPEI contains many polymer bands that interfere with experimental markers for speciation, namely, the triflate absorptions.

Raman spectroscopy, model compound studies, and computational calculations were three additional techniques that were used to help with the investigation of LPEI-salt systems.

Raman spectroscopy was employed to simplify complicated areas in the IR spectra. The polymer bands that complicate the IR spectra are not all Raman active and therefore do not complicate the areas of interest in the Raman spectra. *N,N'*-dimethylethylenediamine (DMEDA) was used by our group as a model compound. DMEDA was studied spectroscopically and used to help elucidate the mode assignments for LPEI. Boesch and York[71] also performed infrared and Raman spectroscopic studies on salts dissolved in DMEDA and compared the results to corresponding LPEI-salt samples. Lastly, computational studies of pure DMEDA and dissolved salt in DMEDA helped in the mode assignments. Boesch and York[71] were able to correlate which vibrational modes were present in the spectrum of DMEDA based upon computational (Hybrid Hartree-Fock density functional calculations) and experimental work. York was then able to assign absorption bands to vibrational modes of LPEI based upon the DMEDA mode assignments.

LiTf and sodium triflate (NaTf) were dissolved in LPEI and the corresponding samples were investigated using IR spectroscopy, Raman spectroscopy, DSC, and AC complex impendence measurements. The IR spectrum of pure LPEI is shown in **Figure II-4** and one can clearly see the N-H stretching region (3300-3200 cm^{-1}) has an asymmetric band (**Figure II-5**).

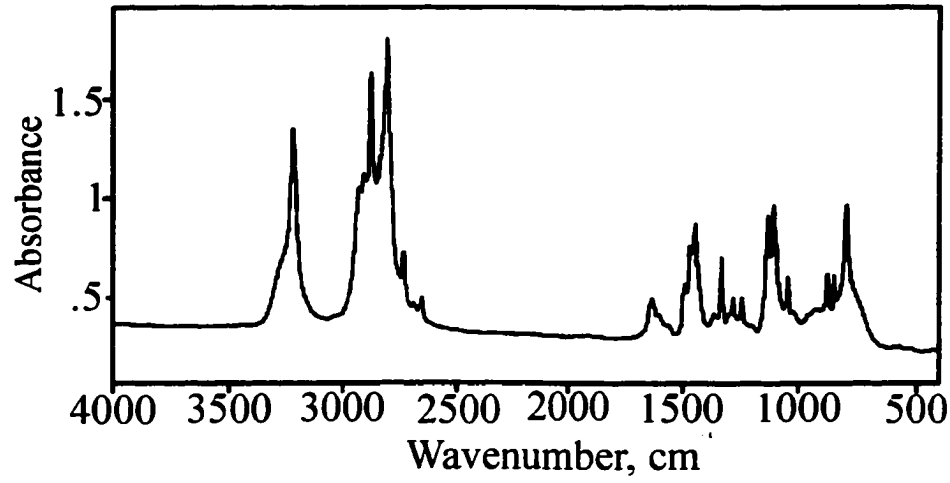

Figure II-4 IR Spectrum of LPEI

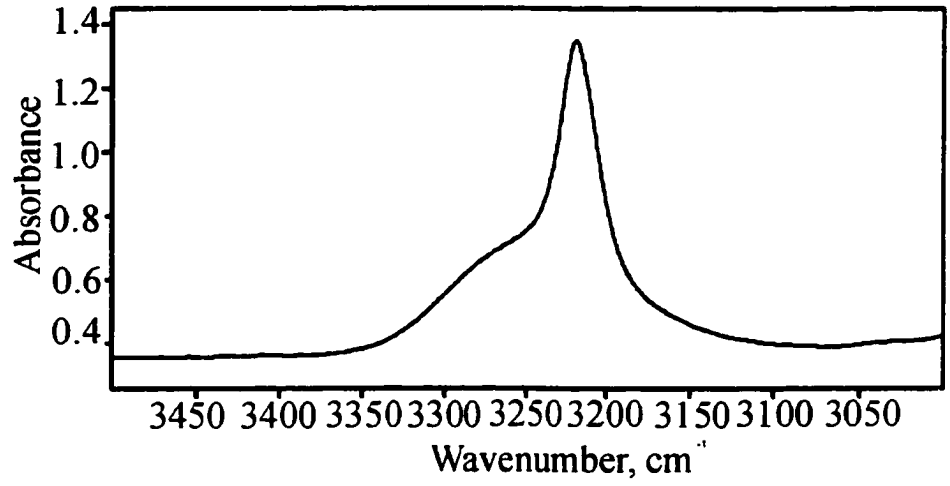

Figure II-5 IR Spectrum of LPEI from 3500 to 3000 cm^{-1}

The asymmetric N-H stretching band of LPEI consists of two absorptions, one centered at 3210 cm^{-1}which is due to crystalline domains in LPEI whereas the second absorption is centered at 3270 cm^{-1} and is due to amorphous domains in LPEI. Two key regions which we looked at were the $\delta_s(CF_3)$ (~765-750 cm^{-1}) and polymer CH and NH bending and stretching region (1400-1050 cm^{-1}). **Figures II-6** and **II-7** shows the IR and

Raman spectra for LPEI and LPEI-LiTf samples in the $\delta_s(CF_3)$ region, respectively. The environment that surrounds the triflate anion influences the $\delta_s(CF_3)$ absorption frequency which spans from ~765-750 cm^{-1}. The $\delta_s(CF_3)$ region shows a large shift of the absorption bands to higher wavenumbers as the amount of LiTf is increased. At the 5:1 N:Li salt composition the $\delta_s(CF_3)$ absorption frequency is at 760 cm^{-1} and this shift is also clearly seen in the Raman spectra.

The IR and Raman spectra in **Figures II-6** and **II-7** show several LPEI-LiTf samples. The low salt concentration sample, 20:1 N:Li, has an absorption band centered at 753 cm^{-1} and the frequency is near the "free" triflate ion frequency in PEO systems.[38] The $\delta_s(CF_3)$ band shifts significantly to higher wavenumbers with increased salt concentration, 757 cm^{-1} and 760 cm^{-1} for the 10:1 and 5:1 N:Li samples respectively. LPEI-sodium salt samples act slightly differently than the LPEI-lithium salt samples. The LPEI-sodium salt samples are mainly ion pair whereas the LPEI-lithium salt samples

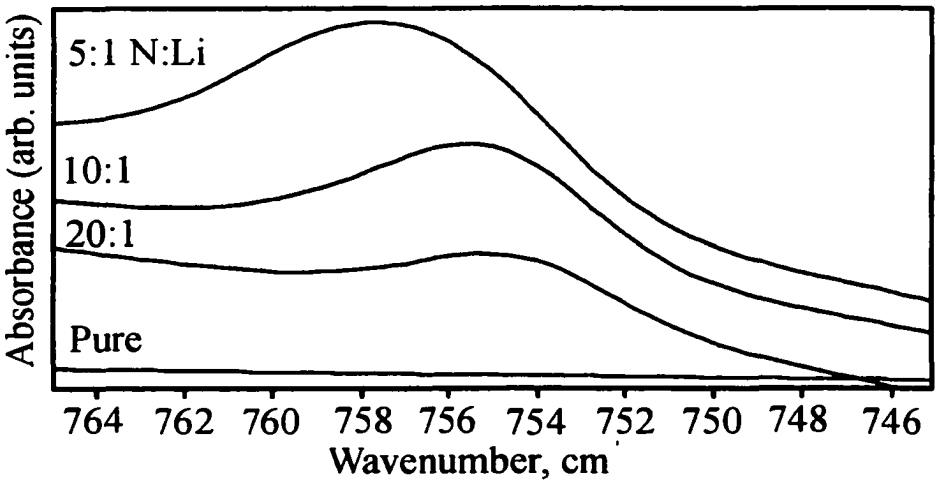

Figure II-6 IR Spectra of LPEILLiTf in varying compositions

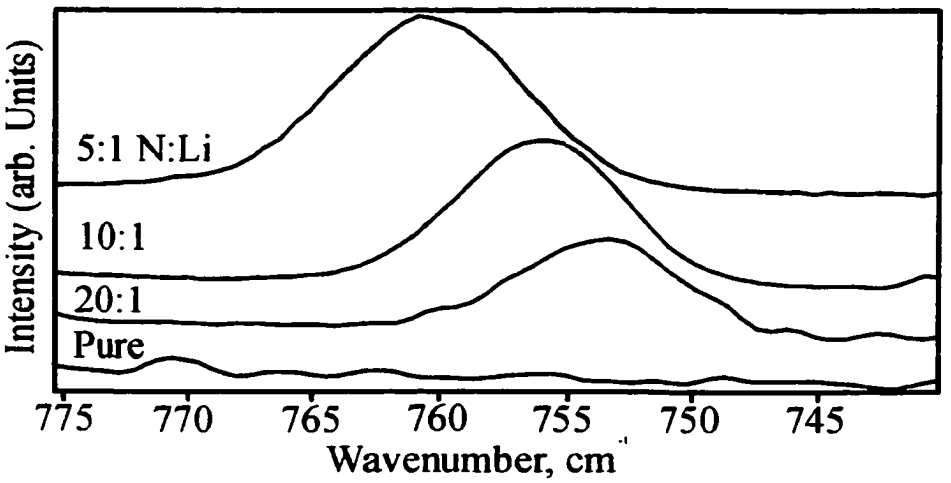

Figure II-7 Raman Spectra of LPEI:LiTf in varying compositions

contain three different species; "free" ion, ion pair, and aggregates. The behavior of the two different LPEI-salt systems is interesting. If the interactions between the backbone nitrogens and the metal cations increase, a decrease in the relative amounts of ion pairs and possibly aggregate should be observed spectroscopically. Nitrogen, lithium cations, and sodium cations are all consider hard atoms/ions (hard/soft acid/base theory, HSAB theory[77]), but lithium is harder than the sodium. The spectroscopic results indicate the lithium system contains relatively more relative "free" ions than the softer sodium system, suggesting that nitrogen interacts more strongly with lithium cations. However, hydrogen bonding within the polymer electrolyte system does complicate the cation-nitrogen interactions. The removal of hydrogen bonding by methylation of LPEI should clarify its role within the polymer electrolyte system and will be discussed further in **Chapter III**. The other interesting point to make is sodium cations normally form higher order ionic species and contain aggregates. However, the LPEI-NaTf salt system does

not contain a significant amount of aggregate species.

The trend for the sodium and lithium salts is not the same; a shift to higher wavenumber is seen for the lithium salt as the concentration of the salt is increased. The sodium salt does not contain, to any reasonable extent, "free" ion at low salt concentration and contains mostly ion pairs at all salt concentrations sampled. **Figures II-8** and **II-9** show the IR and Raman spectra for LPEI and LPEI-NaTf samples in the

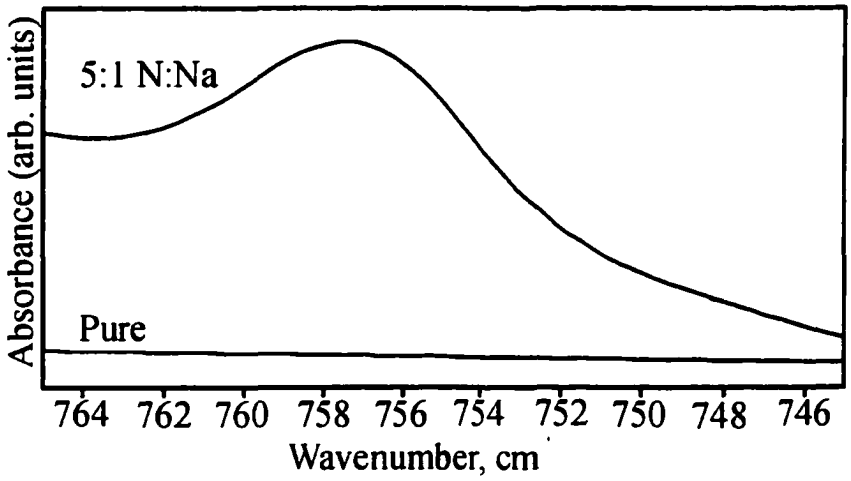

Figure II-8 IR Spectra of LPEI and LPEI:NaTf 5:1 N:Na

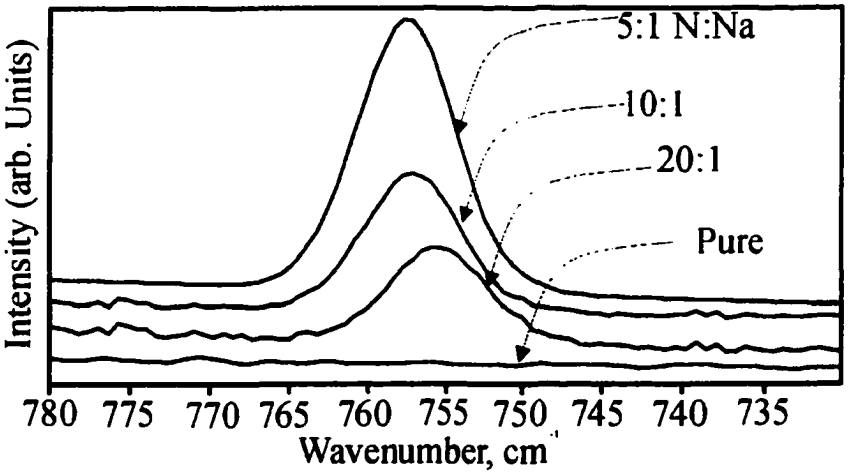

Figure II-9 Raman Spectra of LPEI:NaTf at various compositions

$\delta_s(CF_3)$ region, respectively. The LPEI-NaTf Raman spectra show $\delta_s(CF_3)$ absorption bands at 756, 757, and 758 cm^{-1} for the sample compositions of 20, 10, and 5:1 N:Li, respectively. We noted that the absorption band frequency is consistent with NaTf contact ion pairs. Curve-fitting analysis of the Raman $\delta_s(CF_3)$ spectral region is reproduced in **Table II-1**.

Table II-1 Curve-Fitting Analysis of Raman $\delta_s(CF_3)$ Spectral Region for LPEI-LiTf and LPEI-NaTf

Sample Composition	Band, cm^{-1} (intensity)	Band, cm^{-1} (intensity)	Band, cm^{-1} (intensity)	Band, cm^{-1} (intensity)
N:Li				
20:1			755 (74%)	752 (26%)
10:		759 (18%)	756 (69%)	753 (13%)
5:1	763 (10%)	760 (83%)	757 (7%)	
N:Na				
20:1			756(100%)	
10:1			757 (100%)	
5:1	692 (9%)		757 (80%)	754 (11%)

A second region of interest was the polymer CH and NH bending and stretching region, 1400-1050 cm^{-1}. The changes in this region for both lithium and sodium salts were drastic. **Figures II-10** and **II-11** show the IR and Raman spectra of LPEI-LiTf from

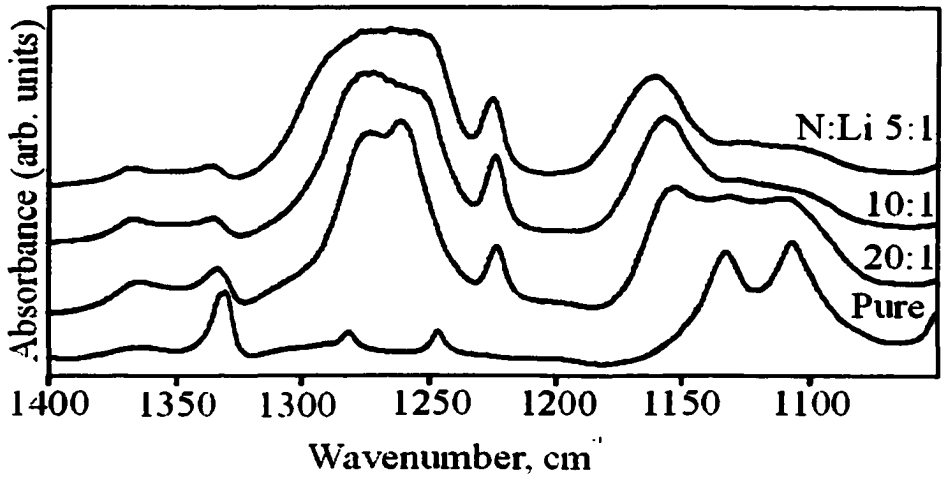

Figure II-10 IR Spectra of LPEI:LiTf at various compositions

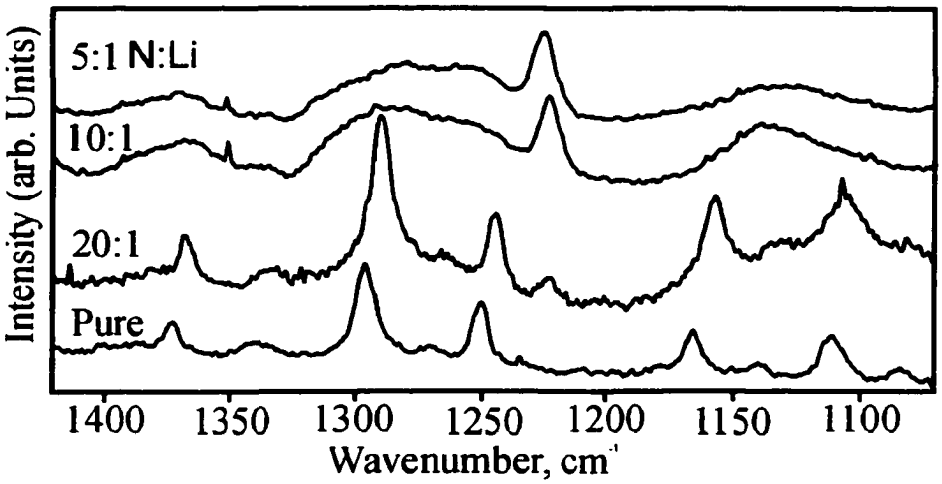

Figure II-11 Raman Spectra of LPEI:LiTf at various compositions

1400-1000 cm^{-1}, respectively. **Figures II-12** and **II-13** show the IR and Raman spectra for LPEI-NaTf from 1400-1000 cm^{-1}, respectively. The modes in this region are very complex; not only do polymer bands appear in this region, so do triflate bands. **Figure II-12** shows two absorption bands that are over absorbed at ~1280 and 1260 cm^{-1},

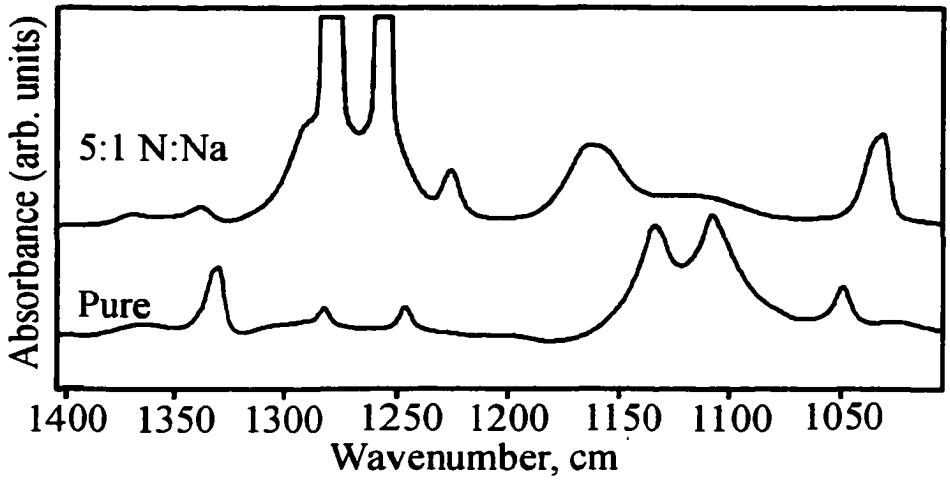

Figure II-12 IR Spectra of LPEI and LPEI:NaTf 5:1 N:Na

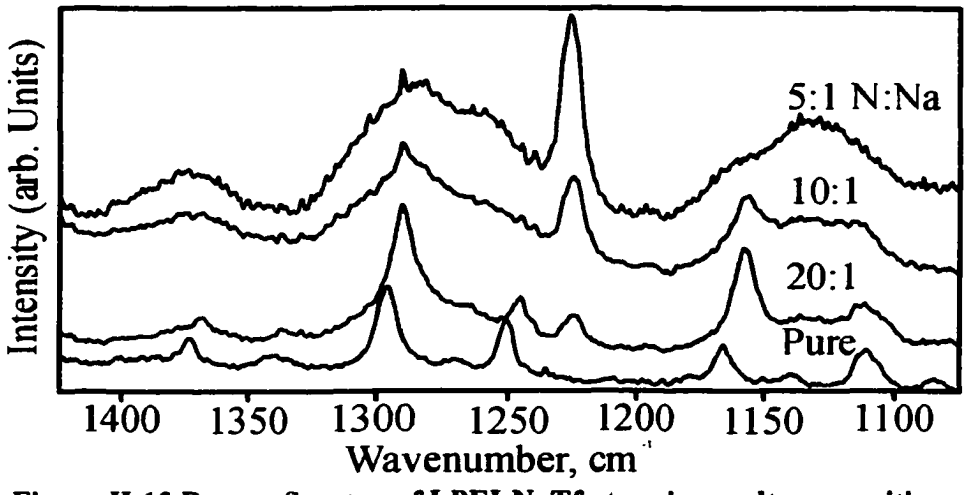

Figure II-13 Raman Spectra of LPEI:NaTf at various salt compositions

however the peaks (~1050-1030 cm^{-1}) of interest are not. The trends seen for both lithium and sodium triflate were that polymer bands broadened, losses of band intensity are observed, and there is an overall loss of vibrational band structure (~1350-1250 cm^{-1}, **Figure II-11** for example).

It is interesting to note that there is a total loss of vibrational band structure that occurs for samples between 20:1 and 10:1 N:Li ratios. This loss of vibrational band structure is also seen in the NH stretching region. **Figure II-14** shows the NH stretching

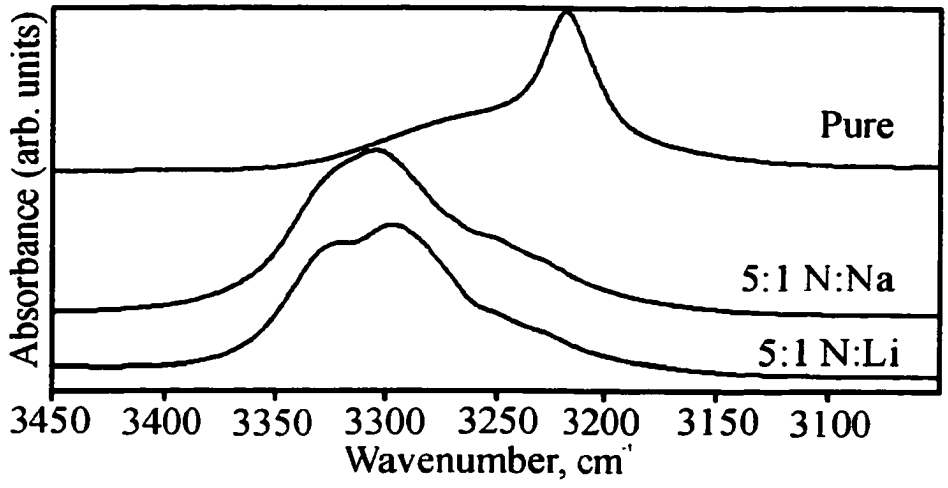

Figure II-14 IR of LPEI, LPEI:LiTf and LPEI:NaTf at a 5:1 N:Cation Ratio

region for both LPEI-LiTf and LPEI-NaTf. It is clearly shown that the NH absorption band; which initially contained two components, amorphous and crystalline domains, has changed significantly at high salt concentrations. In both LPEI-salt samples, the NH stretching region due to the crystalline domains has completely been suppressed. LPEI-salt samples become totally amorphous at high (>10:1 N:M^+) salt concentrations. The loss of crystallinity was also shown in two other experiments. The DSC, see **Figure II-15**, thermogram clearly shows a sharp T_m for pure LPEI at ~65°C, however upon addition of LiTf (20:1 N:Li) the sharp T_m becomes a weak transition and at 5:1 N:Li the transition

is completely gone.

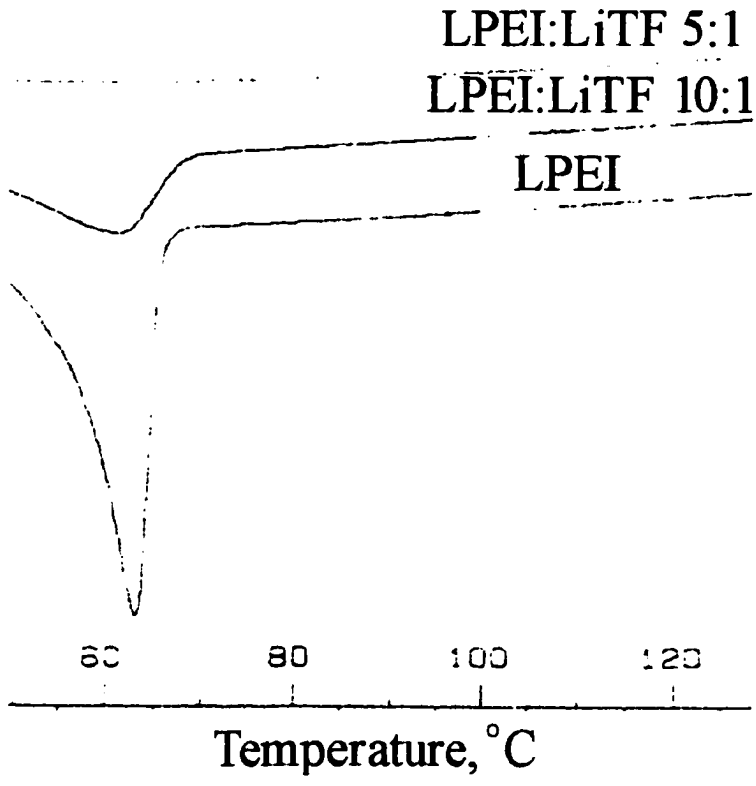

Figure II-15 DSC Thermogram of LPEI and LPEI:LiTf Samples

The second experiment also verified the amorphous nature of the polymer-salt samples. X-ray diffraction data on the LPEI-LiTf and LPEI-NaTf 5:1 samples were obtained which indicated that these two samples were highly amorphous. One interesting side note is that Harris[57] reported the existence of a LPEI-NaTf crystalline compound. The stoichiometry is thought to be 4:1 N:Na. However, this has not been verified.

Impedance measurements, see **Figure 16**, were carried out on the LPEI-LiTf polymer electrolyte system. The 20:1 and 5:1 N:Li compositions samples (at two different temperatures, 20 and 40°C) have conductivities of ca.10^{-7} S/cm^{-1}. The

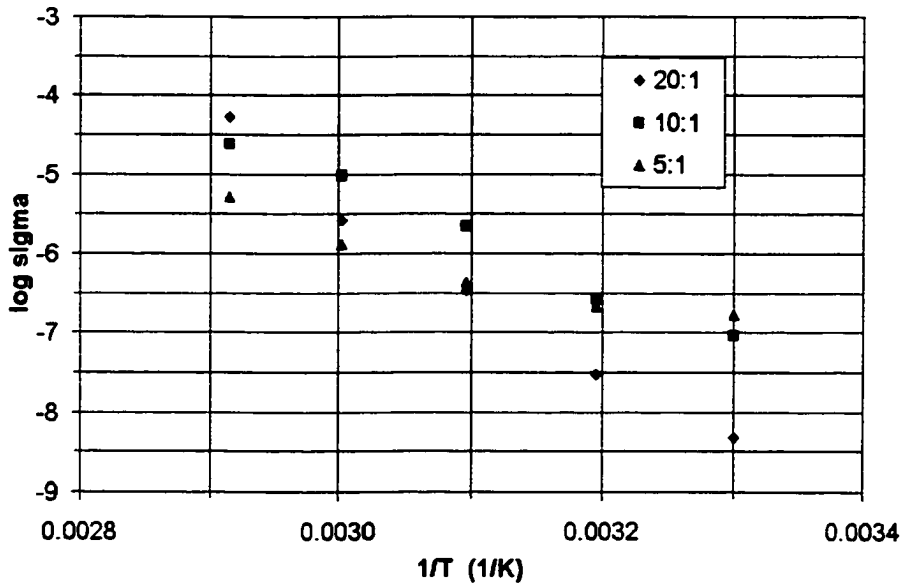

Figure II-16 Temperature Dependant Conductivity of LPEI:LiTf at various salt compositions

conductivity of the 5:1 sample was a little lower at both temperatures than the corresponding 20:1 sample. The conductivity of both LPEI-LiTf samples is relatively low for use as a polymer electrolyte host (> 10^{-4} S/cm would be optimum). This is likely due to the extensive hydrogen bonding which makes LPEI a highly crystalline polymer. However, anions and cations may also be hydrogen bonded to the polymer and therefore the mobility of the lithium cations has decreased. The conductivity of the LPEI-salt systems decrease as the amount of salt is increased. The 20:1 N:Li LPEI-LiTf sample has a conductivity of 3 X 10^{-6} S/cm and the 5:1 N:Li has a conductivity of 1 X 10^{-6} at 60°C. "Free" ions are thought to be the major contributor to conductivity. One can make a simple comparison of conductivity of the polymer electrolyte to its relative amount of "free" ion speciation, however a direct correlation cannot be made. The conductivity of

the 20:1 N:Li sample at 60°C is 3 X 10^{-6} S/cm and we see 26% "free" ion, whereas the 5:1 sample has a conductivity of 1 X 10^{-6} S/cm 60°C and we see fewer "free" ions suggesting that "free" ions are not solely responsible for the ion conductivity. The morphology of LPEI changes as salt is added, becoming more amorphous as the concentration of LiTF is increased. However, a rise in conductivity is not seen for the respective increase in amorphous character of the polymer system. Another point to address is the behavior of LPEI relative to PEO.

LPEI differs from PEO in the relative amount of "free"ions that are contained in the 20:1 X:Li samples (where X is either O or N). PEO has 6% "free" ion whereas LPEI has 26%. LPEI has hydrogen bonding interactions and behaves quite differently than PEO. As the amount of salt is increased, it is more likely that PEO will form crystalline complexes. As the sample will becomes more crystalline, the ionic conductivity will drops due to decreased mobility and increased ionic speciation. The hydrogen bonding in LPEI is suppressed as the amount of salt increases, therefore makes the LPEI-salt system more amorphous. Triflate provides spectroscopic markers that can be used with both PEO and LPEI salt systems. The markers can monitor ionic speciation in both systems, however one must account for hydrogen bonding interactions in the LPEI-salt system.

Conclusions and Future Directions:

LPEI was used as a polymer electrolyte host and provided further information about, and a better understanding of polymer electrolyte host systems. The speciation

data suggests the nitrogen atoms of LPEI interacts with lithium cations more than with sodium cations, but is complicated by hydrogen bonding. The LPEI-LiTf polymer electrolyte system contains a significant amount of "free" ion which is in consistent with HSAB theory.[77] A spectroscopic study of LPEI revealed that triflate salts dissolved in LPEI exhibit similar trends to those of PEO-triflate salt systems, i.e. a change from "free" to more ion pairs and aggregates as salt concentration is increased. The two major differences in LPEI-salts systems and PEO-salt systems are that LPEI exhibits drastic effects due to hydrogen bonding and the second difference is that LPEI-NaTf samples did not exhibit drastic changes in ionic speciation with changing NaTf concentration, while PEO-NaTf has two distinct highly associated ionic species.[78] The LPEI vibrational mode assignments were made by correlation of computational and experimental spectroscopic work. These assignments provide a further understanding of how polymers interact with dissolved salts.

In the future, work on LPEI will be carried out in two areas: extension to work on BPEI and synthetic modification of LPEI. LPEI can be modified in two different ways. LPEI can be synthetically modified to provide a new polymer or it can be crosslinked using a variety of dihalides to provide an elastomeric network. Crosslinking LPEI has a variety of potential uses. Crosslinked LPEI is a potential proton conductor since the crosslinking process generates H-X as a byproduct (where X is the halide used). The nitrogen in the polymer backbone can act as a proton shuttle site. A second use of crosslinked LPEI is as a battery polymer electrolyte layer. A common problem

with polymer electrolytes is that the systems have poor physical properties. However, crosslinked LPEI is a relatively robust elastomeric system which has better mechanical properties than other systems. Initial cross-linking experiments indicated that LPEI can be crosslinked easily, however, the concentrations (in methanol) of both LPEI and the dihalide must be appropriate for the cross-linking to occur. Iodide, chloride, and bromide sources were all used as crosslinking agents and were successful. One other type of crosslinking reagent used was acrolein and acrolein type michael acceptors. The Michael acceptor provided a internal cross that is charge neutral. A complete understanding of the cross-linking process and cross-linked systems is beyond the scope of this dissertation.

A different area of synthetic modification of LPEI is to make new non-crosslinked polymers from LPEI. Linear poly(*N*-methylethylenimine) (LPMEI) is an example of a synthetically modified LPEI. LPMEI is a polymer electrolyte host that will facilitate study of hydrogen bonding effects (by removing them) which will be discussed in **Chapter III**. A second polymer that can be synthesized from LPEI is a polymer that has tethered oligo(ethylene oxide) side chain units off of the LPEI nitrogen. This PEO/PEI hybrid polymer is very promising since it has the crosslinking ability of LPEI and the tethered side chains like poly(bismethoxyethoxyethoxyphosphazene) (MEEP) that may increase the conductivity of the polymer electrolyte host, Chapter IV. Once synthetic modifications of LPEI are complete, application of the synthetic methodology to BPEI system can be carried out. It can't be stressed enough that any

commercialization of PEI as a polymer electrolyte host will be with BPEI until an economical synthesis of LPEI is developed.

Experimental:

All common reagents and solvents were commercially available and used as received unless otherwise noted. All ^{1}H and $^{13}CNMR$ were obtained using a Varian 300 or 400 MHZ spectrometer. All deuterated solvents were used as is and the residual proton solvent peaks were used as references.

Polymerization of 2-Methyloxazoline

Figure II-17 shows the polymerization of 2-methyloxazoline. A 100 mL round bottom flask was charged with 2-methyl-2-oxazoline (monomer, 9.096 g, 0.1068 mol) dissolved in 45 mL of dry CH_3CN. The flask was purged with N_2. Methyl-*p*-toluenesulfonate (initiator, 1.2 g, 0.0065 mol), dissolved in ~5 mL of dry CH_3CN, was added to the monomer solution by pipet. The flask was sealed with a septum and placed in thermostated bath at 60°C for ~24 hours. Reaction was stopped and all solvent was removed under reduced pressure. The residue was dissolved in a minimal amount of dry $CHCl_3$ and the solution was added drop wise to dry diethylether

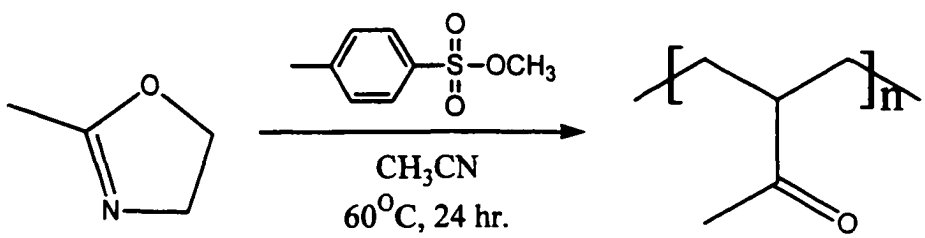

Figure II-17 Synthetic Scheme for Polymerization of 2-methyloxazoline

with stirring and the desired polymer precipitated. The precipitation process was repeated at least once and the polymer was collected by filtration and dried in a vacuum oven for 4 days at room temperature. Molecular weight (Mw) was estimated by GPC (PEOz standards (200,000 and 50,000 g/mol), Ultrahydrogel linear GPC column 6-13 μm, 7.8 X 300 mm; Shodex RI-71 RI detector). The molecular weight of the polymer was between ~1200 - 2000 g/mol. This procedure gave an 85% yield. ^{1}H-NMR(CD_3OD) δ(ppm) 3.2 (4H), 2.0 (3H)

Synthesis of Low MW LPEI

Poly(2-methyloxazoline) (Mw ~1200 - 2000 g/mol, ~9 g) was dissolved in 100 mL distilled water. To the PMOz solution, 10.3710 g NaOH was added and the solution was heated to reflux solvent for 24 hours. After 24 hours, the mixture was allowed to cool. The low molecular weight LPEI that solidified was collected by filtration and was washed with cold distilled water until the filtrate was ~ pH 7. This procedure gave 85% yield. ^{1}H-NMR (CD_3OD) δ(ppm) 2.65 (4H); ^{13}C-NMR(CD_3OD-d_4) δ(ppm) 48.6.

Synthesis of High MW LPEI

A 3 L round bottom flask was charged with ~30 g of linear poly(2-ethyl-2-oxazoline) (Aldrich. Avg. MW 200,000) and 1800 mL of 3 M HCl . The solution was heated until solvent reflux for 5 days. After 5 days, the solution was allowed to cool to room temperature. The solvent was removed under reduced pressure using a rotary evaporator until the resulting ammonium hydrochloride salt was dry. The salt was normally used without verifying its identity. The salt was dissolved in 3 L of

distilled water and neutralized with NaOH pellets until the pH was much greater than 10. The polymer precipitates out of solution as the concentration of NaOH is increased. The basic solution was warmed until all the polymer dissolved. The solution was removed from the heat and allowed to cool. The resulting polymer, LPEI, crystallized from solution and was collected by filtration in a fritted glass funnel. The collected polymer-hydrate was re-dissolved by warming in distilled water (3500 mL). Once the polymer was completely dissolved, the mixture was removed from heat and allowed to cool. The polymer crystallized from solution and was collected by filtration again. This process of washing the LPEI was repeated until the pH of the filtrate was neutral. The resulting LPEI-hydrate was dried overnight by pulling air through the funnel. The LPEI-hydrate was removed from the collection funnel and placed in a jar and further dried by heating under reduced pressure at ~ 50°C for one day followed by heating at ~70°C for one day. The anhydrous LPEI was only soluble in methanol, ethanol, 2-propanol, *t*-butyl alcohol. This procedure gave an 85% yield. ^{1}H-NMR (CD_3OD) δ(ppm) 2.65 (4H); $^{13}C(CD_3OD\text{-}d_4)$ δ(ppm) 49.8.

Preparation of Polymer Electrolytes:

To prepare the electrolyte materials, LPEI was dried under vacuum at 75°C for 48 h. Lithium triflate, $LiCF_3SO_3$ (LiTf), obtained from Aldrich was dried under reduced pressure at 120 °C for 24 h. Sodium triflate, $NaCF_3SO_3$ (NaTf), obtained from Aldrich was dried under reduced pressure at 120°C for 24 h. Anhydrous methanol (99.8%, water, 0.002%) from Aldrich was redistilled and stored over molecular sieves. All materials

were stored in a nitrogen-atmosphere glove box with a moisture less than 1 ppm. Desired ratios of LPEI and LiTf or NaTf were dissolved in anhydrous methanol in the glove box and stirred for 24 h. The composition of an LPEI-salt system is described by the N:M ratio, which is the ratio of nitrogen atoms to cations. To obtain thin films of the samples, the polymer solutions were cast onto glass slides (for Raman) and AgBr salt plates (for IR) and the methanol was allowed to evaporate at room temperature in the glove box. The resulting films were dried under vacuum for 48 h at 45°C.

Raman Spectroscopy:

Raman spectra were taken using an ISA Jobin-Yvon T64000 Raman spectrometer. The 514 nm line of an argon laser was used as the exciting line at a power of 300 mW at the laser head. The Raman spectra of the films were taken in a back-scattering geometry under a microscope.

FTIR Spectroscopy:

Infrared spectra were recorded using a Bruker IFS66V FT-IR spectrometer over a range of 4000-400 cm^{-1} at a resolution of 1 cm^{-1}. The IR spectra of the films were taken between AgBr plates in an evacuated sample chamber at room temperature. Curve-fitting analysis of the spectral data was done using a commercial program (Galactic Grams version 5.05). The spectra were curve-fit to a straight base line and one Gaussian-Lorenzian product function for each band using a non-linear least-squares method.

Differential Scanning Calorimetry:

Sample solutions were cast onto Teflon, dried in a nitrogen environment for 24 hours, and placed under vacuum for 24 hours. After the samples were dried, a 7.1-7.7 mg sample was sealed in a 40 μL aluminum pan. Thermal data were collected using a Mettler DSC 820 calorimeter with commercially available software from Mettler Toledo (Stare v.6.10) under a dry nitrogen purge. The temperature range was -25 - 175 °C

Complex Impedance:

Complex impedance measurements were made over the range of 5 Hz to 10,000 KHz using an HP 4192A LF impedance analyzer. Samples were sandwiched between 12.5 mm stainless steel electrodes in an airtight cell, which was maintained at a desired temperature using a circulating bath. Impedance plots were fitted using LEVM version 7.1.

Chapter III

POLY(N-METHYLETHYLENIMINE), PMEI

Introduction:

LPEI has strong hydrogen bonding interactions which are of interest since hydrogen bonding clearly affects speciation of dissolved salts. Little work has been done on LPMEI.[48,51,54,68,69] Tanaka[68], in 1978, used LPEI to make LPMEI. Tanaka used the Eschweiler-Clarke variation of the Leuckart reaction to methylate either LPEI or poly(*N*-formylethlenimine) (POZ). The degree of methylation was shown to be over 90% for both LPEI and POZ at different temperatures, see **Table III-1**.

Table III-1 Degree of Methylation for LPMEI at Different Temperatures

Sample	105°C	115°C	125°C
LPEI	94%	97%	92%
POZ	100%	100%	96%

Isolation of LPMEI was accomplished by acidifying the polymer followed by either extraction, dialyses, or anion-exchange. Tanaka noted that the extraction and dialysis experiments were both poor methods. Both methods were complicated by low yields and the extractions were contaminated with various inorganic salts. Anion-exchange was the most efficient method used and Tanaka noted *"this method enabled an almost quantitative recovery of the free amines"*. Tanaka also reported that LPMEI was a hygroscopic viscous liquid when thoroughly dry.

Saegusa[54], in the same year (1978), used a similar method to synthesize LPMEI.

However, Saegusa did not characterize LPMEI. Saegusa's results were comparable to those of Tanaka and the synthesis was considered "*almost perfect.*" The molecular weights of LPMEI made by both Tanaka and Saegusa were low. Later, Tanaka [51] synthesized LPMEI in high molecular weights (~47-136 X 10^3 g/mol) The resulting polymer was characterized by proton and carbon NMR spectroscopy. LPMEI is soluble in water, methanol, ethanol, dimethylformamide, THF, chloroform, and benzene and insoluble in diethyl ether and hexane. The degree of substitution was complete within detection limits. LPMEI absorbs moisture readily and forms a solid hydrated polymer. The LPMEI-hydrate has a melting point of 56°C and has one water molecule per four repeat units of polymer. DSC thermograms for the LPMEI hydrate were not reproducible, however, once the polymer hydrate was dried, the DSC thermograms showed a Tg at -82 to -84 °C. In 1993, Tanaka[48] et al. studied ionic conduction in LPMEI-Li salt systems. Tanaka used two different salts, lithium perchlorate ($LiClO_4$) and LiTf. Tanaka noted "*the PEI systems are much more conductive than the corresponding PMEI systems.*" The highest conductivity that Tanaka observed for LPMEI-LiTf was 10^{-6} S/cm at 120 °C for a 10:1 N:Li sample. No extensive study of LPMEI has been carried out. A systematic study was undertaken in our lab to help understand the behavior of LPMEI. Three areas of fundamental research were started. The first area was the synthesis and study of LPMEI. The second area of study was the use of *N, N, N', N'*-tetramethyethlyenediamine (TMEDA) as a model compound for LPMEI. Lastly, computational work on TMEDA was used to help understand and assign

vibrational modes of LPMEI. The utilization of data from these three areas of research just mentioned will help provide a better understanding of the potential of LPMEI for use as a polymer electrolyte host.

Results and Discussion:

LPMEI was synthesized using three different methods. The first and second methods were taken from the literature. The first synthesis was an Eschweiler-Clarke methylation of LPEI and the second synthesis was an in situ hydrolysis followed by an Eschweiler-Clarke methylation using PEOz as the starting material. Both syntheses used formic acid and formaldehyde. The Eschweiler-Clarke methylation of LPEI gave LPMEI in good yields, and over 95% methyl substitution. The degree of methyl substitution was calculated using simple Beers Law calculations. IR spectra were taken of PEOz and LPMEI dissolved in CH_2Cl_2. The molar absorptivity of PEOz (on a repeat unit basis) was ~581 cm^{-1} M^{-1} (1669 cm^{-1}), see Appendix, **Figures A-23** and **A-24**. LPMEI was calculated to have a C=O impurity of less than 6% using the calculated molar absorptivity for PEOz and assuming that the impurity was due to residual amide carbonyls, see Appendix, **Figures A-23** and **A-24**. However, both NMR (Appendix, **Figures A-7** and **A-8**) and IR (**Figure III-7** and **III-8**) spectroscopy indicated complete substitution for the synthesis of LPMEI. The appearance of only two peaks in the proton and carbon NMR spectra ($N\text{-}CH_2$ and $N\text{-}CH_3$) and the absence of N–H stretching absorption bands (3300-3200 cm^{-1}) in the IR spectrum indicated that the substitution was 100%.

The in situ hydrolysis and Eschweiler-Clarke methylation did not work on poly(2-ethyloxazoline), see **Figure III-1**. **Figure III-1** clearly shows the CH_3 (~0.8 ppm)

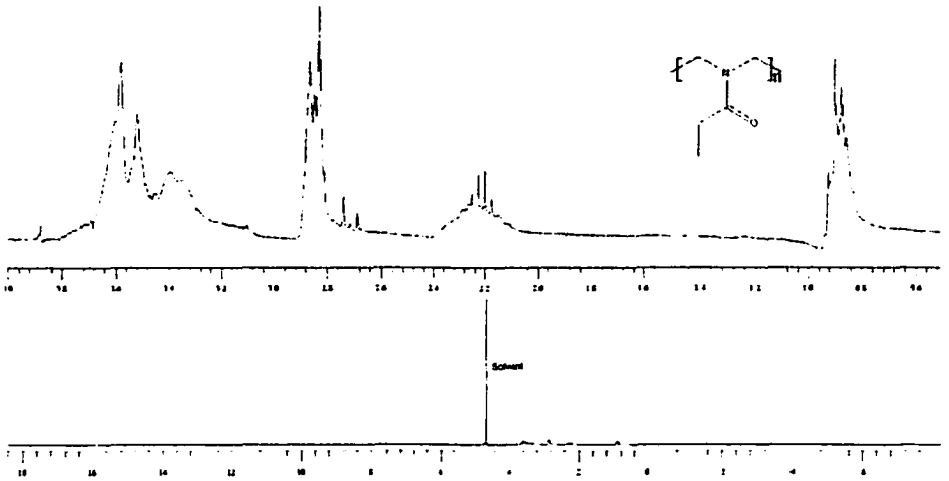

Figure III-1 ^{1}H NMR Spectrum of Crude Reaction Mixture of LPMEI Synthesis

of the ethyl group of the poly(2-ethyloxazoline) indicating that the parent polymer was not hydrolyzed. This method of synthesizing LPMEI was not investigated further. The majority of LPMEI syntheses presented here used the first method. A problem that we encountered with the first Eschweiler-Clarke synthesis was paraformaldehyde contaminated our LPMEI. The paraformaldehyde was difficult to remove and an alterative synthesis method was sought. The alterative method that was developed was a modification of Eschweiler-Clarke methylation, see **Figure III-2**.

Paraformaldehyde is the contaminant which was attributed to excess formaldehyde used. A new formaldehyde source was used to control the amount of formaldehyde in the reaction vessel. Diethoxymethane, an acetal, was used as the

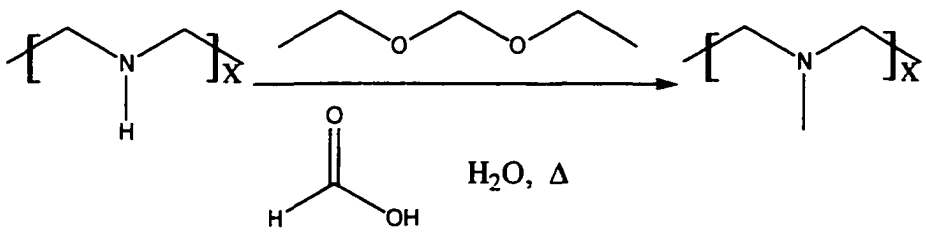

Figure III-2 Synthetic Scheme for New LPMEI Synthesis

formaldehyde source since it could be measured more accurately than the formalin solution. Acetals decompose in acidic media to provide the corresponding aldehydes. The solvent for the reactions is, of course, formic acid which will decompose the diethoxymethane into formaldehyde and ethanol. There is no literature precedent for this type of modification of the Eschweiler-Clarke methylation. It is common to see formic acid used with formaldehyde or acetals used with sodium borohydride.

The conditions for the experiment were decided upon considering previous experiences with the LPMEI synthesis. The initial reaction experiment was successful, see **Figures III-3** and **III-4**. However, upon repeating the experiment the reaction did not rovide 100 % substitution of LPEI, see **Figures III-5** and **III-6**. **Figure III-6** is a blow up of **Figure III-5** and it clearly shows a side peak indicating incomplete substitution of the polymer backbone. The reaction conditions need to be explored more throughly before the reaction can be used on a large scale basis. The vast majority of LPMEI synthesized used the first Eschweiler-Clarke methylation of LPEI. The calculated average molecular weight of LPMEI is 115,000 (assuming no polymer degradation). LPMEI is a light amber-brown viscous polymer which is very hygroscopic. The LPMEI

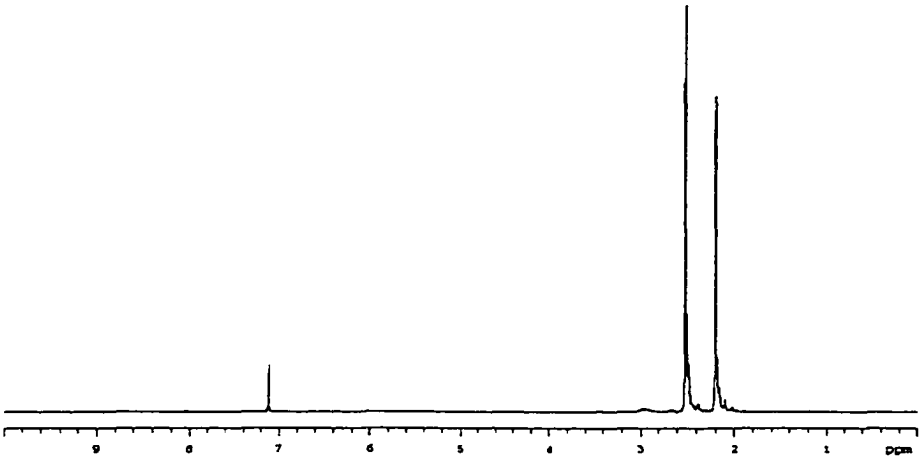

Figure III-3 ^{1}H NMR Spectrum of "Good" LPMEI, New Synthesis

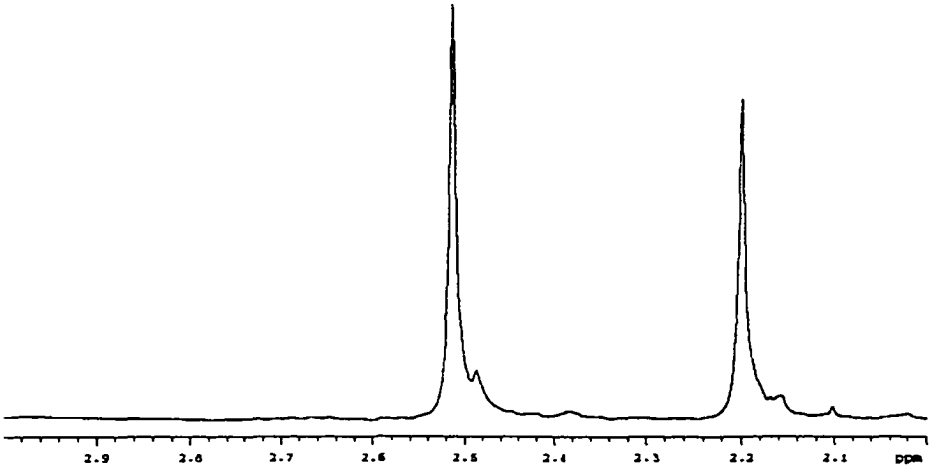

Figure III-4 Expansion of ^{1}H NMR Spectrum of "Good" LPMEI, New Synthesis

was used in spectroscopic studies containing two different salts. LiTf and NaTf salts were dissolved in LPMEI and the corresponding samples were studied using IR spectroscopy, DSC, complex impedance, and X-ray diffraction measurements.

For IR spectroscopic analysis of LPMEI, see **Figure III-7**, it was convenient to

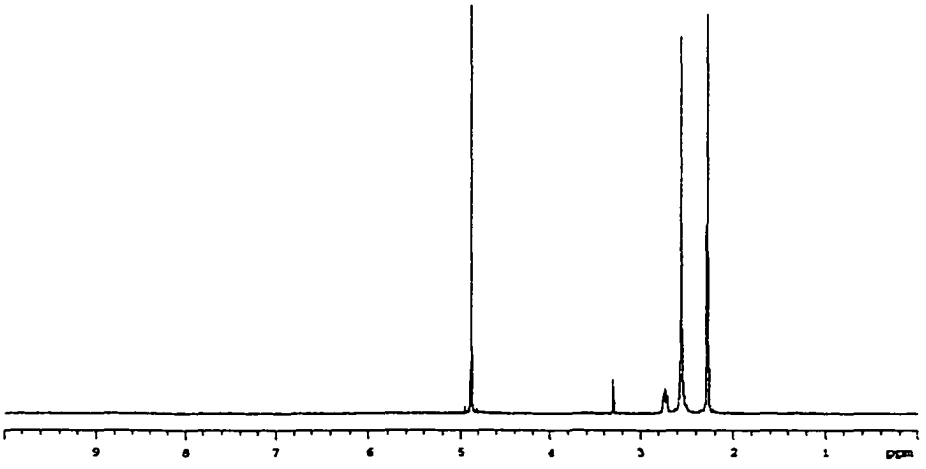

Figure III-5 ^{1}H NMR Spectrum of "Bad" LPMEI, New Synthesis

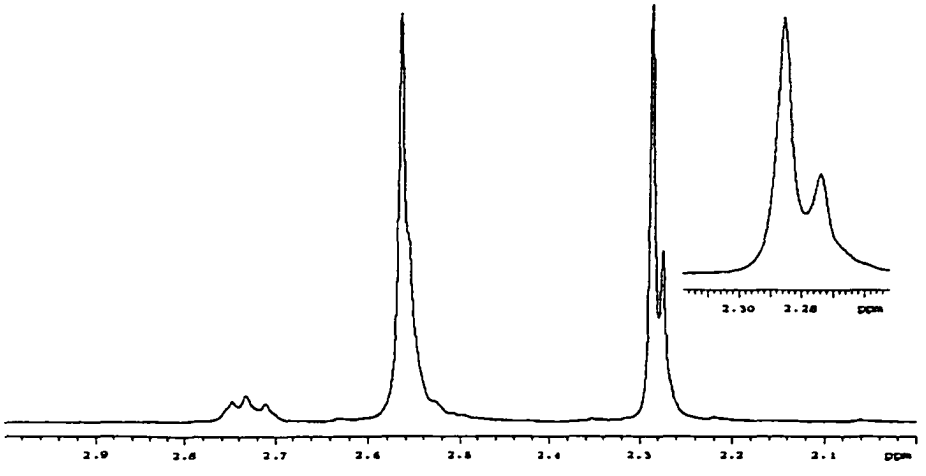

Figure III-6 Expansion of ^{1}H NMR Spectrum of "Bad" LPMEI, New Synthesis

split the spectral range into three different regions. The NH stretching region in the IR did not show any N-H stretching absorptions and indicated that the substitution was ca. 100%, see **Figure III-8.** The removal of hydrogen bonding should cause LPMEI to behave similarly to PEO, since neither system is able to hydrogen bond on its own. The

two other regions that were studied were the $\delta_s(CF_3)$, and $\nu_{as}(SO_3)$ and $\nu_s(SO_3)$ regions.

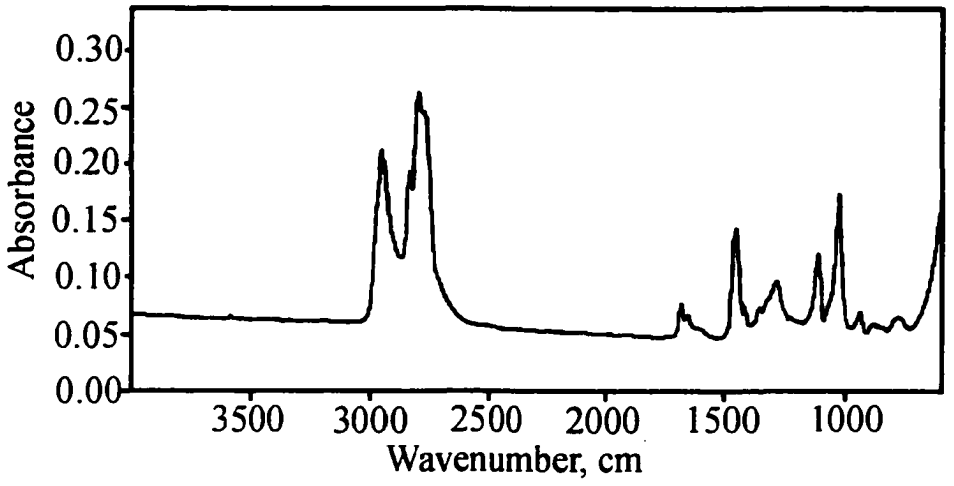

Figure III-7 IR Spectrum of LPMEI from 4000 to 600 cm^{-1}

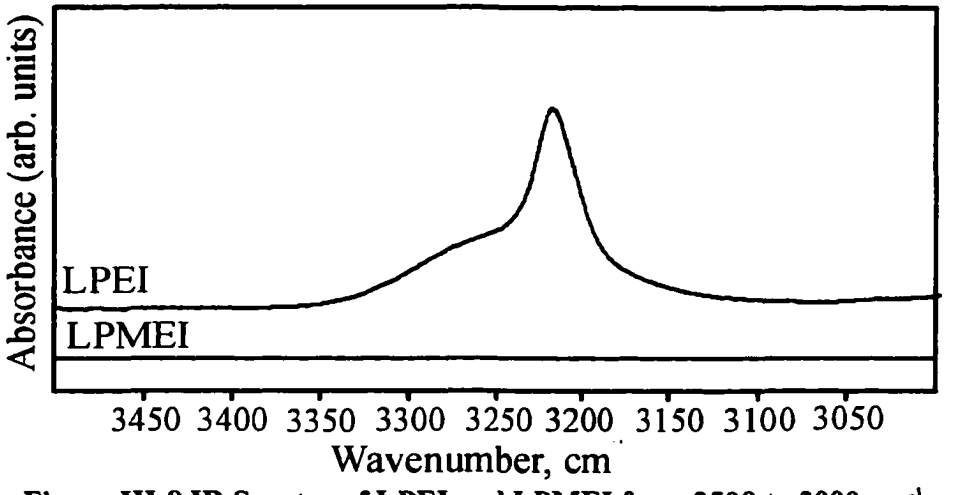

Figure III-8 IR Spectra of LPEI and LPMEI from 3500 to 3000 cm^{-1}

These two regions were extensively studied for samples with both LiTf and NaTf salts. The lithium and sodium triflate polymer electrolytes systems behaved differently from what was expected. This difference came as a shock to us. NaTf tends to form higher order ionic species in PEO. Instead of having "free" ions, NaTf will form ion pair

and aggregates. However, this trend was not seen in the LPMEI-NaTf salt system. The $\delta_s(CF_3)$ absorption bands for LPMEI-LiTf systems (see **Figure III-9**) were broader than for the NaTf systems, see **Figure III-10.** The asymmetric nature of the band indicates

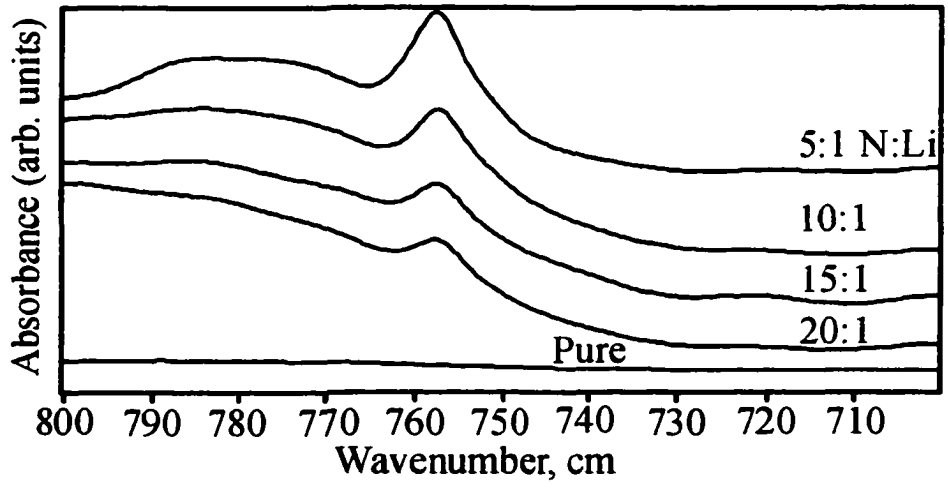

Figure III-9 IR Spectra of LPMEI:LiTf at various compositions

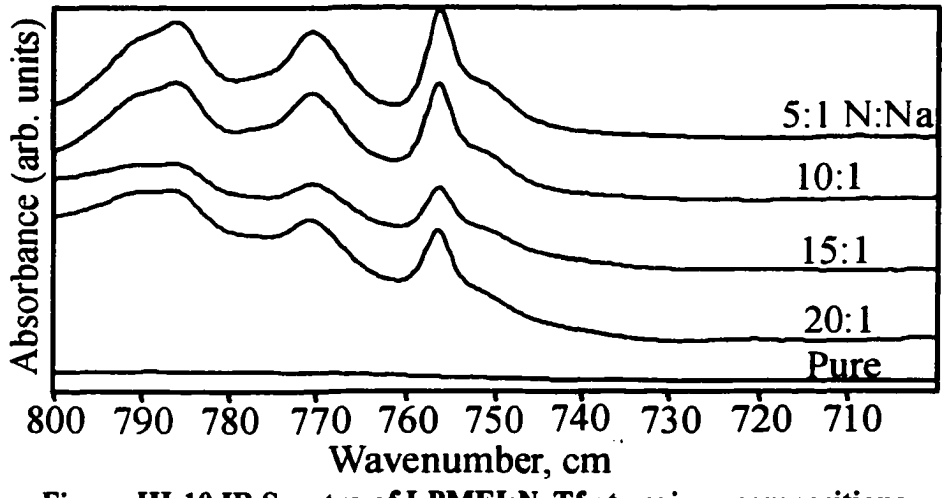

Figure III-10 IR Spectra of LPMEI:NaTf at various compositions

that there is more than one ionic species in the polymer electrolyte. A change in the $\delta_s(CF_3)$ band can be seen by a shift to higher wavenumber in the LPMEI-LiTf polymer

electrolyte sample as the salt concentration is increased.

All LPMEI-LiTf samples contain a small proportion (< 20%) of aggregate ($[Li_2Tf]^+$), whereas the LPMEI-NaTf polymer electrolyte system did not contain any. Spectral deconvolution of this region by curve fitting analysis for the LPMEI-LiTf salt samples indicated that a significant portion of the ions present were either "free" ion or contact ion pairs, see **Table III-2**. The 20:1 N:Li sample contains 36% "free" ions which is a significant proportion. An intriguing note can be made about the 5:1 N:Li sample. The 5:1 N:Li sample contains 24% "free" ion. At high salt concentrations PEO contains only ion pairs and aggregates. The LPMEI-LiTf polymer electrolyte system shows increasing ion speciation as the concentration of the lithium salt was increased. The speciation goes from "free" ion (low speciation) to ion pair (more speciation) to aggregates (high speciation). This trend is very common in other systems but was not seen in the LPMEI-NaTf polymer electrolyte system.

The LPMEI-NaTf polymer electrolyte system actually shows a decrease in speciation with an increase in salt concentration. HSAB theory may explain this trend. As mentioned earlier, nitrogen atoms, lithium cations, and sodium cations are all hard, however, sodium cations are softer than lithium cations. The backbone nitrogens appear to interact more strongly with lithium cations than with the sodium cations. This generalization holds true for LPMEI as well as LPEI at low salt concentrations. The importance of hydrogen bonding is shown by simply considering that the hydrogen bonding effects NaTf more than LiTf.

Table III-2 Curve-Fitting Analysis of IR $\delta_s(CF_3)$ Spectral Region for LPMEI-LiTf and LPMEI-NaTf.

Sample Composition	Band, cm^{-1} (relative intensity)	Band, cm^{-1} (relative intensity)	Band, cm^{-1} (relative intensity)
N:Li	Aggregate	Contact Ion Pair	"Free"
20:1		757 (64%)	752 (36%)
15:1	762 (12%)	758 (61%)	752 (27%)
10:	762 (14%)	757 (60%)	752 (26%)
5:1	762 (20%)	758 (56%)	752 (24%)
N:Na			
20:1		757 (73%)	752 (27%)
15:1		756 (62%)	751 (38%)
10:		756 (54%)	751 (46%)
5:1		756 (48%)	751 (52%)

The LiTf-polymer electrolyte systems (LPEI and LPMEI) both contain "free" ions. However, the LPEI-NaTf does not contain any "free" ions whereas the LPMEI-NaTf contains significant portions of "free" ions. This observation indicates that hydrogen bonding effects can be more significant than HSAB effects, but the exact nature of these effects is still under investigation.

The LPMEI-NaTf polymer electrolyte system actually shows a decrease in ion pairs with an increase in "free" ions. This trend is very interesting and a larger concentration range needs to be explored to substantiate this trend. Although this trend

is unique, it also needs to be pointed out that the NaTf system might not exhibit the normal trends seen for other polymer electrolytes systems because the LPMEI and NaTf may be forming crystalline compounds at high salt concentrations. Spectral deconvolution was carried out on the $\delta_s(CF_3)$ absorption bands in the LPMEI-NaTf polymer electrolyte system and is reproduced in **Table III-2.**[69] It can be seen that NaTf speciation does change with increasing concentration. However, the speciation does not go through any drastic redistribution to form higher order ionic species, rather more "free" ions are formed. The redistribution to form more "free" ions is difficult to explain and may be due the LPMEI-NaTf forming a crystalline complex. The LPMEI-NaTf polymer electrolyte sample contains mainly contact ion pairs for the entire composition range, which is very interesting. The local structure of LPMEI-NaTf could be better understood if a crystal structure can be solved for a LPMEI-NaTf crystalline complex. A crystalline LPMEI-NaTf complex could help substantiate many of the vibrational mode assignments that have been made using experimental and computational methods.

The other significant region (1200-1000 cm^{-1}) contains the $\nu_{as}(SO_3)$ and $\nu_s(SO_3)$ absorption bands which showed interesting trends as the salt concentration was varied. **Figures III-11** and **III-12** show the $\nu_{as}(SO_3)$ and $\nu_s(SO_3)$ absorption bands for LPMEI-LiTf and LPMEI-NaTf polymer electrolyte samples, respectively. The $\delta_s(CF_3)$ absorption bands become broader and shifted to higher wavenumbers as salt concentration was increased. This trend is also seen in the $\nu_{as}(SO_3)$ and $\nu_s(SO_3)$ spectral regions. The LPMEI-LiTf polymer electrolyte $\nu_{as}(SO_3)$ absorption bands are broader

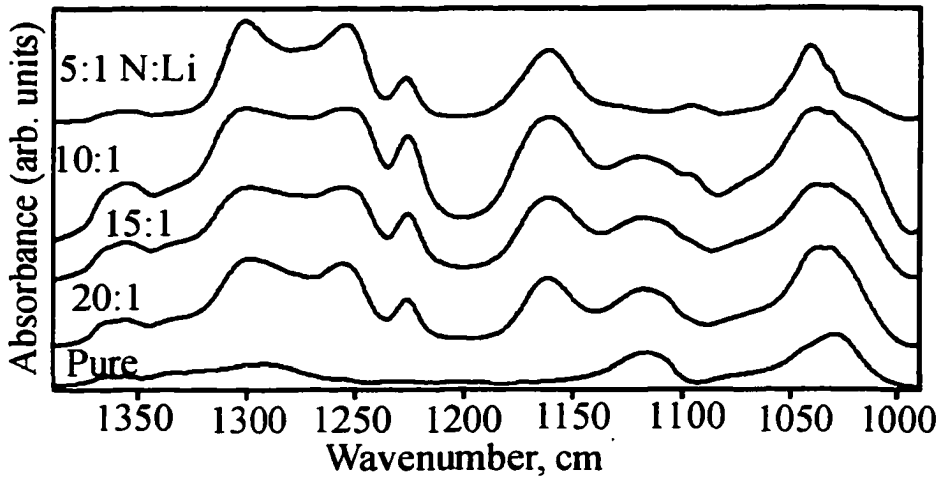

Figure III-11 IR Spectra for LPMEI:LiTf at various compositions

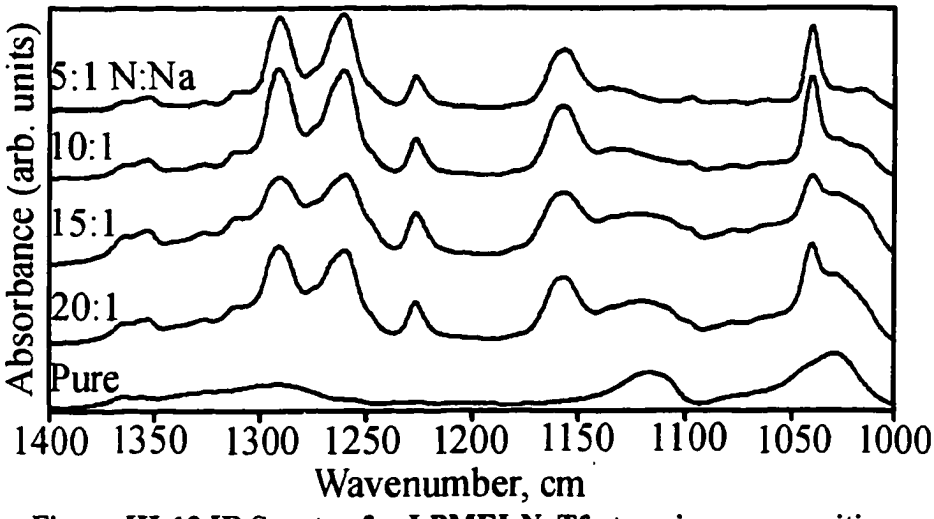

Figure III-12 IR Spectra for LPMEI:NaTf at various compositions

than the corresponding NaTf samples. The $\nu_s(SO_3)$ absorption band shifts to higher wavenumbers as the concentration of salt is increased. The NaTf sample, however, does not show any change or shift in wavenumber. The LPMEI-LiTf sample also shows a broad absorption from roughly 1315 cm^{-1} to 1240 cm^{-1} and at high salt concentrations (5:1 N:Li) this broad absorption separates into at least two different absorption bands.

This trend is not seen in the NaTf sample. The two distinct bands are present at all salt concentrations studied.

DSC analysis of LPMEI and LPMEI-salt systems was carried out and indicated that the polymer was completely amorphous at room temperature. The pure polymer has a Tg of -91°C. **Figure III-13** is a representative DSC thermograph for pure LPMEI. Tg

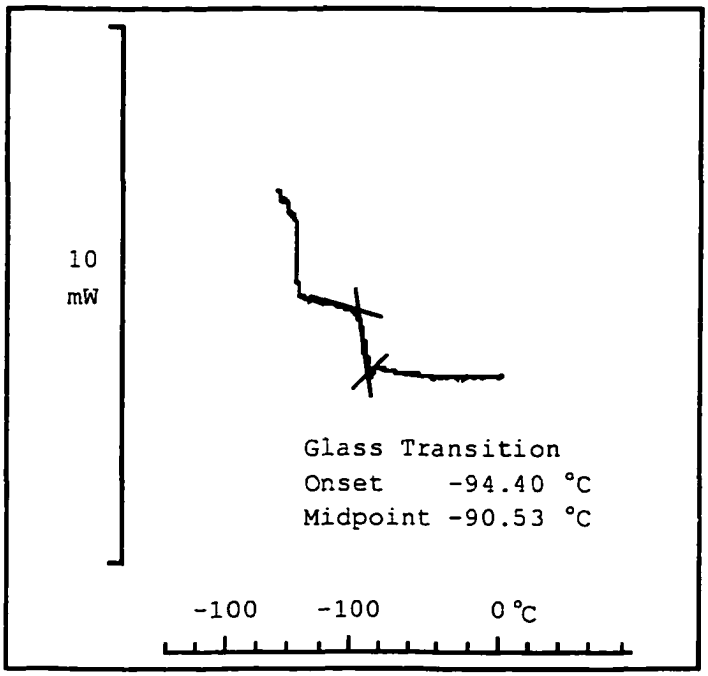

Figure III-13 DSC Thermogram for LPMEI

increases as the concentration of salt is increased. However, the extent Tg increases is different for the two salts. The Tg of the NaTf samples only increases three degrees from -91 to -88 °C from pure LPMEI to 10:1 N:Na. **Table III-3** contains the glass transition and melting temperatures for LPMEI, LPMEI-Li or NaTf samples.

Table III-3 Glass Transition and Melting Temperatures of LPEI and LPEI Salt Systems

Composition	Tg	Composition	Tg	Tm
N:Li	°C	N:Na	°C	°C
LPMEI	-91		-91	
20:1	-63	20:1	-90	119
15:1	-53	15:1	-89	119
10:1	-48	10:1	-88	128, 133
5:1		5:1		125, 141

The LPMEI-NaTf samples also exhibit melting endotherms (Tm). We suggest that these melting transitions are due to crystalline regions within the polymer electrolyte. The crystallinity of the LPMEI-NaTf samples was also verified by X-ray diffraction data.[69]

The conductivity of LPMEI salt systems is displayed in **Figure III-14.** The LPMEI-LiTf samples show a decrease in conductivity as the concentration of salt increased. The 20:1 N:Li sample, which contained the highest relative concentration of "free" ion, has the highest conductivity for all LPMEI samples at the temperatures studied. On comparing the LPEI to LPMEI, one also notices that LPMEI:LiTf (20:1) has a higher conductivity at 30 °C (1 X 10^{-5} S cm^{-1}) than at the same salt concentration for LPEI-LiTf (5 X 10^{-9} S cm^{-1}). This can be explained by hydrogen bonding interactions, since LPEI still contains extensive hydrogen bonding interactions at the low salt concentrations. At high salt concentration (5:1 N:Li) however, the hydrogen bonding interactions in LPEI are disrupted and the conductivity is higher at 30 °C (2 X 10^{-7} S cm^{-}

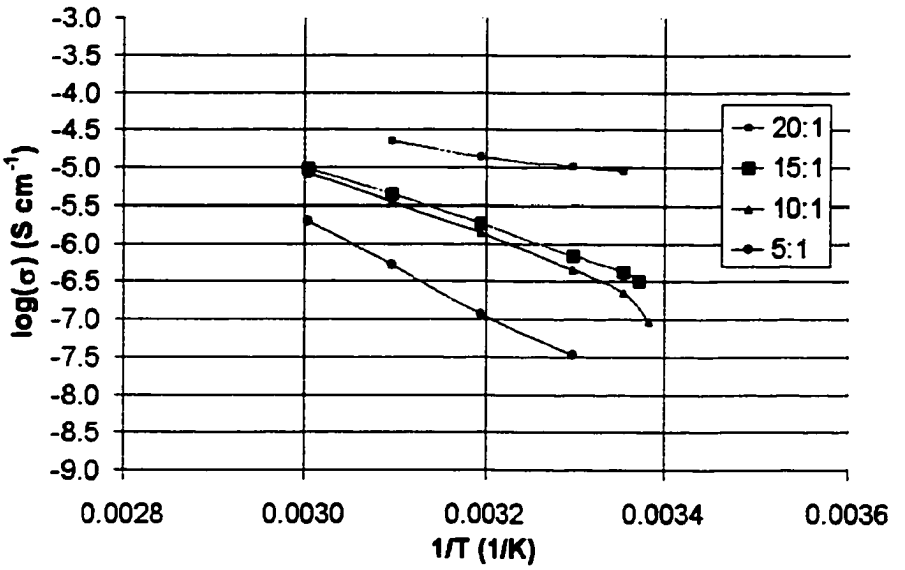

Figure III-14 Temperature Dependent Conductivity of LPEI:LiTf at various compositions

^{1}) than that of the same concentration LPMEI-LiTf sample (3 X 10^{-8} S cm^{-1}). The conductivity of the LPMEI:NaTf salt systems were low and difficult to acquire.

Conclusion and Future Directions:

The use of LPMEI as a polymer electrolyte host has potential, however the physical properties of LPMEI and LPMEI salt complexes are poor since they are viscous liquids rather than free standing films. LPMEI used as a polymer electrolyte host provided further information on hydrogen bonding interactions and their role in establishing crystallinity. Removal of hydrogen bonding allows the polymer electrolyte host to behave similarly to PEO, i.e. $\delta_s(CF_3)$ will be 751cm^{-1} instead of being shifted to higher wavenumber. It should be stated that conductivity is not solely due to "free" ions. If "free" ion were the only contributors to ionic conductivity, then LPMEI-salt systems

should have higher conductivities than the corresponding PEO-salt systems which is not true. LPMEI complements both LPEI and PEO by providing a similar system with minimal changes.

The difference between LPMEI and LPEI is that extensive hydrogen bonding in LPEI is removed in LPMEI. A microscopic spectroscopic study of LPMEI and LPMEI-triflate salt systems revealed triflate salts dissolved in LPMEI show similar spectroscopic trends to LPEI-triflate salt systems, i.e. going from "free" to more ion pair and aggregates as salt concentration is increased. The major difference in LPMEI-salts systems and LPEI-salt systems is that LPMEI vibrational modes are not drastically affected by changes in salt concentrations, whereas LPEI vibrational modes are affected by changes in salt concentration by disruption of the hydrogen bonding interactions. The LPMEI mode assignments were made using computational and experimental results for the model compound *N, N, N', N'*-tetramethylethylene diamine (TMEDA).[71] These assignments provide a further understanding of how LPMEI interacts with dissolved salts by indicating how each mode changes as the concentration of salt is changed.

In the future, work on LPMEI will be carried out in two areas: extension to work on BPEI /BPMEI and synthetic modification of LPMEI. Branched poly(*N*-methylethylenime) (BPMEI) has been synthesized (Appendix, **Figure A-12**) using the Eschweiler-Clarke synthesis and has not been investigated as a possible polymer electrolyte host. Synthetic modification of LPMEI using a variety of dihalides can provide a crosslinked elastomeric network polymer. Crosslinking LPMEI has a variety

of potential uses. Crosslinked LPMEI may be used as a battery polymer electrolyte layer. A common problem with polymer electrolytes is that the systems have poor physical properties. However, crosslinked LPMEI is a relatively robust elastomeric system which has better mechanical properties than the other systems. Initial cross-linking experiments indicated that LPMEI can be crosslinked easily, however, concentration of both LPMEI and the dihalide, in methanol, must be appropriate for the cross-linking to occur. A complete understanding of the cross-linking process and cross-linked systems was not investigated and is beyond the scope of this dissertation. Once again, it can't be stressed enough that any commercialization of LPMEI as a polymer electrolyte host will be with BPEI as a starting material until an economical synthesis is developed for LPMEI.

Experimental:

All common reagents and solvents were commercially available and used as received unless otherwise noted. All ^{1}H and $^{13}CNMR$ were obtained using a Varian 300 or 400 MHz spectrometer. All deuterated solvents were used as is and referenced to residual solvent protons.

Synthesis of LPMEI:

Method One: A 1 L round bottom flask was charged with LPEI, 5.274 g (0.122 5 moles) and 50 mL distilled water. The water was heated until the LPEI dissolved. To this heated solution 200 mL of formic acid (88% solution) and 125 mL of formalin (37 % solution) were added. The solution was heated to reflux solvent for 24 hours. The

solution was allowed to cool to room temperature and 150 mL of concentrated HCl was added. The solvent, both acids, and formaldehyde were removed under reduced pressure to yield the corresponding LPMEI ammonium chloride salt. The LPMEI ammonium chloride salt was dissolved in a minimal amount of distilled water which was neutralized by passing through an ion-exchange resin (Amberlite IRA(Cl), -OH exchanged resin, >100 meq. excess). Solvent was removed under reduced pressure using a rotorary evaporator. The sample was dissolved in benzene and any excess water was removed by azeotropic distillation. The resulting LPMEI solution was cooled to room temperature and centrifuged to collect any remaining salts and filtered. The benzene was removed under reduced pressure and the resulting polymer was dried under reduced pressure. The anhydrous LPMEI was soluble in methanol, benzene, and other common organic solvents. This procedure gave a 95% yield. ^{1}H-NMR (Benzene-d_6) δ(ppm) 2.6 (4H) and 2.2 (3H); ^{13}C-NMR (Benzene-d_6) δ(ppm) 56.4, 43.2.

Method Two: A 100 mL round bottom flask was charged with PEOz, 3.900 g (0.03937 moles), 15 mL formic acid (80% solution), and 30 mL formalin (37% solution). The mixture was heated to reflux solvent for six days. The mixture was cooled to room temperature and 50 mL concentrated HCl was added to the solution. The solvent was removed under reduced pressure. Proton NMR spectroscopy of the resulting LPMEI tertiary ammonium chloride salt crude mixture showed that the reaction had failed, see Appendix, **Figure A-9**.

Method Three: A 250 mL round bottom flask was charged with LPEI, 2.006 g

(0.04657 moles) and 41 mL of formic acid (80% solution). The LPEI was allowed to dissolve in the formic acid solution. Diethoxymethane, 5.296 g (0.05085 moles), was added to the reaction solution and the sample was heated to reflux solvent for 24 hours. Concentrated HCl, 10 mL, was added to the cooled solution and the solvent was removed under reduced pressure. The remaining LPMEI ammonium chloride salt was dissolved in a minimal amount of distilled water and the solution was slowly passed through an ion-exchange resin (Amberlite IRA(Cl), -OH exchanged resin, > 100 meq. excess). The solvent was removed under reduced pressure using a rotorary evaporator. The anhydrous LPMEI was soluble in methanol, benzene, and other common organic solvents. This procedure gave a 97% yield. ^{1}H-NMR (Benzene-d_6) δ(ppm) 2.6 (4H) and 2.2 (3H).

Synthesis of BPMEI:

A 250 mL round bottom flask was charged with BPEI, 1.782 g (0.04138 moles) and 10 mL distilled water. To this solution 30 mL of formic acid (88% solution) and 30 mL of formalin (37 % solution) were added. The solution was heated to reflux solvent for 48 hours. The solution was allowed to cool to room temperature and 20 mL of concentrated HCl was added. The solvent was removed under reduced pressure to yield the corresponding BPMEI ammonium chloride salt. The BPMEI ammonium chloride salt was dissolved in a minimal amount of distilled water and run through an ion-exchange resin (Amberlite IRA(Cl), -OH exchanged resin, > 10 fold excess meq.). The solvent was removed under reduced pressure. The anhydrous BPMEI was soluble in methanol, benzene, and other common organic solvents. This procedure gave a 88%

yield. ^{1}H-NMR (CD_3OD) δ(ppm) 2.55-2.41(b), 2.40-2.36 (b), 2.36-2.28 (b), and 2.18-2.10 (b).

Preparation of Polymer Electrolytes:

To prepare the LPMEI-LiTf solutions of a desired composition, the appropriate amount of LiTf was added to 0.175 g of LPMEI. All of the LPMEI, LPMEI:LiTf, and LPMEI:NaTf samples were dissolved in dry acetonitrile to prepare homogeneous solutions. The composition of the samples are reported as a nitrogen to cation ratio. LPMEI:LiTf samples were prepared at 5:1, 10:1, 15:1, and 20:1 compositions, and 5:1, 10:1, 15:1, and 20:1 compositions were used for LPMEI:NaTf.

FTIR Spectroscopy:

Samples were prepared by casting thin films onto ZnSe windows and drying under a dry air purge for ~ 12 hours. The thin films were translucent with a faint tint of golden brown coloration. All FTIR data was collected on a Bruker IFS66V FT-IR spectrometer with a KBr beam splitter over a range of 4000-600 cm^{-1}. All spectra were collected with the samples under reduced pressure (8 mbar) and at a 1 cm^{-1} spectral resolution. Commercially available software (Thermo Galactic, Grams/AI 7.00) was used for spectral analysis. The spectral bands were fitted using a mixed Gaussian-Lorenzian product function and a straight baseline.

Differential Scanning Calorimetry:

Sample solutions were cast onto Teflon, dried in a nitrogen environment for 24 hours, and placed under reduced pressure for 24 hours. After the samples were dried, a

10-15 mg sample was sealed in a 40 μL aluminum pan. Thermal data were collected using a Mettler DSC 820 calorimeter with commercially available software from Mettler Toledo (Stare v.6.10) under a dry nitrogen purge. All of the samples were heated to 60°C for thirty minutes followed by two cooling and heating cycles between -100°C and ~140°C (5°C/min). After a pin hole was punched in the pan's lid, the samples were cycled twice between 25°C and 150°C (5°C/min) to insure that the samples were dry.

Complex Impedance:

Sample films were made by casting onto Teflon, dried in a nitrogen environment for 24 hours, and placed under reduced pressure for 24 hours. The film thickness was measured using a micrometer built into the conductivity cell. Conductivity measurements were made over the frequency range 0.005 to 10,000 kHz using a Hewlett-Packard 4192A LF impedance analyzer (National Instruments, LabviewTM 5.1). The conductivity data for all of the LPMEI:LiTf and LPMEI:NaTf compositions were collected at temperatures ranging from 25°C to 60°C in 10°C increments. All of the impedance plots were curve-fitted using commercially available software (Solartron Instruments LTD, LEVM 7.1v).

CHAPTER IV

PEI/PEO HYBRIDS,

LINEAR POLY(OLIGO-(ETHYLENE OXIDE)ETHYLENIMINES)

Introduction:

It has been shown in the last two chapters that PEI based polymer electrolytes are viable, however, they do not have "high" (>10^{-4} S/cm) conductivities at room temperature. The highest generally accepted room temperature conductivity for a solid, single phase polymer electrolyte system was reported by Allcock[79] in 1998 and was based on poly(bis-methoxyethoxyethoxyphosphazene), MEEP, which contains oligo(ethylene oxide) side chains pendant to the phosphorus-nitrogen backbone. MEEP:lithium triflate (LiTf) has a room temperature conductivity of 2.7 X 10^{-5} S/cm (O:Li at 24:1). Allcock used poly(phosphazenes) as a foundation for studies of tethered side groups that will solvate metal cations. **Figure IV-1** shows a few of Allcock's poly(phosphine)

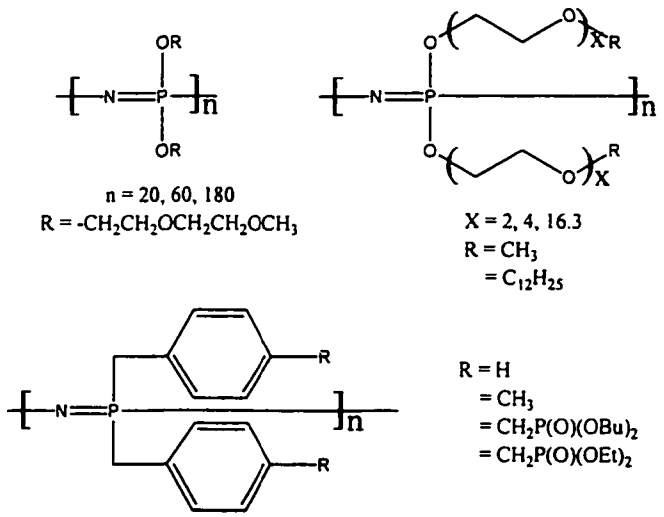

Figure IV-1 Poly(phosphazene) Derivatives

derivatives.[80-82] An interesting trend can be seen in Allcock's work; many derivatives contain oligo(ethylene oxide) side chains. The main systems of interest for our research are those side chains that contain linear oligo(ethylene oxide) units. These tethered linear oligo(ethylene oxide) side chains mimic PEO.

PEO is difficult to modify. Synthetic modification of PEO to add a tethered oligo(ethylene oxide) side chains provides an interesting challenge. John Kerr[83] has developed a novel synthesis of such a system, but in general, PEO systems are difficult to modify. In contrast, LPEI can be modified in straight forward ways. Reductive alkylations of amines are common in the organic chemistry literature. The most common source of alkylating agents are aldehydes. However, specific aldehydes to add oligo(ethylene oxide) tethered side chains are not as readily available as one would hope. A good source of alkylating agents would be carboxylic acids. However, there are not many methods that use carboxylic acids as alkylating agents. Nonetheless, Gribble[84,85] showed that amines can be alkylated using $NaBH_4$ and carboxylic acids under specific conditions. The application of Gribble's method to PEI has been carried out.

Results and Discussion:

LPEI (or BPEI) has been modified to incorporate tethered ethoxy side chains using 2-oligo(ethylene oxide) acetic acids. The resulting polymers have been characterized using both ^1H and ^{13}C NMR spectroscopy. The functionality that was added is shown in **Figure IV-2.** The synthesis is fairly straightforward. The corresponding acid (RCH_2CO_2H, where R is the oligo(ethylene oxide) chain of a given

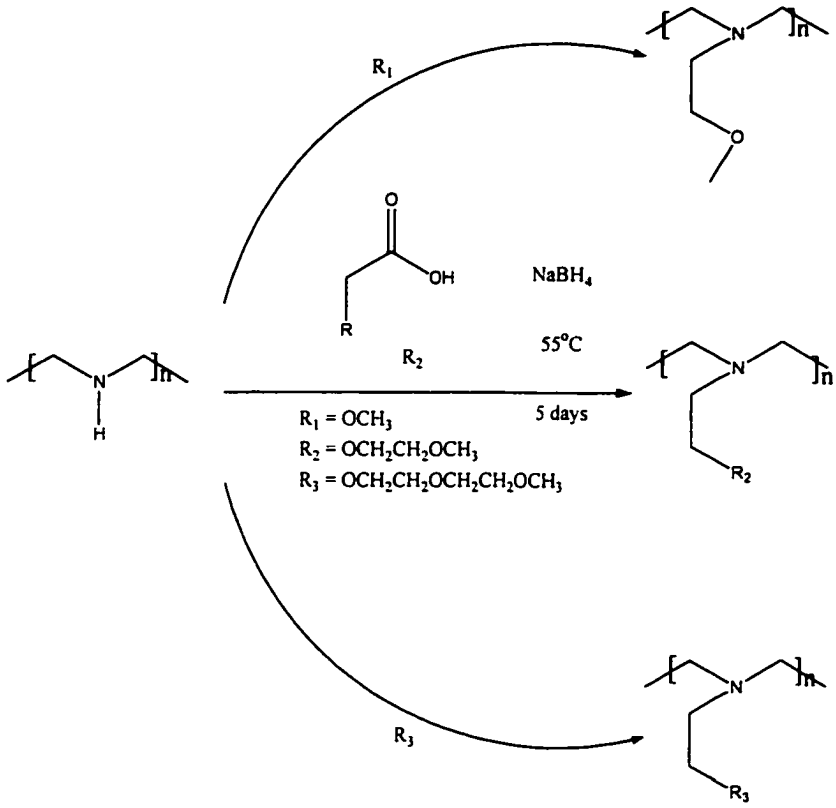

Figure IV-2 Synthetic Routes for LPEI-GX Polymer Series

length) is used as both reactant and solvent. LPEI is dissolved in the acid and the polymer solution is cooled and $NaBH_4$ is added. $NaBH_4$ must be added in the form of chunks rather than powder to prevent the solution from overheating. The reaction was run for five days. There are three steps in the reaction that are critical. First, the reaction time is critical. The yields suffered drastically if the reaction was not allowed to go the full five days when using LPEI as a starting reagent. Second, the extraction of the polymer was done with CH_2Cl_2, and if the aqueous layer was not extremely basic (pH well above 10) the extraction was poor. Thirdly, the separation of the two layers in the extraction process was difficult. The emulsion that formed took an extremely long time

to separate. Therefore, all three samples (LPEI-G1,LPEI-G2,and LPEI-G3) were centrifuged to separate the two layers. The timed saved was tremendous. The yields for the three reactions were all high, e.g. LPEI-G2 was >90%. All three polymer systems were made and were given the abbreviations of LPEI-G1, LPEI-G2, and LPEI-G3. The acronyms given were based on the two components of the polymers systems. The backbone of the polymer systems are similar to LPEI (CH_2NCH_2) and the tethered side chains are similar to glymes (G1, $CH_3OCH_2CH_2OCH_3$). The ^1H NMR spectrum for LPEI-G1 is shown in **Figure IV-3.** The spectrum of LPEI-G1 clearly shows the corresponding peaks that one would expect. **Figure IV-4** is an expansion of **Figure IV-3** and the splitting patterns of the tethered ethylene unit can clearly be seen (two triplets). The other two peaks are the polymer CH_2 backbone hydrogen, which should be a singlet at ~ 2.75 ppm, and the OCH_3, which should be a singlet at ~3.25 ppm. The ^{13}C NMR spectrum also confirmed that the synthesis was successful. **Figure IV-5** shows the full

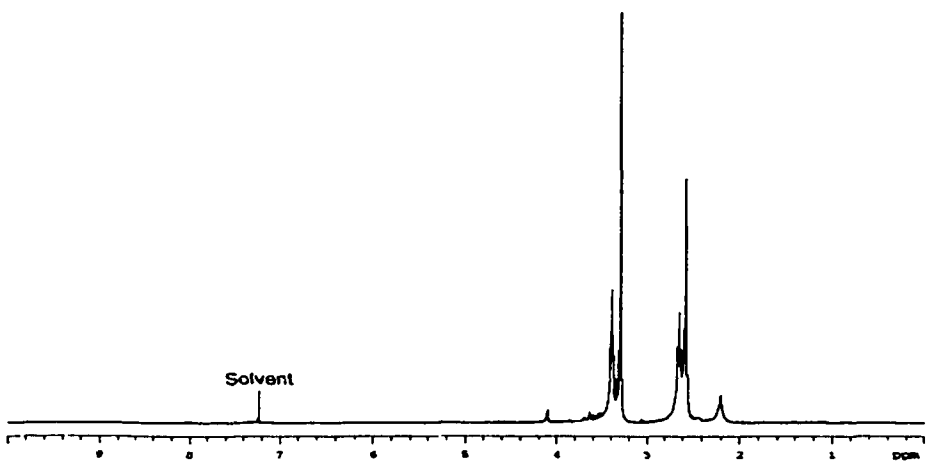

Figure IV-3 ^1H NMR Spectrum of LPEI-G1

^{13}C NMR spectrum of LPEI-G1.

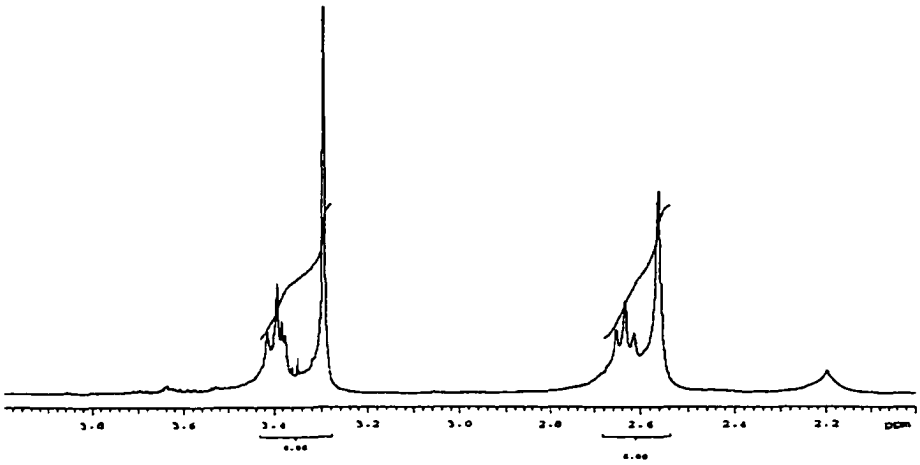

Figure IV-4 Expansion of ^{1}H NMR Spectrum of LPEI-G1

A key piece of information from the ^{13}C NMR spectrum is the lack of a peak at or above 150 ppm. Carbonyl carbon ^{13}C NMR peaks are above 150 ppm and the lack of one for LPEI-G1 supports the fact that amide and acid functionalities were not present. A second point to mention is that the ^{13}C NMR data reveals that the polymer is fairly

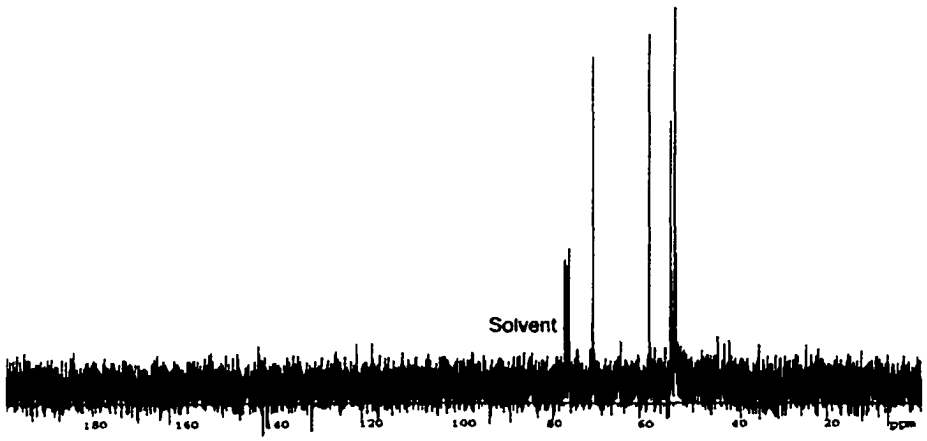

Figure IV-5 ^{13}C NMR Spectrum of LPEI-G1

clean. Only four peaks can be seen in the ^{13}C NMR spectrum of LPEI-G1, see **Figure IV-6**. The only two complications with the LPEI-G1 synthesis are: 1) the polymer (LPEI) is not highly soluble in methoxyacetic acid, and 2) the resulting polymer product (LPEI-G1) is brown-amber in color and may not be a good candidate for Raman spectroscopy.

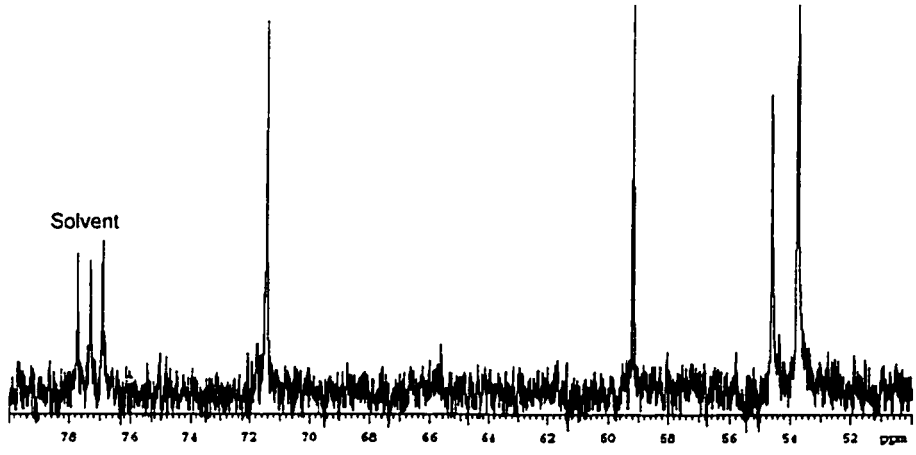

Figure IV-6 Expansion of ^{13}C NMR Spectrum of LPEI-G1

The reaction of the remaining two acids, 2-(methoxyethoxy)acetic acid and 2-(2-(methoxyethoxy)ethoxyacetic acid, with LPEI were more difficult. The solubility of LPEI in both acids decreases as the length of the ethylene oxide side chain is incresed. Gribble, however, did mention a modification to his method. The use of a co-solvent, specifically THF, can increase the solubility of the corresponding amine in the acid. LPEI is not soluble in THF, however, THF was used to reduce the viscosity of the solution. The addition of THF to the mixture did not cause LPEI to precipitate out of solution. The use of a co-solvent did help provide the corresponding new polymer from

the respective acid. LPEI-G2 was chosen as the first candidate to be studied as a polymer electrolyte host.

The synthesis of LPEI-G2 has been reported in the literature.[70] Characterization of LPEI-G2 by ^{1}H and ^{13}C NMR spectroscopy was performed. **Figure IV-7** and **IV-8**

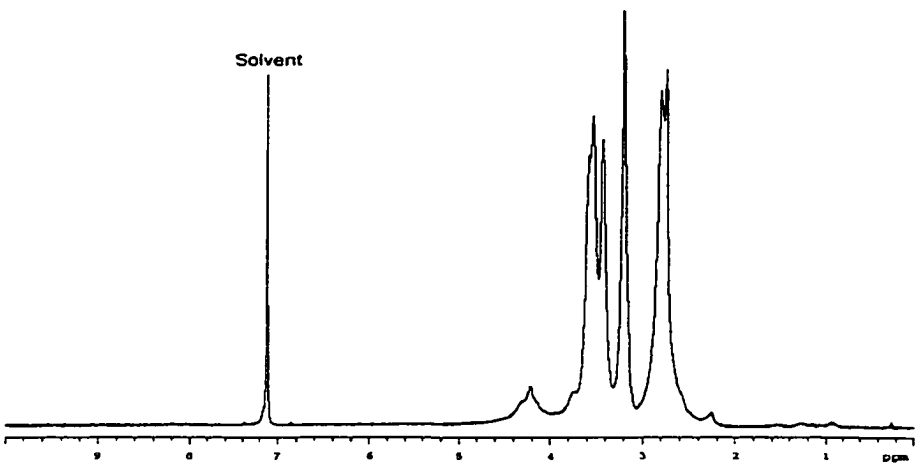

Figure IV-7 ^{1}H NMR Spectrum of LPEI-G2

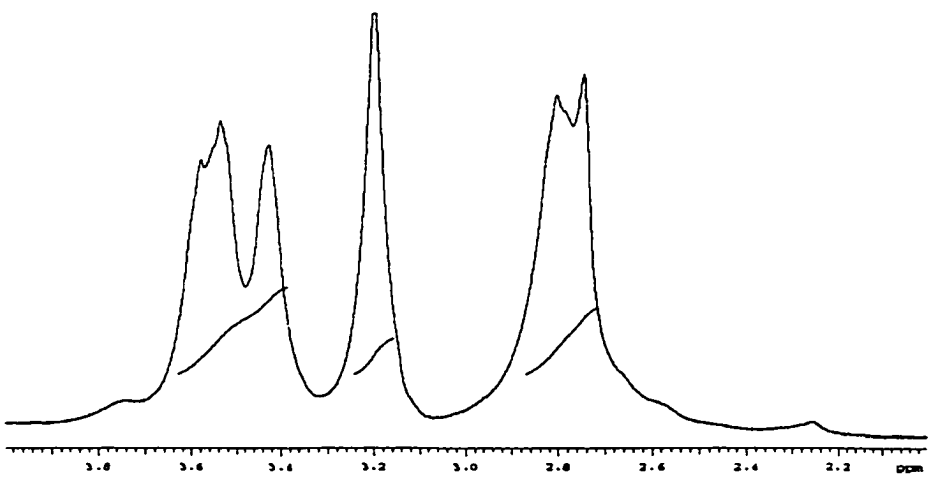

Figure IV-8 Expansion of ^{1}H NMR Spectrum of LPEI-G2

show proton NMR spectrum of LPEI-G2. **Figure IV-7** clearly shows no other peaks are

appearing in the spectral window that was surveyed. **Figure IV-8** is an expansion of **Figure IV-7** in the range from 2-4 ppm. **Figure IV-8** shows exactly what one would expect for the respective polymer. The polymer back bone CH_2 protons and the CH_2 protons of the tethered side adjacent to the N are both at 2.70 and 2.85 ppm, respectively. The OCH_2 and OCH_3 absorptions are all seen downfield from 3 ppm which is consistent with small molecule ether units.

The ^1H NMR peaks of LPEI-G2 were assigned with the help of a model compound. (*N*-3,6-Dioxaheptyl)diethylamine (DEA-G2), see **Figure IV-9**, was synthesized in our lab using Gribble's method. The ^1H NMR spectrum of DEA-G2 clearly showed the correct splitting patterns for this model compound. **Figure IV-10** shows the assignments of each hydrogen and carbon environments for both LPEI-G2 and

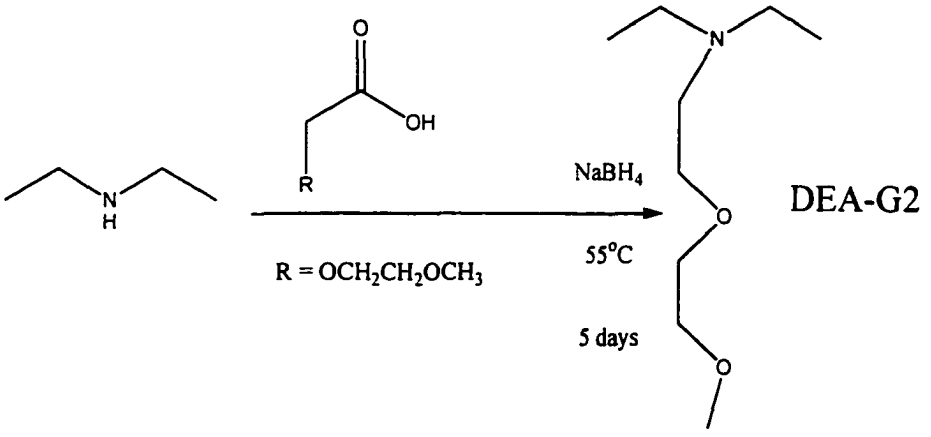

Figure IV-9 Synthesis of DEA-G2

DEA-G2. **Figure IV-11** and **IV-12** show the ^1H NMR spectra of DEA-G2. The assignment of the peaks for DEA-G2 are as followed: protons A are at 0.9 ppm, protons

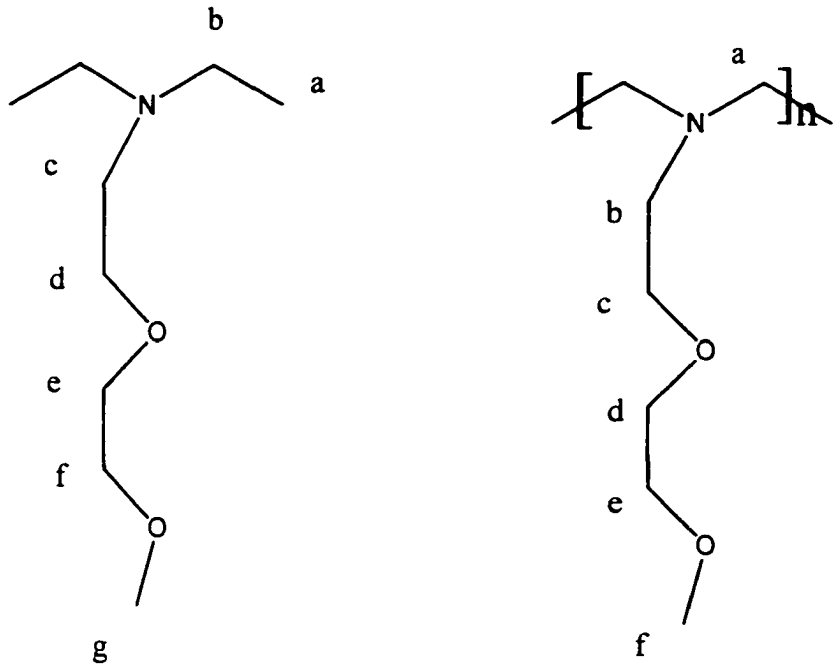

DEA-G2 LPEI-G2

Figure IV-10 Hydrogen and Carbon Environment Assignments

B are at 2.4, protons C are at 2.6,protons F are at 3.3, protons G are at 3.1, and protons D and E overlap from 3.5-3.4. Protons F was assigned to the multiplet at 3.3 ppm since the gCOSY, see **Figure IV-13**, spectrum clearly shows coupling of protons F to a second set of protons that are grouped in the region from 3.5-3.4 ppm. D and E protons are in very similar environments so incidental overlap is not unusual. However, proton F is next to an oxygen that is attached to a methyl group instead of a methylene group, and this small difference could easily separate protons F from the other two protons, D and E.

The DEA-G2 peak assignments were used to help in the assignments of the LPEI-

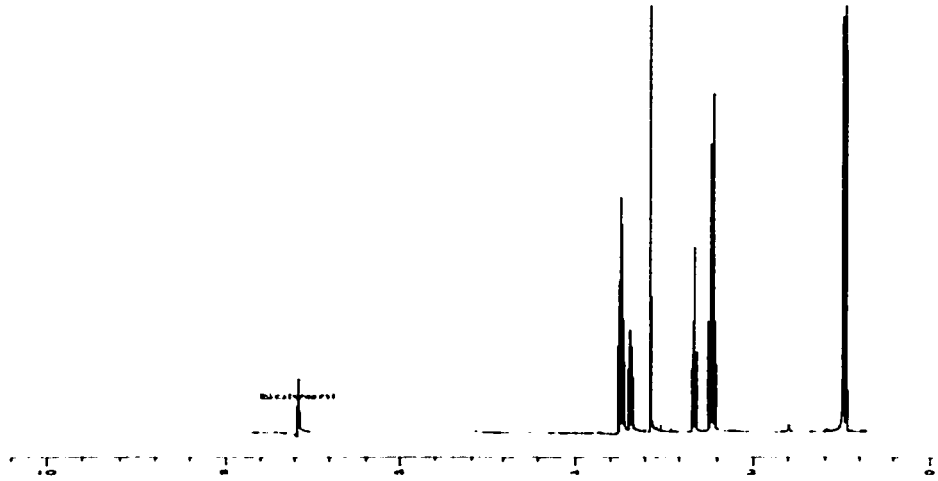

Figure IV-11 ^{1}H NMR Spectrum of DEA-G2

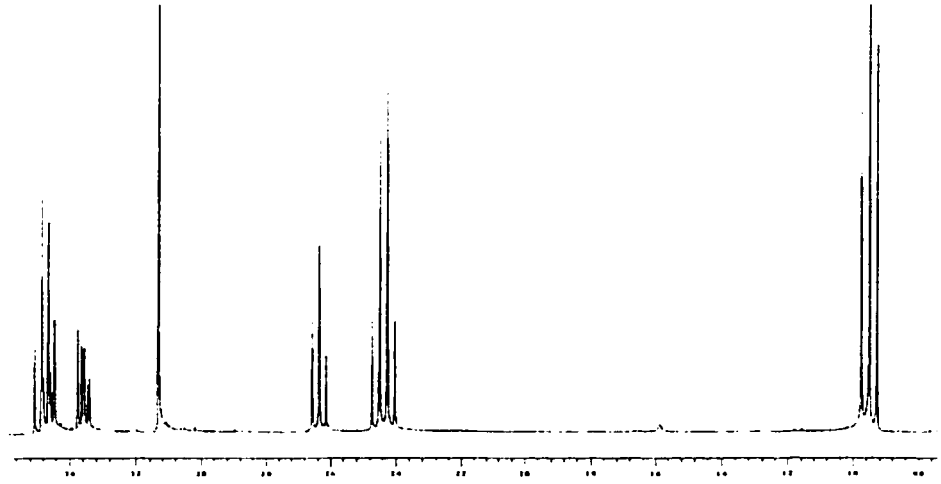

Figure IV-12 Expansion of ^{1}H NMR Spectrum of DEA-G2

G2 polymer peak assignments. The peak assignments are as follows: protons A and B are at 2.9-2.7 ppm, protons E are at 3.45-3.35 ppm, protons F are at 3.25-3.15 ppm, and protons C and D overlap at 3.65-3.50 ppm. The ^{13}C NMR spectrum was also consistent with the structure of the polymer. **Figure IV-14** shows the entire spectral range that was studied for LPEI-G2. An important feature of this NMR spectrum is the absence of a

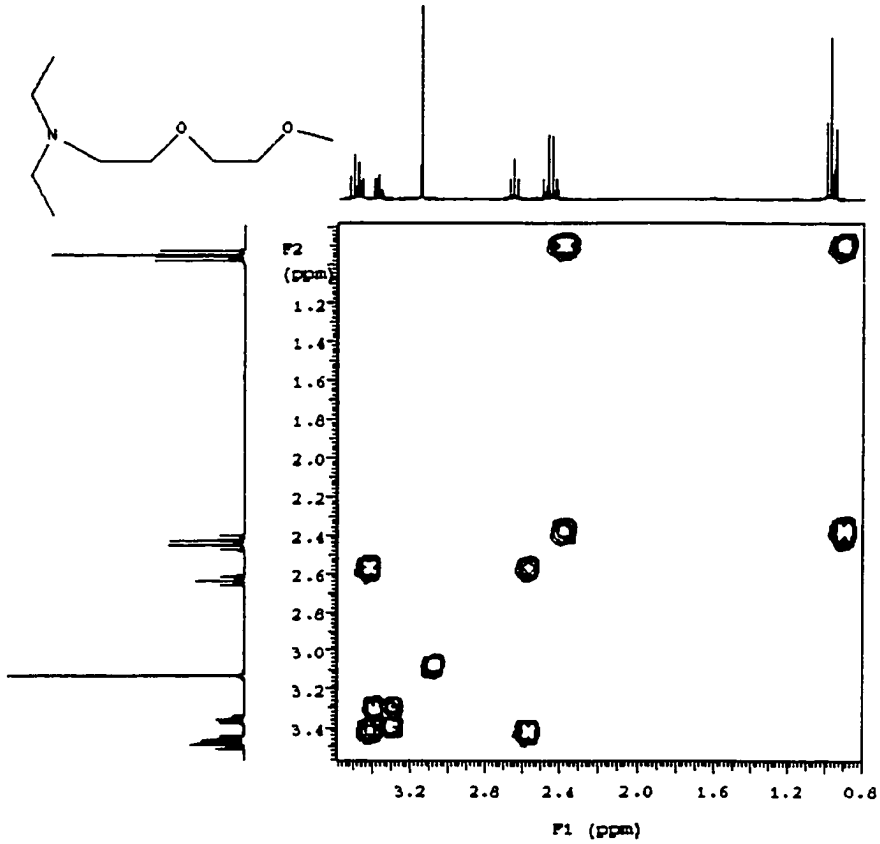

Figure IV-13 gCOSY Spectrum of DEA-G2

carbonyl peak at or above 150 ppm. Carbonyl carbons have ^{13}C NMR peaks above 150 ppm, and the lack of them is consistent with complete substitution. If the substitution was not complete the ^{13}C NMR spectrum would become more complicated. The ^{13}C NMR spectrum would contain more peaks due to the carbons being in different environments. **Figure IV-15** is an expansion of **Figure IV-14.**

LPEI-G2 has six different carbons within the polymeric repeat unit which should result in six peaks in the ^{13}C NMR spectrum. However, the actual ^{13}C NMR spectrum showed only five peaks. The missing peak is explained by incidental overlap of two of

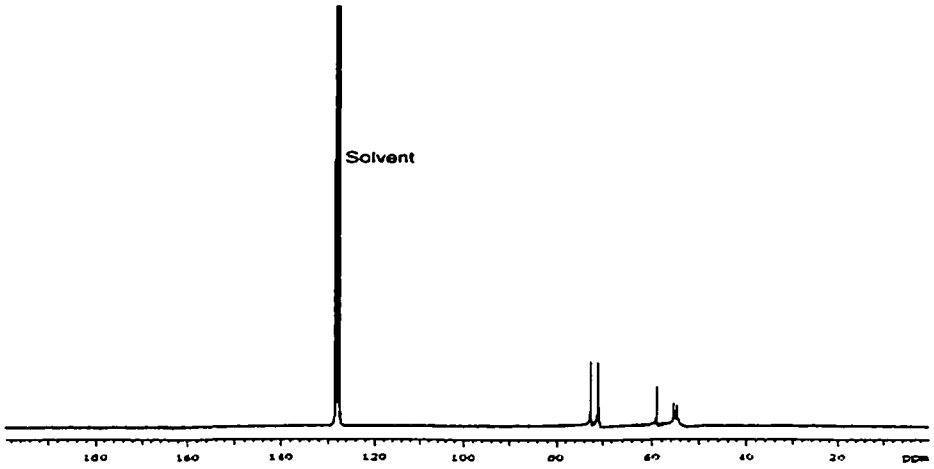

Figure IV-14 ^{13}C NMR Spectrum of LPEI-G2

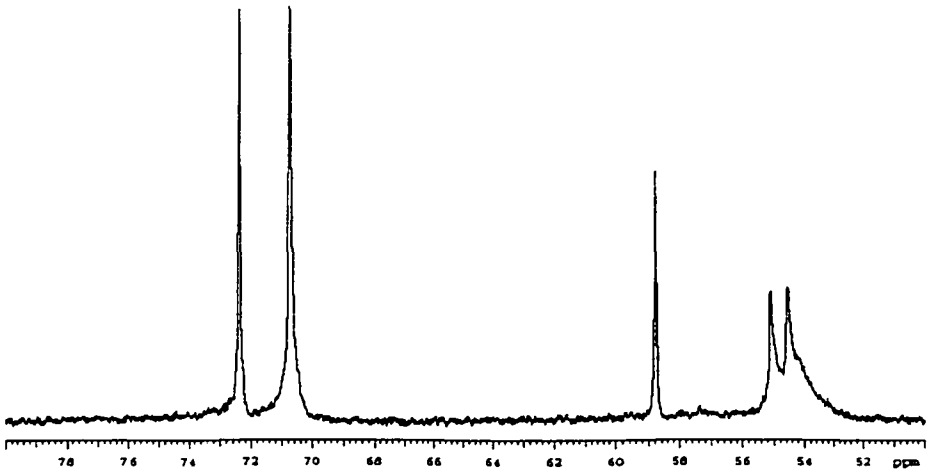

Figure IV-15 Expansion of ^{13}C NMR Spectrum of LPEI-G2

the OCH_2 carbons. This can easily be seen since the line width of one of the peaks is much wider than the other peaks (second peak from the left in **Figure IV-15**). The ^{13}C NMR spectrum peak assignments for LPEI-G2 were made with the help of ^{13}C NMR spectral data of DEA-G2. Both ^{13}C NMR and gHMQC experiments were carried out. **Figure IV-16** and **IV-17** are ^{13}C NMR spectra of DEA-G2. DEA-G2, just like LPEI-G2,

is missing one peak in the ^{13}C NMR spectrum. DEA-G2 should have seven different carbon atoms. However, only six peaks are seen in the ^{13}C NMR spectrum. Expanding the region around ~72 ppm two peaks are overlapped. The ^{13}C NMR spectrum peak assignments for DEA-G2 are as followed: carbon A is at 12.7 ppm, carbon B is at 48 ppm, carbon C is at 53.2 ppm, carbon F is at 58.7 ppm, carbon G is at 72.4 ppm, and carbons D and E are overlapping at 70.75 ppm.

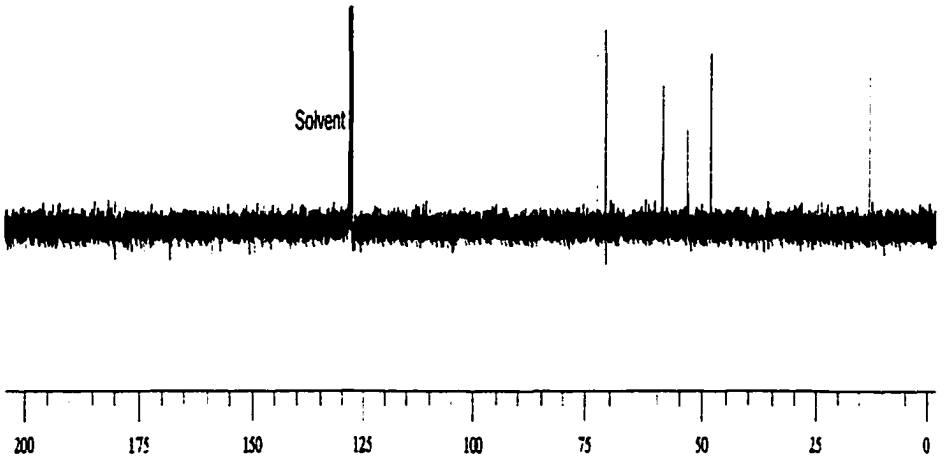

Figure IV-16 ^{13}C NMR Spectrum of DEA-G2

The gHMQC, **Figure IV-18**, also confirmed our initial assignments for the ^{1}H NMR spectrum were correct. The gHMQC clearly shows which carbon atoms goes with which protons. The ^{13}C NMR peak assignments of DEA-G2 were used to help assign the carbon peaks for LPEI-G2. The assignments for LPEI-G2 are as followed: carbon A is at 54.5 ppm, carbon B is at 55.1 ppm, carbon E is at 72.4 ppm, carbon F is at 58.7 ppm, and carbons C and D overlap at 70.8 ppm. It should also be pointed out that carbons A and B are both broad; this is due to the molecular weight of distribution of the polymer.

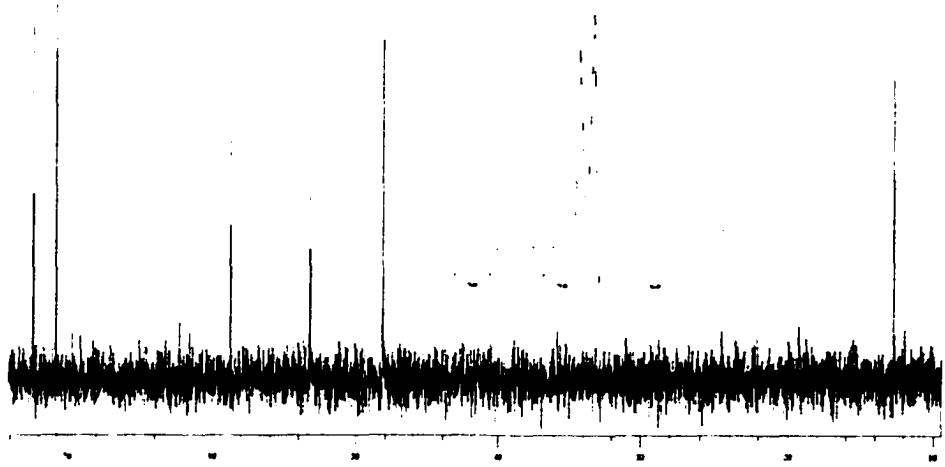

Figure IV-17 Expansion of ^{13}C NMR Spectrum of DEA-G2

The slight change in the electronic environment will change the chemical shift slightly broadening the peak.

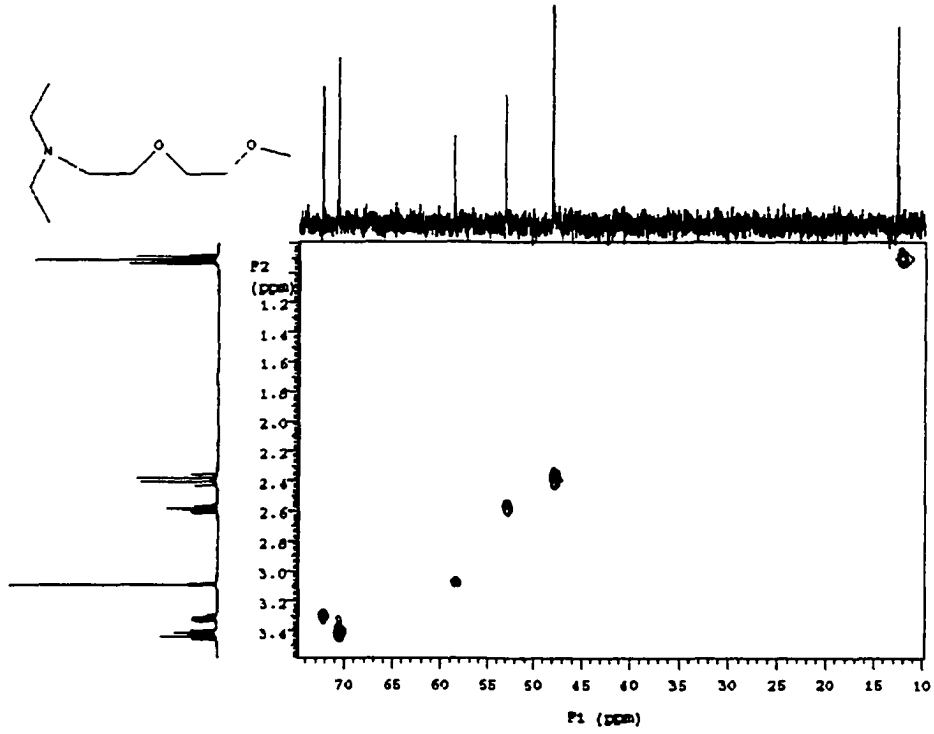

Figure IV-18 gHMQC of DEA-G2

Figure IV-19 shows the IR spectrum of LPEI-G2. The absence of NH stretching absorption bands, see **Figure IV-20,** indicate that the degree of substitution is 100 % or

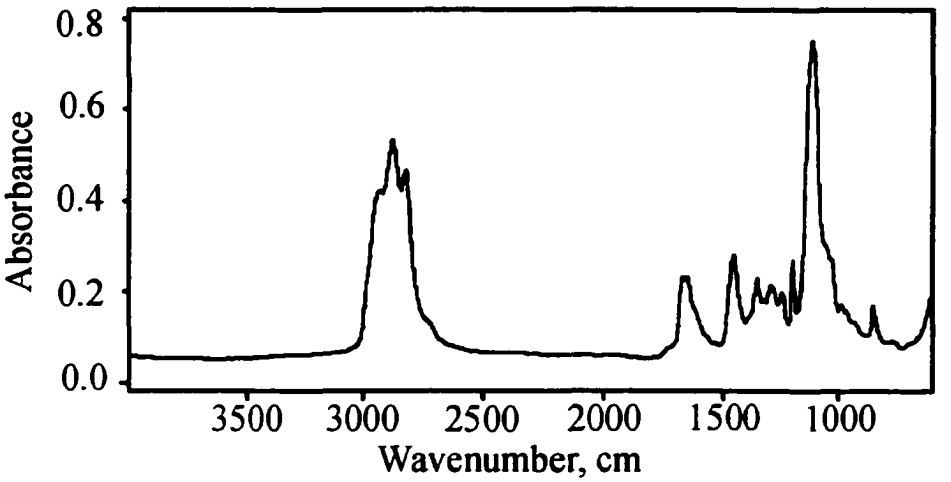

Figure IV-19 IR Spectrum of LPEI-G2 from 4000 to 600 cm^{-1}

within the detection limits of the IR spectrometer. One last point that needs to be made is that one can consider LPEI-G2 a non-MEEP MEEP in that it has oligo(ethylene oxide) side chains tethered to a low Tg polymer backbone. The advantages of the LPEI-G2

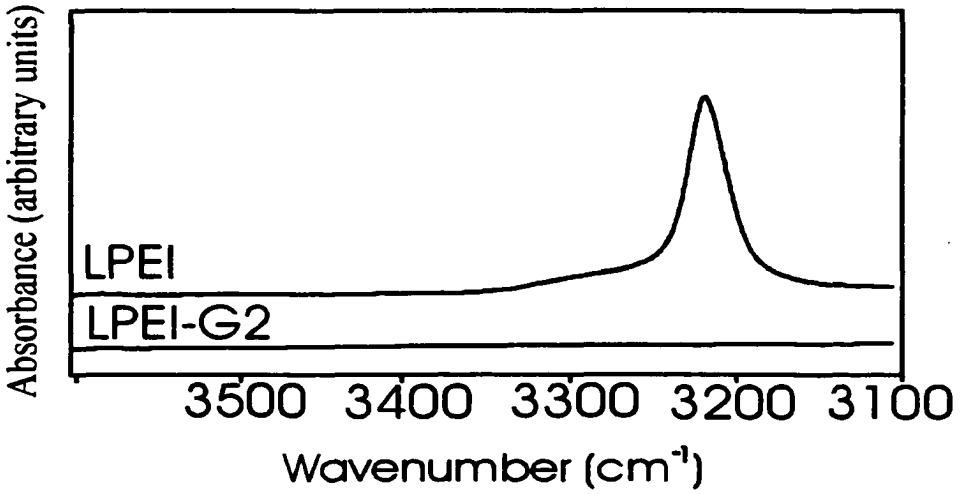

Figure IV-20 IR Spectra of LPEI and LPEI-G2 from 3600 to 3100 cm^{-1}

system are the synthesis is easier than working with phosphazenes and the reaction is not substantially air sensitive.

LPEI-G2 has been investigated as a possible polymer electrolyte host. The polymer electrolyte was formed by dissolving LiTf in LPEI-G2 and was investigated using Fourier transform infrared spectroscopy (FTIR), differential scanning calorimetry (DSC), and room temperature complex impedance measurements. We also investigated DEA-G2, see **Figure IV-21**, as a model compound for LPEI-G2 using the same

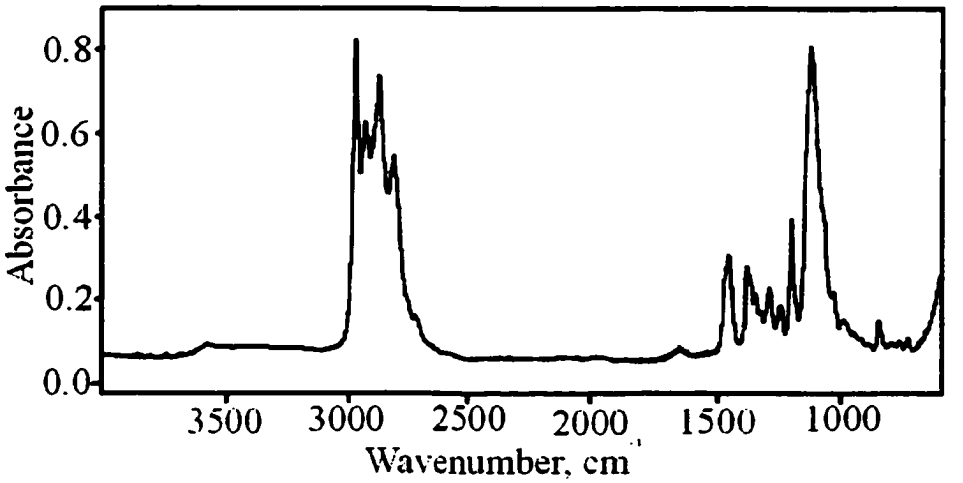

Figure IV-21 IR Spectra of DEA-G2 from 4000 to 600 cm^{-1}

techniques. One point to make is the DEA-G2 does have a small broad absorption in the spectral range of ~3600-3400 cm^{-1} suggesting trace amounts of water or O-H containing molecules may be present. **Figure IV-22** compares the IR spectrum of LPEI-G2 and DEA-G2 from ~1800-600 cm^{-1}. DEA-G2 has an IR spectrum similar to that of LPEI-G2. The only glaring difference is in the absorption band that is centered at ~1650 cm^{-1}. LPEI-G2 has an intense absorption in this area whereas DEA-G2 does not. We originally

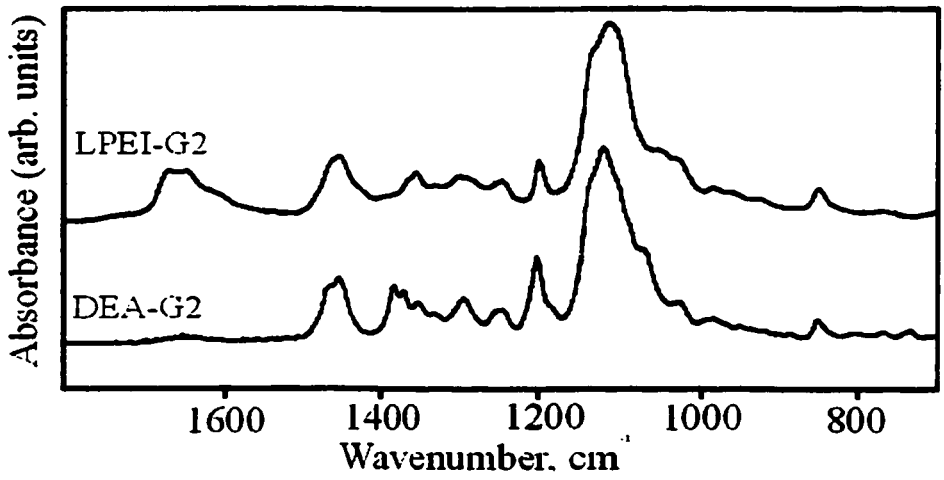

Figure IV-22 Comparison IR Spectra of LPEI-G2 and DEA-G2 from 1800 to 600 cm^{-1}

attributed this to residual C=O, however this has not been verified. An explanation of why the impurity concentration is lower for DEA-G2 centers around the observation that diethyleamine is more soluble in the corresponding acid. The reaction solution was not heated initially and therefore the possibility of amide formation was lowered. A ^{13}C NMR peak for a C=O carbon does not appear in the ^{13}C NMR spectrum (**Figure IV-16**) for DEA-G2 and suggests amide formation did not occur.

Three spectroscopic regions are specifically important. The ranges are ~760-750 cm^{-1}, $\delta_s(CF_3)$; ~1100-1000 cm^{-1}, $\nu_s(SO_3)$; and 1000-800 cm^{-1}. The $\delta_s(CF_3)$ and $\nu_s(SO_3)$ regions are very sensitive to ionic speciation and have multiple bands associated with different ionic species. Three species have been identified in PEO systems. The three ionic species are: "free" ion (or solvent separated ion pair, low speciation), a contact ion pair (more speciation), and an aggregate species ($[Li_2Tf]^+$, high speciation). **Figure IV-23** shows three IR spectra in the $\nu_s(SO_3)$ region for LPEI-G2:LiTf. The three samples

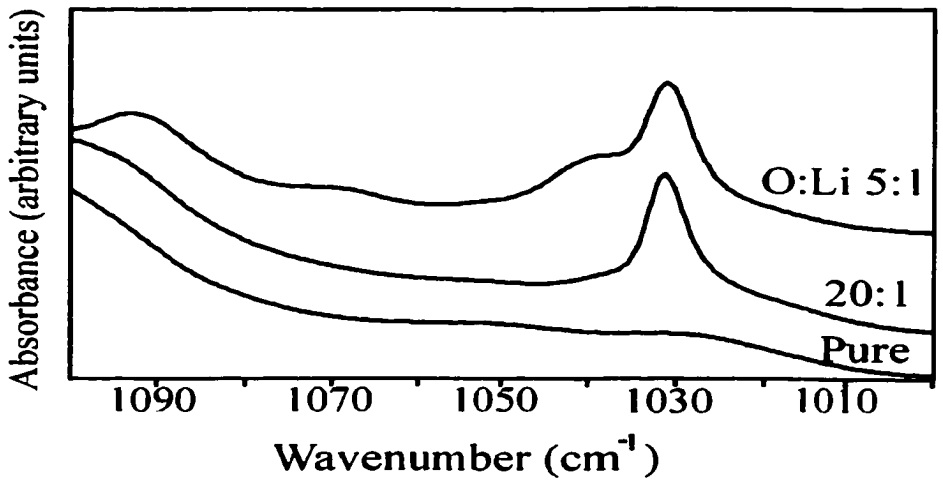

Figure IV-23 IR Spectra of LPEI-G2:LiTf at various compositions

shown are the pure LPEI-G2 polymer, and two LPEI-G2:LiTf salt complexes. The two compositions of the LPEI-G2 salt complexes are 20:1 and 5:1 (O:Li). The polymer does not have any significant polymer absorption bands in this region, and spectral deconvolution using commercial available software is straightforward. Comparing DEA-G2 to LPEI-G2 in this region, see **Figure IV-24** and **IV-25**, at the same salt

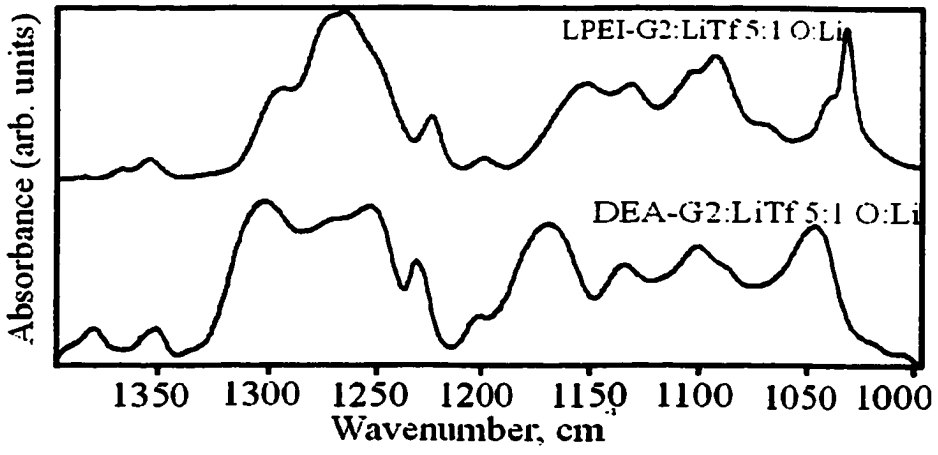

Figure IV-24 Comparison IR Spectra for LPEI-G2:LiTf and DEA-G2:LiTf 5:1 O:Li Samples

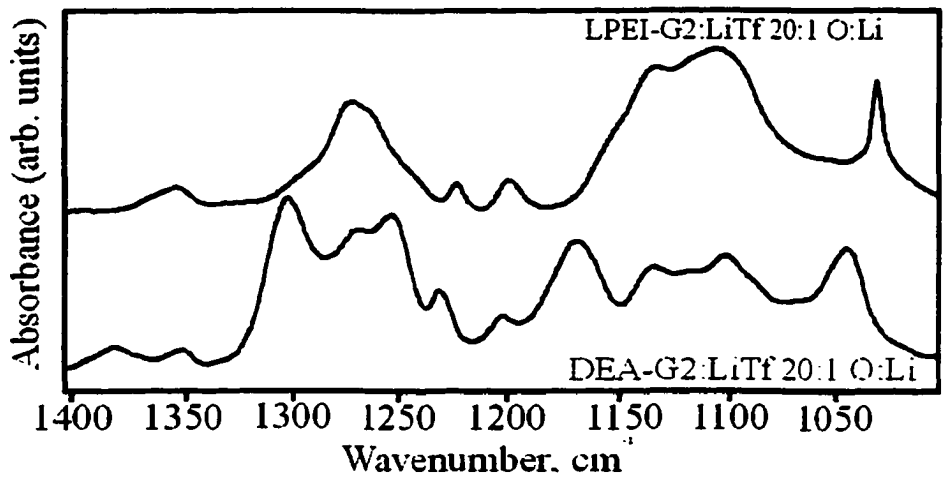

Figure IV-25 Comparison IR Spectra for LPEI-G2:LiTf and DEA-G2:LiTf 20:1 O:Li Samples

concentrations revealed that the LPEI-G2 absorption bands change drastically as salt concentration is increased, whereas the DEA-G2 absorption bands do not. More specifically, the $\nu_s(SO_3)$ absorption band for the LPEI-G2 :LiTf samples shows growth of a shoulder at ~1040 cm^{-1}. The $\nu_s(SO_3)$ absorption band in DEA-G2:LiTf samples does not show any significant change upon addition of more salt. **Table IV-1** reports the relative composition of the integrated band intensities of each of the LPEI-G2:LiTf samples. The percentage will be used as an estimate of the relative concentration of each species. Addition of LiTf decreased the relative amount of "free" ion from 50% to 26%. It should be pointed out that the 26% of "free" ion is a high quantity at a high salt concentration and significant quantities of "free" ion have not been observed in PEO systems at high salt concentrations. PEO systems will start to form crystalline species and high order aggregates, and the relative amount of "free" ion becomes minuscule. This striking trend should also be seen in the other significant spectral region, 765-750

cm^{-1} ($\delta_s(CF_3)$). The $\nu_s(SO_3)$ spectral region for DEA-G2 is complicated by DEA-G2 absorption bands and the integrated band intensities were not obtained for DEA-G2.

Table IV-1 Percent of Triflate Ionic Species in LPEI-G2:LiTf from Curve-fitting of $\nu_s(SO_3)$ Band.

$\nu_s(SO_3)$ cm^{-1}	1031	1038/1039	1052/1054
LPEI-G2:LiTF O:Li	% "free"	% pair	% aggregate
20:1	50	43	7
5:1	26	73	1

Figure IV-26 shows the same three samples (pure LPEI-G2, 20:1, and 5:1 O:Li complexes) in the spectral region of 765-750 cm^{-1}($\delta_s(CF_3)$). The polymer has a very

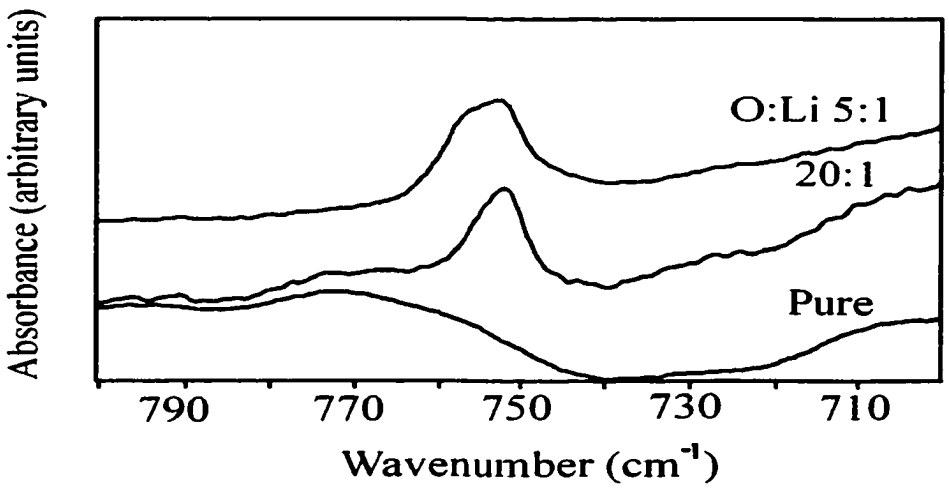

Figure IV-26 IR Spectra for LPEI-G2:LiTf at various compositions

broad absorption in this region which is centered at 770 cm^{-1}. Comparing the LPEI-G2:LiTf samples to the DEA-G2:LiTf samples in this region, **Figure IV-27** and **IV-28**, the broad absorption band has shifted to higher wavenumbers, i. e. from ~770 cm^{-1} for

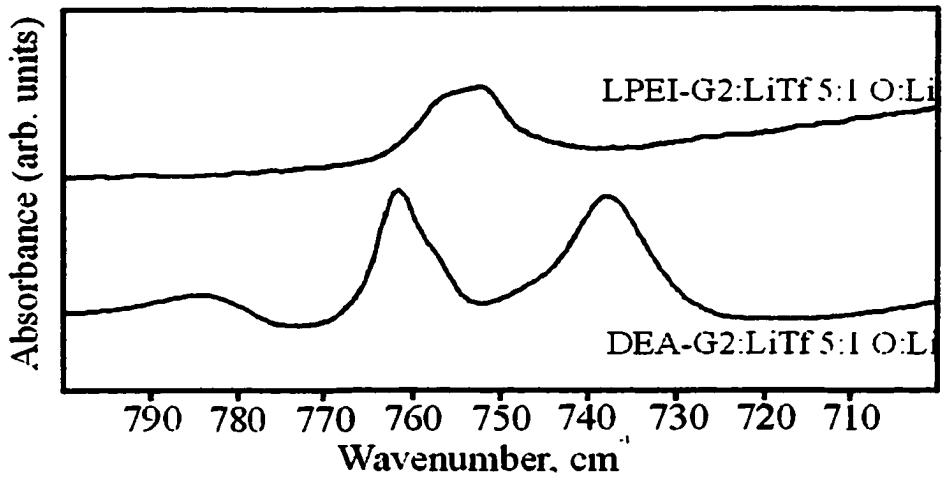

Figure IV-27 Comparison of IR Spectra of LPEI-G2:LiTf and DEA-G2:LiTf 5:1 O:Li Samples

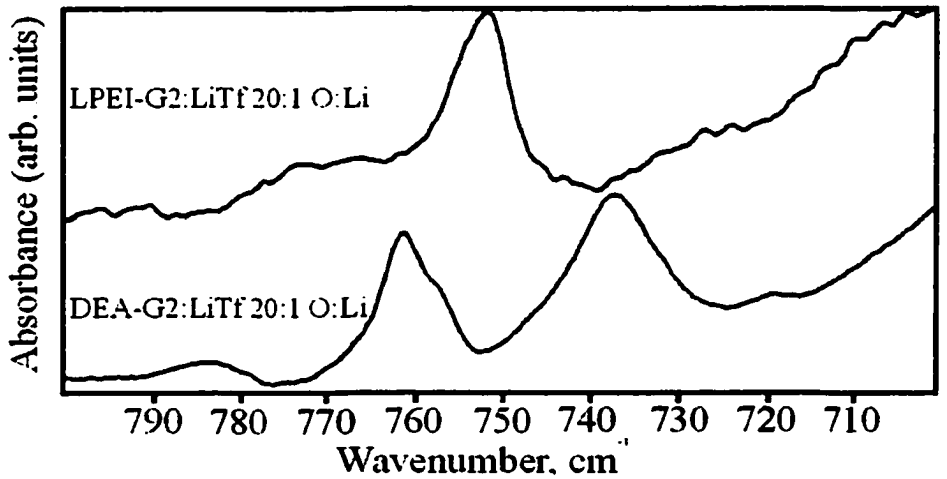

Figure IV-28 Comparison of IR Spectra of LPEI-G2:LiTF and DEA-G2:LiTf 20:1 O:Li Samples

the LPEI-G2 system to 785 cm^{-1} for DEA-G2 systems. This broad absorption in the LPEI-G2:LiTf IR spectra causes a problem in the spectral deconvolution of $\delta_s(CF_3)$. However the "free" ion will be the least affected for these LPEI-G2:LiTf samples. The $\delta_s(CF_3)$ region has different relative intensities for the respective ionic speciation than the

$\nu_s(SO_3)$ region. This is attributed to interference by the broad polymer absorption band. Consequently, deconvolution of the $\delta_s(CF_3)$ region was difficult. **Table IV-2** contains the relative percentages for both LiTf samples, 20:1 and 5:1 in the $\delta_s(CF_3)$ spectral region for both LPEI-G2 and DEA-G2 systems.

Table IV-2 Percent of Triflate Ionic Species in LPEI-G2:LiTf and DEA-G2:LiTf from Curve-fitting of $\delta_s(CF_3)$ Band.

$\delta_s(CF_3)$ cm^{-1}	% "free" (Frequency)	% pair (Frequency)	% aggregate (Frequency)
LPEI-G2:Li 20:1	45 (751)	39 (755)	17 (758)
LPEI-G2:Li 5:1	25 (751)	25 (755)	50 (758)
DEA-G2:Li 20:1	0	33 (757)	67 (761)
DEA-G2:Li 5:1	0	68 (757)	32 (762)

The broad polymer band does change the calculated relative percentages for the pair and aggregates. The 20:1 O:Li sample contains 50 and 45 % "free" ion and the 5:1 O:Li contains 26 and 25 % "free" for **Tables IV-1** and **IV-2**, respectively. The difference is small, 1%. The differences between the $\delta_s(CF_3)$ and the $\nu_s(SO_3)$ in the other two bands, however is more significant. The 20:1 O:Li sample contains 43 and 39 % ion pair and the 5:1 O:Li contains 73 and 25 % ion pair for the $\nu_s(SO_3)$ and $\delta_s(CF_3)$, respectively. The difference in ionic speciation of the $\delta_s(CF_3)$ and the $\nu_s(SO_3)$ for the 20:1 sample is small but for the 5:1 sample has a large difference of 48 %. The difference between the

ionic speciation in the $\delta_s(CF_3)$ and the $\nu_s(SO_3)$ is also see in the aggregate speciation. The 20:1 O:Li sample contains 7 and 17 % ion pair and the 5:1 O:Li sample contains 1 and 50 % ion pair for $\nu_s(SO_3)$ and the $\delta_s(CF_3)$ respectively. The drastic differences are attributed to the broad polymer band that was mentioned earlier. For this reason, the conclusions are based mainly upon the $\nu_s(SO_3)$ relative band intensities. Two items need to be mentioned, the first being the DEA-G2:LiTf samples are drastically different spectroscopically (IR) than the LPEI-G2:LiTf system. The drastic changes seen in the IR absorption bands for LPEI-G2:LiTf samples with addition of LiTf are not seen in the IR spectra for the DEA-G2:LiTf samples. The second point to make is that it is extremely rare to see significant amounts of "free" ions at high salt concentrations for PEO-like systems.

Structural changes in the tethered side chain of LPEI-G2 have also been investigated, see **Figure IV-29. Figure IV-29** shows the same three samples (pure

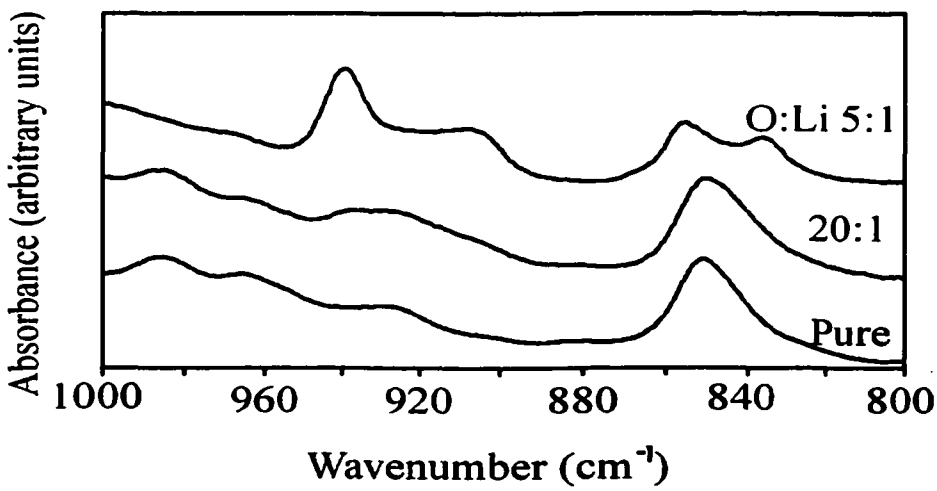

Figure IV-29 IR Spectra for LPEI-G2:LiTf at various compositions

LPEI-G2, 20:1, and 5:1 O:Li complexes) in the spectral window of 1000-800 cm^{-1}. It has been shown[37,86-91] that in both PEO and diglyme the modes in this spectral region consist of mixed CH_2 rocking, $\rho(CH_2)$, and CO stretching, $\nu(CO)$. It is known that these bands are sensitive to the interaction of the lithium ion with the heteroatom and the local conformation of the tethered chain. LPEI-G2 has a medium intensity polymer absorption band centered at 851 cm^{-1} and three weak absorption bands centered at 929, 966, and 985 cm^{-1}, receptively. Comparing the LPEI-G2 samples to the DEA-G2 samples in this region, **Figure IV-30**, it can be seen that DEA-G2 is similar to LPEI-G2. **Figure IV-30** shows the IR spectra for LPEI-G2 and DEA-G2 from 1000-800 cm^{-1}. The main

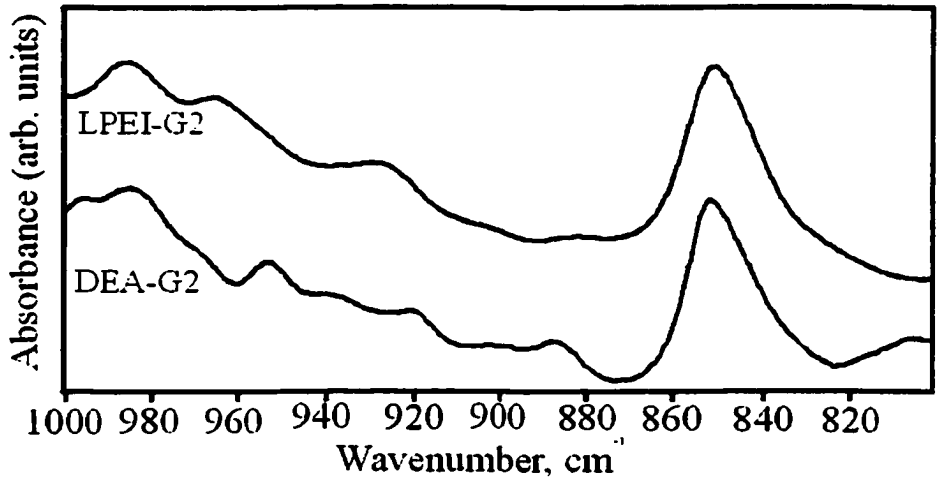

Figure IV-30 Comparison of IR Spectra of LPEI-G2 and DEA-G2

difference between the two spectra is the polymer bands are broader and have less structure. For example, LPEI-G2 has a small broad absorption from ~940-920 cm^{-1} and DEA-G2 has two definite absorptions bands in this range at ~938 and 920 cm^{-1}. The IR

absorption bands for LPEI-G2 change slightly when LiTf is added. **Figures IV-31** and **IV-32** show the IR spectra of the 5:1 O:Li and 20:1 O:Li samples. It can be easily seen

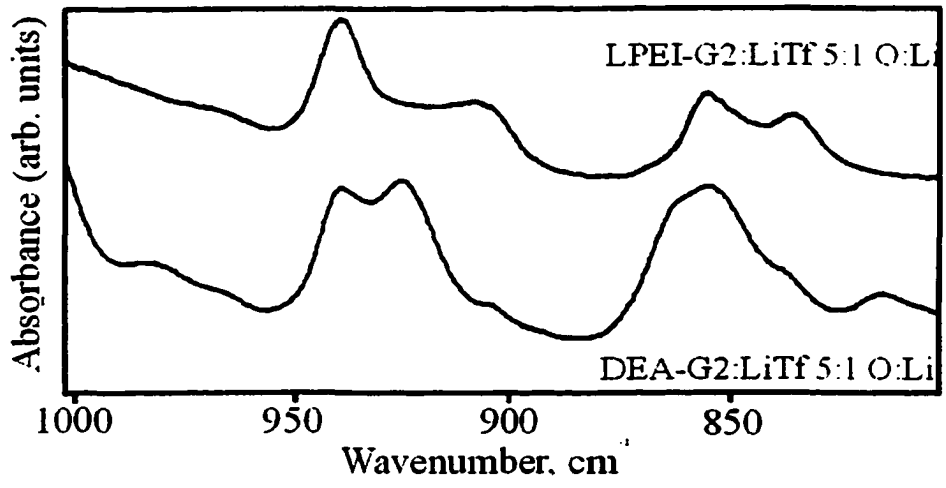

Figure IV-31 Comparison of IR Spectra of LPEI-G2:LiTf and DEA-G2:LiTf 5:1 O:Li Samples

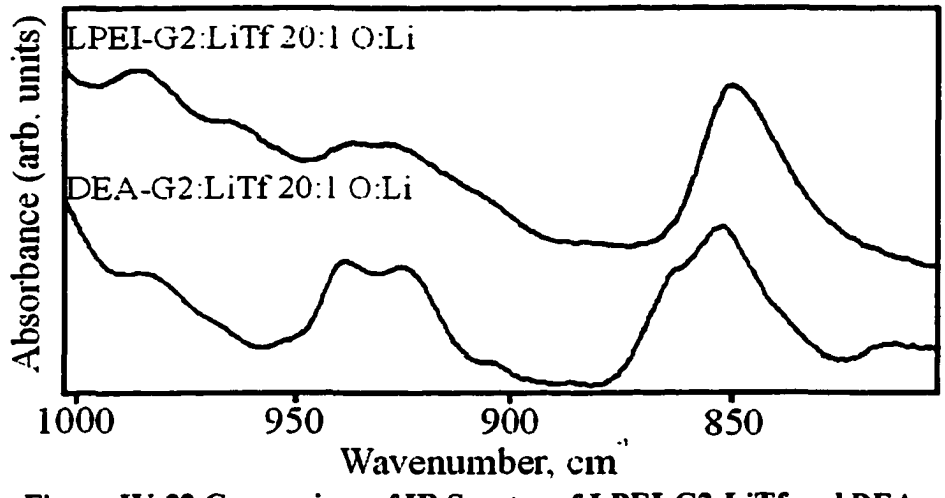

Figure IV-32 Comparison of IR Spectra of LPEI-G2:LiTf and DEA-G2:LiTf 20:1 O:Li Samples

that the absorption bands for DEA-G2:LiTf samples do not change significantly with addition of LiTf. However, the absorption bands of LPEI-G2:LiTf samples drastically change with addition of LiTf.

Drastic changes in the absorption bands for the 5:1 O:Li LPEI-G2:LiTf sample are seen in the IR spectra. The band at 851 cm^{-1} is lost and two new bands are seen at 860 and 830 cm^{-1}. The appearance of the band at 860 cm^{-1} is very significant. This band signals a change in the local conformation of the ethylene oxide sidechain in response to the interaction of the lithium cation with the ether oxygen atoms. Similar studies of crystalline and liquid or amorphous phases of glyme-salt or PEO-salt systems has shown that a decrease in the gauche angle of the O-C-C-O dihedral angle accompanies the spectral shift. The second significant change in the LPEI-G2 :LiTf samples is seen in the absorption band at ~940 cm^{-1}. In the 20:1 sample , a very weak band at ~940 cm^{-1} can be seen, however, this band grows in intensity with increasing salt concentration and becomes the most intense band in this region for the 5:1 O:Li sample. These spectral changes are similar to those seen in diglyme systems upon addition of LiTf.[92]

Diglyme could be considered a model compound for LPEI-G2 since both have three heteroatoms per repeat unit. **Table IV-3** contains a simple comparison of IR absorption bands in the 1000-800 cm^{-1} spectral region. **Figure IV-33** shows the IR

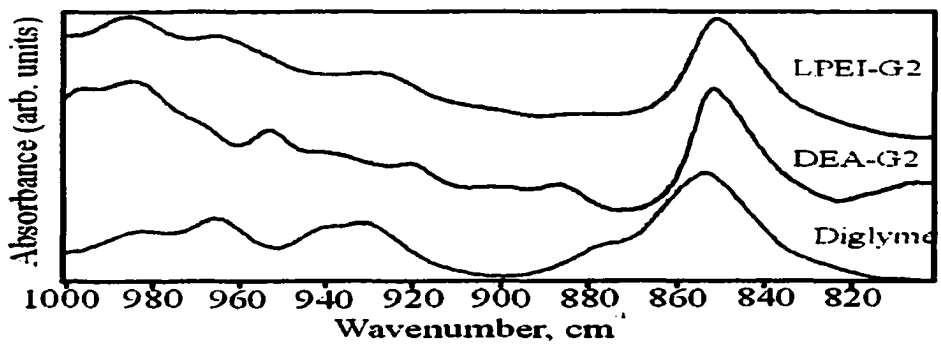

Figure IV-33 Comparison of IR Spectra for LPEI-G2, DEA-G2, and Diglyme

spectra of LPEI-G2, DEA-G2, and diglyme. The three samples have similar absorption bands. It is interesting to note that two areas within this spectral region are different. LPEI-G2 is very similar to DEA-G2 and the only glaring difference is the broad polymer absorption band centered at 929 cm^{-1}, as mentioned earlier. The main difference in the IR spectrum of diglyme relative to the IR spectra of LPEI-G2 and DEA-G2 is the absorption band centered at 851 cm^{-1} for diglyme is much broader than the absorption band for LPEI-G2 or DEA-G2. However, one similarity does exist for diglyme. The absorption band of diglyme centered at ~930 cm^{-1} is broad just like the absorption band of LPEI-G2 that is centered at 929 cm^{-1}.

Table IV-3 Comparison of IR Band Frequencies (cm^{-1})

for LPEI-G2 and Diglyme in the region 1000 cm^{-1} to 800 cm^{-1}

LPEI-G2	Diglyme
851	854
929	932
966	966
985	981

LPEI-G2 behaves drastically different than DEA-G2 when LiTf is dissolved in it. One possible explanation for this is DEA-G2 is more flexible than LPEI-G2 and may wrap around the lithium cations and form a complex, see **Figure 34a**. LPEI-G2 on the other hand is not as flexible and would have to form some other type of transient species, see **Figure 34b**. The two structures in **Figure 34** are only conjecture and have not been

proven.

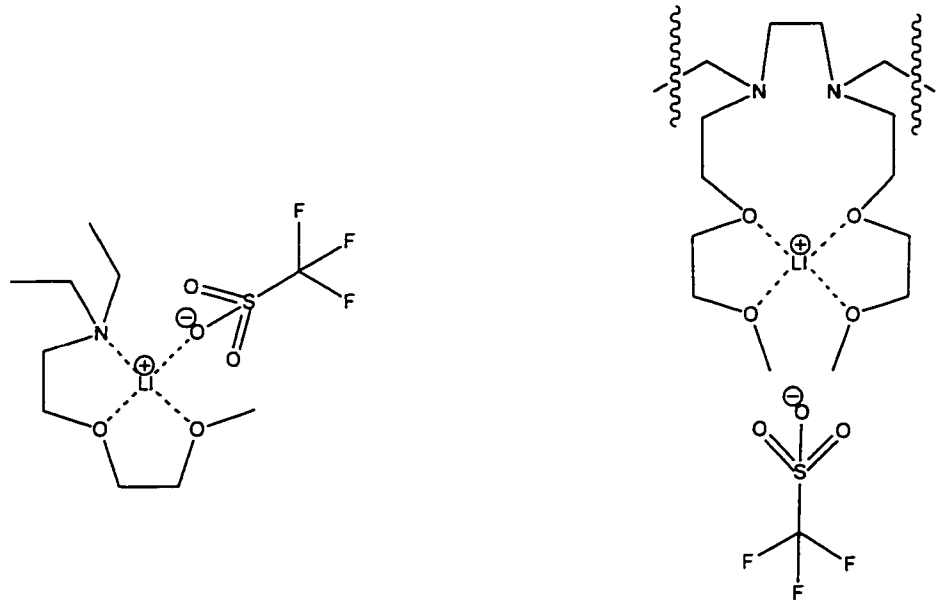

A B

Figure IV-34 Possible Species Present in DEA-G2:LiTf (A) and LPEI-G2:LiTf (B)

The last two areas that need to be discussed are the conductivity of LPEI-G2:LiTf salt complexes and the corresponding DSC thermograms. The LPEI-G2:LiTf salt compositions have conductivities in the range of 10^{-7} - 10^{-5} S/cm. The highest conductivity that was obtained was 7 X 10^{-5} S/cm at 60°C for the 20:1 O:Li sample, see **Figure IV-35**. The 20:1 O:Li sample had a conductivity of 5 X 10^{-6} S/cm at 25°C and 7 X 10^{-5} S/cm at 60°C. The 20:1 O:Li sample contains roughly 50% "free" ions as determined spectroscopically. Over the temperature range of this study, the conductivity values of the 5:1 sample are markedly lower than the corresponding values of the 20:1 sample. A decrease in the relative amount of "free" ion is seen for the 5:1 O:Li sample.

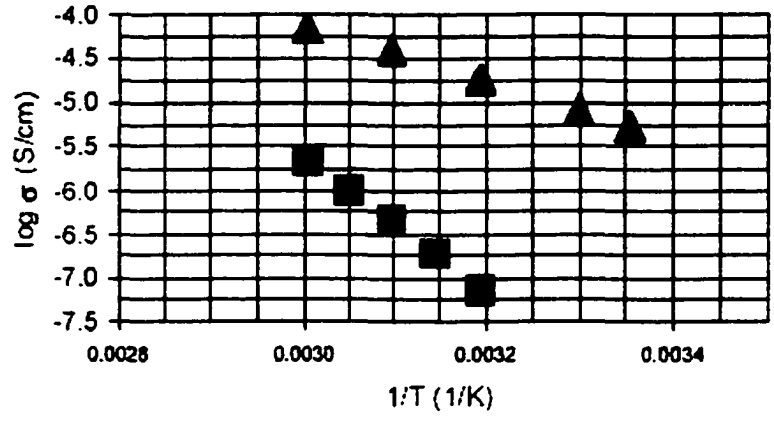

Figure IV-35 Plot of log σ vs 1/T for LPEI-G2:LiTf at 20:1 (▲) and 5:1 (■) O:Li Samples

The 5:1 O:Li sample contains roughly 25 % "free" ions and has ionic conductivities of 1 X 10^{-7} S/cm at 25°C and 2 X 10^{-6} S/cm at 60°C. Although the total amount of "free" ion may increase in the 5:1 O:Li sample, conductivity likely decreases due to a large increase in the volume fraction of the more poorly conducting phase associated with ion pair and aggregate species. This decrease in conductivity at high salt concentration is consistent with trends seen in the literature.[19]

It should be pointed out that the LPEI-G2:LiTf system has the highest conductivities for the three polymer systems (LPEI, LPMEI, LPEI-G2) that have been studied. The behavior of the polymer electrolytes system is more like Arrhenius behavior and not William, Landel, and Ferry (WLF) behavior.[93] This can explain since the conductivity measurements were performed over a small temperature range. A larger temperature range must be studied to accurately depict what type of behavior the LPEI-

G2:LiTf polymer electrolyte follows.

Table IV-4 contains the Tg data for the three samples that have been studied. LPEI-G2 has a low Tg and is clearly amorphous at room temperature since a Tm has not been seen for any type of crystalline species for this polymer system (up to ~140°C).

Table IV-4 Glass Transition (Tg) Temperatures of LPEI-G2:LiTf with Different O:Li Ratios

Sample (O:Li)	Tg °C
LPEI-G2	-76
LPEI-G2:20:1	-60
LPEI-G2:5:1	16

A large change is seen between the 5:1 and 20:1 O:Li LPEI-G2LiTf samples The 20:1 O:Li sample has a Tg of -60°C and the 5:1 O:Li sample has a Tg of 16°C whereas the pure polymer has a Tg of -76°C.

LPEI-G3 was made in the same manner as LPEI-G1 and LPEI-G2. After LPEI is completely dissolved in the acid, the polymer solution is cooled and $NaBH_4$ is added as chunks to prevent the solution from over heating. The reaction is heated at 55°C for five days. The extraction proved to be difficult and centrifugation was used to separate the emulsion. The solvent was removed under reduced pressure and proton NMR spectrum was recorded. **Figure IV- 36** shows the crude proton NMR spectrum of LPEI-G3. The spectrum is fairly complicated, see **Figure IV-37**. The spectrum contains many of the features that one would expect for LPEI-G2. A broad peak at ~2.8 ppm

would be attributed to the protons adjacent to the nitrogen atom and the peaks that are at 3.8-3.0 ppm fall where protons adjacent to an oxygen would be.

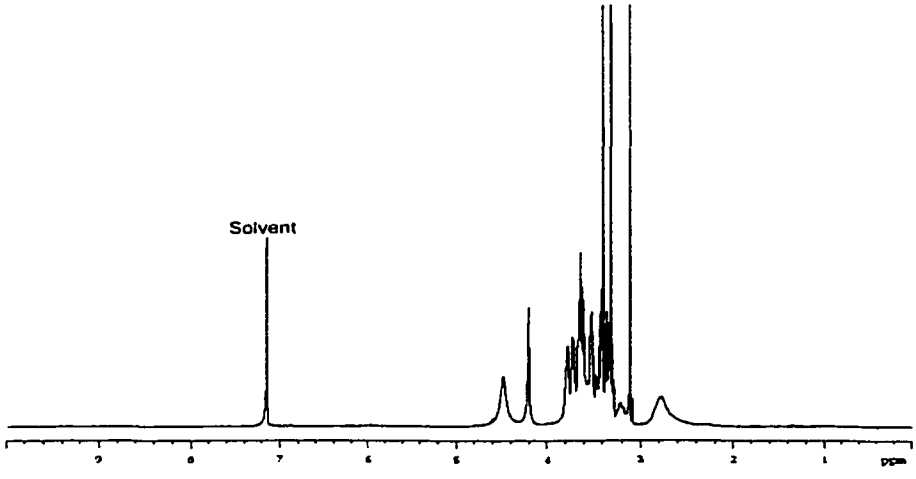

Figure IV-36 ^{1}H NMR Spectrum of LPEI-G3

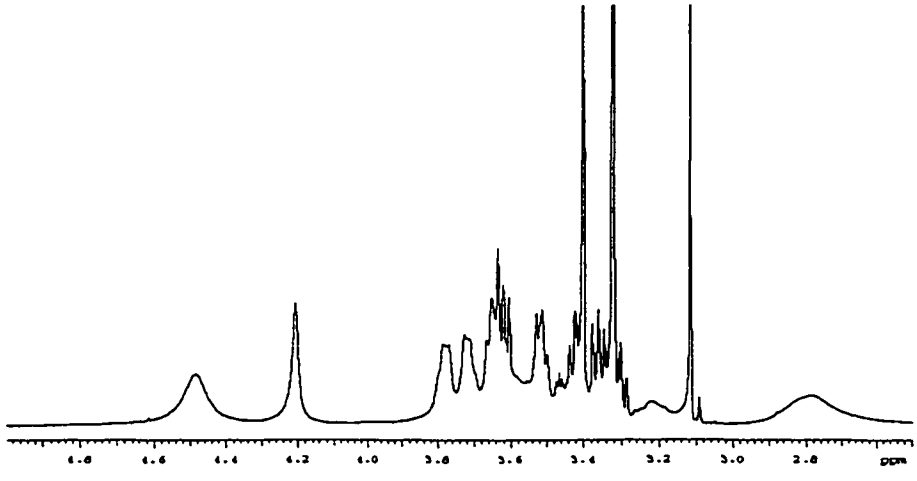

Figure IV-37 Expansion of ^{1}H NMR Spectrum of LPEI-G3

The only peak that can be assigned is the polymer backbone CH_2 protons. The CH_2 protons of the polymer backbone can be seen at ~2.8 ppm and are broad. ^{13}C NMR spectral analysis would help, however it has not been done to date. It can be clearly seen

that the reaction for the LPEI-G3 was not as clean as LPEI-G1 or LPEI-G2. The polymer will need some type of purification process before it can be studied.

Conclusion and Future Directions:

Synthetic modification of LPEI and BPEI has been carried out and incorporation of oligo(ethylene oxide) tethered side chains has been accomplished. The use of LPEI-GX (X=1,2,3) as a polymer electrolyte host has potential. The first advantage that LPEI-GX systems have over other polymer systems, such as MEEP, is a synthetic route has been worked out that is simple and not air sensitive. Even though the synthesis had initial problems, those problems have been solved and the synthesis can be considered straightforward. However , the synthetic route can still be improved. Specifically, the most astounding trait that LPEI-G2 has is the portion of "free" ionic species that are present in high salt concentration polymer electrolytes. This significant portion of "free" ion has not been observed in other PEO-based polymer electrolyte systems. The LPEI-G2 modes will be assigned using data collected from both experimental and computational studies of the model compound (without dissolved salt). These assignments may provide further insight to how the polymer interacts with the dissolved salts.

In the future, work on LPEI-G2 will be carried out in two areas: extension to BPEI /BPEI-G2 and synthetic modification of LPEI-G2. Branched poly(*N*-(2-methoxyethylene)ethylenime) (BPEI-G1) has been synthesized (Appendix, **Figure A-14**) using Gribble's method, however, BPEI-G1 has not been investigated as a possible

polymer electrolyte host. Synthetic modification of LPEI -G2 using a variety of dihalides can provide a crosslinked elastomeric network polymer. Crosslinking LPEI-G2 has a variety of potential uses. Crosslinked LPEI-G2 may be used as a battery polymer electrolyte layer. A common problem with polymer electrolytes is the system has poor physical properties. However, crosslinked LPEI -G2 is a relatively robust elastomeric system which has better mechanical properties than other systems. Initial cross-linking experiments indicated that LPEI-G2 can be crosslinked, however, concentration of both LPEI-G2 and the dihalide, in methanol, must be appropriate for the cross-linking to occur. The cross-linking process using LPEI-G2 is slightly different than that for LPEI and LPMEI. The latter two will crosslink easily and methanol solutions will gel. However, LPEI-G2 may crosslink, but until the solvent is removed the crosslinking process remains incomplete and the system still flows. After removal of solvent the crosslinking process continues and a gel eventually forms. A complete understanding of the cross-linking process and cross-linked systems was not investigated and is beyond the scope of this dissertation.

The extension of the model compound work will also provide valuable information. The synthesis, computational calculations, and spectroscopic study of the corresponding model compounds for LPEI-G1 and LPEI-G3 will provide the data that may help deconvolute the experimental data for the corresponding polymers. If the model compounds and triflate salts form crystalline complexes, the local structure of the crystal complex can be investigated spectroscopically. Solving the crystal structure of

these crystalline complexes will provide information on the local structure. Knowing the local structure may solidify the mode assignments that were made on the model compounds and polymers.

Experimental:

All common reagents and solvents were commercially available and used as received unless otherwise noted. All ^{1}H and $^{13}CNMR$ were obtained using a Varian 300 or 400 MHz spectrometer. All deuterated solvents were used as received and referenced to residual solvent protons.

Synthesis of LPEI-G1

Linear poly(*N*-(2-methoxyethylene)ethylenimine) (LPEI-G1) was synthesized from LPEI, cut into small pieces, by placing 2.103 g (0.04883 mol) into a three neck 250 mL round bottom flask and adding methoxyacetic acid (77.0 mL) to the reaction flask. The mixture was warmed until all the LPEI dissolved. The solution was cooled to 5°C and $NaBH_4$ (7.57 g, 0.224 mol) was added in the form of small chunks. Tetrahydrofuran, THF, (25 mL) was added to decrease the viscosity of the thick solution and the solution was stirred to insure homogeneity. The solution was heated to 55°C for five days. The resulting solution was cooled to room temperature and 50 mL of distilled water was added. NaOH pellets were added to the solution until dissolved and the pH of the solution was much greater than 10. The solution was extracted with CH_2Cl_2 (5 X 25 mL, Fisher). Centrifugation was used to separate the organic layer from the aqueous layer and the organic layers were combined. The organic layer was dried over Na_2SO_4,

filtered, and the solvent was removed under reduced pressure. This procedure gave a 94% yield. ^{1}H-NMR ($CDCl_3$) δ(ppm) 3.4(2H, t), 3.3 (3H), 2.64 (2H, t) 2.56 (4H); ^{13}C-NMR ($CDCl_3$) δ(ppm) 71.5, 59.2, 58.8, 54.6, 53.8.

Synthesis of BPEI-G1

Branched poly(*N*-(2-methoxyethylethylenimine) (BPEI-G1) was synthesized from BPEI by placing 3.217 g (0.07469 mol) into a three neck 500 mL round bottom flask and adding 2-methoxyacetic acid (110.0 mL, Aldrich) to the reaction flask. The mixture was warmed until all the BPEI dissolved. The solution was cooled to 5°C and $NaBH_4$ (10.51 g, 0.3107 mol) was added in the form of small chunks. The solution was heated to 55°C for five days. The resulting solution was cooled to room temperature and 50 mL of distilled water was added. NaOH pellets were added to the solution until the pellets dissolved and the pH of the solution was much greater than 10. The solution was extracted with CH_2Cl_2 (5 X 25 mL). The organic layer was dried over Na_2SO_4, filtered, and the solvent was removed under reduced pressure. This procedure gave a low yield which was not recorded since there was only enough for an NMR sample. ^{1}H-NMR (Benzene-d_6) δ(ppm) 3.65-3.50(b), 3.49 (b), 3.35-3.18(b) 2.95-2.65 (b); ^{13}C-NMR (Benzene-d_6) δ(ppm) 72.4, 70.8, 58.8, 55.1, 54.6

Synthesis of LPEI-G2

Linear poly(*N*-(2-(2-methoxyethoxy)ethyl)ethylenimine) (LPEI-G2) was synthesized from LPEI, cut into small pieces, by placing 1.5620 g (0.03627 mol) into a three neck 250 mL round bottom flask and adding 2-(2-methoxyethoxy)acetic acid (55.0

mL) to the reaction flask. The mixture was warmed until all the LPEI dissolved. The solution was cooled to 5°C and $NaBH_4$ (5.052 g, 0.1494 mol) was added in the form of small chunks. Tetrahydrofuran, THF, (25 mL, Fisher) was added to decrease the viscosity of the thick solution, and the solution was stirred to insure homogeneity. The solution was heated to 55°C for five days. The resulting solution was cooled to room temperature and 50 mL of distilled water was added. NaOH pellets were added to the solution until they dissolved and the pH of the solution was much greater than 10. The solution was extracted with CH_2Cl_2 (5 X 25 mL). Centrifugation was used to separate the organic layer from the aqueous layer and the organic layers were combined. The organic layer was dried over Na_2SO_4, filtered, and the solvent was removed under reduced pressure. A sample was purified by dialysis (2000 MW cutoff membrane, 48 hours) and water was removed under reduced pressure. This procedure gave 94% yield for the crude product. ^{1}H-NMR (Benzene-d_6) δ(ppm) 3.65-3.50(4H), 3.49 (2H), 3.35-3.18 (3H) 2.95-2.65 (6H); ^{13}C-NMR (Benzene-d_6) δ(ppm) 72.4, 70.8, 58.8, 55.1, 54.6

Synthesis of LPEI-G3

Linear poly(*N*-(2-(2-(2-methoxyethoxy)ethoxy)ethylene)ethylenimine) (LPEI-G3) was synthesized from LPEI, cut into small pieces, by placing 2.018 g (0.04685 mol) into a three neck 250 mL round bottom flask and adding 2-(2-(2-methoxyethoxy) ethoxy)acetic acid (30.0 mL) to the reaction flask. The mixture was warmed until all the LPEI dissolved. The solution was cooled to 5°C and $NaBH_4$ (7.037 g, 0.2080 mol) was

added in the form of small chunks. Tetrahydrofuran, THF, (25 mL) was added to decrease the viscosity of the thick solution and the solution was stirred to insure homogeneity. The solution was heated to 55°C for five days. The resulting solution was cooled to room temperature and 50 mL of distilled water was added. NaOH pellets were added to the solution until they dissolved and the pH of the solution was much greater than 10. The solution was extracted with CH_2Cl_2 (5 X 25 mL). Centrifugation was used to separate the organic layer from the aqueous layer and the organic layers were combined. The organic layer was dried over Na_2SO_4, filtered, and the solvent was removed under reduced pressure. This procedure gave a % yield over 100%. The sample is still wet and needs to be purified. See Appendix, **Figure A-22**.

Synthesis of DEA-G2:

DEA-G2 was synthesized from diethylamine by placing 1.998 g (0.02731 mol) into a 100 mL round bottom flask and adding 2-(2-methoxy)ethoxyacetic acid (50.0 mL) to the reaction flask. The mixture was stirred until the solution became homogenous. The solution was cooled to 5°C and $NaBH_4$ (5.485 g, 0.1621 mol) was added in the form of small chunks. The solution was heated to 55°C for four days under a N_2 environment. The resulting solution was cooled to room temperature and 50 mL of distilled water was added. NaOH pellets were added to the solution until they dissolved and the pH of the solution was much greater than 10. The solution was extracted with CH_2Cl_2 (5 X 25). The organic layer was dried over Na_2SO_4, filtered, and the solvent was removed under reduced pressure. The crude mixture purified by distilling over Na metal and under

vacuum. This procedure gave 63% of yield for the crude product. ^{1}H-NMR (Benzene-d_6) δ(ppm) 3.5-3.40(4H, m), 3.3 (2H, m), 3.1(3H, s) 2.6 (2H, t), 2.4 (2H, q), 0.9 (3H, t); ^{13}C-NMR (Benzene-d_6) δ(ppm) 72.4, 70.8, 58.7, 53.2, 48.0, 12.7.

Preparation of Polymer Electrolytes:

To prepare the LPEI-G2:LiTf solutions of a desired composition, the appropriate amount of LiTf was added to 0.2695 g of LPEI-G2 (5.0 mL of stock solution of 0.3712 M in methanol) The sample solution was stirred to insure homogeneity. Sample composition are reported as oxygen to lithium molar ratios (O:Li). LPEI-G2:LiTf ratios of 20:1 and 5:1 were prepared and investigated.

FTIR Spectroscopy:

Samples were prepared by casting thin films onto sodium chloride windows and drying under a dry air purge for ~ 12 hours. The thin films were translucent with a faint tint of golden brown coloration. All FTIR data was collected using a Bruker IFS66V FT-IR spectrometer with a KBr beam splitter over a range of 4000-600 cm^{-1}. All spectra were collected with the samples under reduced pressure (8 mbar) and at a 1 cm^{-1} spectral resolution. Commercially available software (Thermo Galactic, Grams/AI 7.00) was used for spectral analysis. The spectral bands were fitted using a mixed Gaussian-Lorenzian product function and a straight baseline.

Differential Scanning Calorimetry:

Sample solutions were cast onto Teflon, dried in a nitrogen environment for 24 hours, and placed under vacuum for 24 hours. After the samples were dried, a 12-15 mg

sample was hermetically sealed in a 40 mL aluminum pan. Thermal data were collected using a Mettler DSC 820 calorimeter with commercially available software from Mettler Toledo (Stare v.6.10) under a dry nitrogen purge. All of the samples were heated to 60°C for thirty minutes, followed by two cooling and heating cycles between -100°C and ~140°C (5°C/min). After a pin hole was punched in the pan's lid, the samples were cycled twice between 25°C and 150°C to insure that the samples were dry. A reproducible small transition is noticed at 100°C, suggesting that there is a small amount of H_2O or solvent present in the LPEI-G2:LiTf samples.

Complex Impedance:

Sample solutions were cast onto Teflon, dried in a nitrogen environment for 24 hours, and placed under vacuum for 24 hours. The film thickness was measured using a micrometer built into the conductivity cell. Conductivity measurements were made over the frequency range 0.005 to 10,000 kHz using a Hewlett-Packard 4192A LF impedance analyzer (National Instruments, LabviewTM 5.1). The conductivity data for all of the LPEI-G2:LiTf compositions were collected at temperatures ranging from 25°C to 60°C in 10°C increments. All of the impedance plots were curve-fitted using commercially available software (Solartron Instruments LTD, LEVM 7.1v).

OVERALL CONCLUSIONS

Three polymer electrolyte systems were studied. LPEI and LPMEI were studied to provide an understanding of the role hydrogen bonding. Hydrogen bonding does not drastically change the spectroscopic makers ($\delta_s(CF_3)$ for example); small shifts in the absorption wavenumbers are seen. However, hydrogen bonding does effect the ionic conductivity. LPEI-LiTf samples had a lower ionic conductivity than the same LPMEI-LiTf samples. The effect of hydrogen bonding on ionic conductivity is also show in a crossover in the ionic conductivity for the 20:1 N:Li and 5:1 N:Li samples. The 5:1 N:Li sample has a higher ionic conductivity at lower temperature than the 20:1 N:Li sample, but as the temperature is increased the 20:1 N:Li sample surpasses the 5:1 N:Li sample.

The disruption of hydrogen bonding as the polymer nears and passes through its Tm allows the polymer to flow and therefore the ions flow more readily and thus an increase in ionic conductivity is seen. The ionic conductivity of all three polymer systems is roughly from 10^{-6} S/cm - 10^{-5} S/cm. LPEI-G2 has the highest ionic conductivities for the three polymer systems that were studied and is roughly 3/4 of a magnitude lower than MEEP at room temperature.

The design of new polymer electrolyte host systems should take into account hydrogen bonding and remove it completely. Also, an increase in the local concentration of tethered oligo(ethylene oxide) units may increase ionic conductivity.

Bibliography

1) Vincent, C. A.; Scrosati, B. *Modern Batteries, An Introduction to Electrochemical Power Sources*; Wiley & Sons Inc.: New York, 1997.

2) http://www.batteryrecycling.com/; Battery Solutions, I. **2001**, *2001*.

3) *Polyelectrolytes, Science and Technology*; Marcel Dekker, Inc.: New York, 1993.

4) Gray, F. M. *Solid Polymer Electrolytes*; VCH: New York, 1991.

5) Besenhard, J. O. *Handbook of Battery Materials*; Wiley-VCH: New York, 1999.

6) Venkatasetty, H. V. *Lithium Battery Technology*; Wiley & Sons: New York, 1984.

7) Crompton, T. R. *Battery Reference Book*; Butterworths: Boston, 1990.

8) Laskar, A. L.; Chandra, S. *Superionic Solids and Solid Electrolytes, Recent Trends*; Academic Press, INC.: New York, 1989.

9) Ismail, M. I. *Electrochemical Reactors, Their Science and Technology*; Elsevier: New York, 1989.

10) Bode, H. *Lead-Acid Batteries*; Wiley & Sons: New York, 1977.

11) Falk, S. U.; Salkind, A. J. *Alkaline Storage Batteries*; Wiley & Sons Inc.: New York, 1969.

12) Rand, D. A. J.; Woods, R.; Dell, R. M. *Batteries for Electric Vehicles*; Research Studies Press Ltd. & Wiley & Sons Inc.: New York, 1998.

13) Gabano, J.-P. *Lithium Batteries*; Academic Press: Saft, Poitiers, France, 1983.

14) Hagenmuller, P.; Gool, W. V. *Solid Electrolytes, General Principles, Characterization, Materials, Applications*; Academic Press, INC.: New York, 1978.

15) Ingram, W. J. *New Technology Batteries Guide*, 1998.

16) Sequoia, E. *Lead-Acid Batteries: A Reference and Data Book*; Elsevier Sequoia S. A., Lausanne: Switzerland, 1977.

17) Wakihara, M.; Yamamoto, O. *Lithium Ion Batteries*; Wiley-VCH: New York, 1998.

18) Meyer, W. H. *Advanced Materials* **1998**, *10*, 439-448.

19) Bruce, P. G.; Vincent, C. A. *J. Chem. Soc. Faraday Trans.* **1993**, *89*, 3187-3203.

20) Wright, P. V. *Electrochim. Acta* **1998**, *43*, 1137-1143.

21) Armand, M. B. *Solid State Ionics* **1983**, *9-10*, 745-754.

22) Armand, M. B.; Chabagno, J. M.; Duclot, M. *2nd International Meeting on Solid Electrolytes*: St. Andrews, Scotland, 1978.

23) Fenton, D. E. *Polymer* **1973**, *14*, 589.

24) Maxfield, J.; W., S. I. *Polymer* **1975**, *16*, 505-509.

25) Bernson, A.; Lindgren, J.; Huang, W.; R., F. *Polymer* **1995**, *36*, 4471-4478.

26) Dissanayake, M. A. K. L.; Frech, R. *Macromolecules* **1995**, *28*, 5313-5319.

27) Munshi, M. Z. A.; Smyrl, W. H. *Solid State Ionics* **1991**, *45*, 183-189.

28) Qiao, J.; Chen, Y.; Baker, G. L. *Chem. of Materials* **1999**, *11*, 2542-2547.

29) Bruce, P. G.; Krok, F.; Vincent, C. A. *Solid State Ionics* **1988**, *27*, 81-88.

30) Honda, H.; Ono, K.; Murakami, K. *Macromolecules* **1990**, *23*, 515-520.

31) Gadjourova, Z.; Marero, D. M.; Andersen, K. H.; Andreev, Y. G.; Bruce, P. G. *Chem. of Materials* **2001**, *13*, 1282-1285.

32) Doeff, M. M.; Georen, P.; Qiao, J.; Kerr, J.; De Jonghe, L. C. *Solid State Ionics* **1999**, *146*, 2024-2028.

33) Machida, K.; Miyazawa, T. *Spectrochim. Acta* **1964**, *20*, 1865-1873.

34) Matsuura, H.; Miyazawa, T. *Spectochimica Acta.* **1967**, *23A*, 2433-2447.

35) Matsuura, H.; Miyazawa, T. *J. Polym. Sci., Polym. Chem.* **1969**, *7*, 1735-1744.

36) Papke, B. L.; Dupon, R.; Ratner, M. A.; Shriver, D. F. *Solid State Ionics* **1981**, *5*, 685.

37) Papke, B. L.; Ratner, M. A.; Shriver, D. F. *J. Electrochem. Soc.* **1982**, *129*, 1434-1438.

38) Huang, W.; Frech, R.; Wheeler, R. A. *J. Phys. Chem.* **1994**, *98*, 100-110.

39) Kakihana, M.; Schantz, S.; Torell, L. M.; Stevens, J. R. *Solid State Ionics* **1990**, *40-41*, 641-644.

40) Matsuura, H.; Miyazawa, T. *Bull. Chem. Soc. Jpn.* **1968**, *41*, 1798-1808.

41) Hyun, J.; Dong, H.; Rhodes, C. P.; Frech, R.; Wheeler, R. A. *J. Phys. Chem. Part B* **2001**, *105*, 3329-3337.

42) Forsyth, M.; Payne, V. A.; Ratner, M. A.; De Leeuw, S. W.; Shriver, D. F. *Solid State Ionics* **1992**, *53-56*, 1011-1026.

43) Johansson, A.; Wendsjo, A.; Tegenfeldt, J. *Electrochim. Acta* **1992**, *37*, 1487-1489.

44) Ward, I. M.; Boden, N.; Cruickshank, J.; Leng, S. A. *Electrochim. Acta* **1995**, *40*, 2071-2076.

45) Chatani, Y.; Yakura, Y.; Ishioka, T. *Polymer* **1990**, *31*, 208-211.

46) Chatani, Y.; Irie, t. *Polymer* **1988**, *29*, 2126-2129.

47) Chiang, C. K.; Davis, G. T.; Harding, C. A. *Solid State Ionics* **1986**, *18-19*, 300-305.

48) Tanaka, R.; Fujita, T.; Nishibayashi, H.; Saito, S. *Solid States Ionics* **1993**, *60*, 119-123.

49) Harris, C. S.; Shriver, D. F.; Ratner, M. A. *Macromolecules* **1986**, *19*, 987-989.

50) Chiang, C. K.; Davis, G. T.; Harding, C. A. *Macromolecules* **1985**, *18*, 825-827.

51) Tanaka, R.; Ueoka, I.; Takaki, Y.; Kataoka, K.; Saito, S. *Macromolecules* **1983**, *16*, 849-853.

52) Chatani, Y.; Kobatake, T.; Tadokoro, H.; Tanaka, R. *Macromolecules* **1982**, *15*, 170-176.

53) Chatani, Y.; Tadokoro, H.; Saegusa, T.; Ikeda, H. *Macromolecules* **1981**, *14*, 315-321.

54) Saegusa, T.; Yamada, A.; Taoda, H.; Kobayashi, S. *Macromolecules* **1978**, *11*, 435-436.

55) Johnson, T. W.; Klotz, I. M. *Macromolecules* **1974**, *7*, 149-153.

56) Saegusa, T.; Ikeda, H.; Fujii, H. *Macromolecules* **1972**, *5*, 108.

57) Harris, C. S.; Ratner, M. A.; Shriver, D. F. *Macromolecules* **1987**, *20*, 1778-1781.

58) Watanabe, M.; Ikezawa, R.; Sanui, K.; Ogata, N. *Macromolecules* **1987**, *20*, 968-973.

59) Chatani, Y.; Kobatake, T.; Tadokoro, H. *Macromolecules* **1983**, *16*, 199-204.

60) Park, I. H.; Choi, E. *Polymer* **1996**, *37*, 313-319.

61) Chatterjee, S. K.; Misra, N. *Polymer* **1997**, *38*, 1485-1490.

62) Takahashi, T.; Davis, G. T.; Chiang, C. K.; Harding, C. A. *Solid State Ionics* **1986**, *18-19*, 321-325.

63) Tanaka, R.; Yamamoto, H.; Kawamura, S.; Iwase, T. *Electrochim. Acta* **1995**, *40*, 2421-2424.

64) Paul, J. L.; Jegat, C.; Lassegues, J. C. *Electrochim. Acta* **1992**, *37*, 1623-1625.

65) Kokufuta, E.; Suzuki, H.; Yoshida, R.; Yamada, K.; Hirata, M.; Kaneko, F. *Langmuir* **1998**, *14*, 788-795.

66) York, S.; Frech, R.; Snow, A.; Glatzhofer, D. *Electrochim. Acta* **2001**, *46*, 1533-1537.

67) Hashida, T.; Tashiro, K.; Aoshima, S.; Inaki, Y. *Macromolecules* **2002**, *35*, 4330-4336.

68) Tanaka, R.; Koike, M.; Tsutsui, T.; Tanaka, T. *Journal of Polymer Science: Polymer Lettes Edition* **1978**, *16*, 13-19.

69) Sanders, R.; Snow, A. G.; Glatzhofer, D. T.; Frech, R. *Electrochim. Acta* **2002**, *Submitted.*

70) Snow, A. G.; Sanders, R.; Glatzhofer, D. T.; Frech, R. *Electrochim. Acta* **2002**, *Submitted.*

71) Boesch, S. E.; York, S. S.; Rech, R.; Wheeler, R. A. *PhysChemComm* **2001**, *1*.

72) Saegusa, T.; Ikeda, H.; Fujii, H. *Polymer* **1972**, *3*, 35-39.

73) Jang, T.; Rasmussen, P. G. *J. Polym. Sci., Part A, Polym. Chem.* **1998**, *36*, 2619-2629.

74) Geckeler, K.; Lange, G.; Eberhardt, H.; Bayer, E. *Pure & Applied Chemistry* **1980**, *52*, 1883-1905.

75) Saegusa, T.; Ikeda, H.; Fujii, H. *Polymer* **1972**, *3*, 176-180.

76) Smits, T. F.; Kuil, M. E.; Mandel, M. *Macromolecules* **1993**, *26*, 6808-9816.

77) Shriver, D.; Atkins, P. *Inorganic Chemistry*; W. H. Freeman and Company: New York, 1999.

78) Rhodes, C. P.; Frech, R. *Solid State Ionics* **1999**, *121*, 91.

79) Allcock, H.; Napierala, M. E.; Olmeijer, D. L.; Cameron, C. G.; Kuharcik, S. E.; Reed, C. S.; O'Connor, S. J. M. *Electrochim. Acta* **1998**, *43*, 1145-1150.

80) Allcock, H. R.; Hofmann, M. A.; Wood, R. M. *Macromolecules* **2002**, *34*, 6915-6921.

81) Allcock, H. R.; Kuharcik, S. E.; Reed, C. S.; Napierala, M. E. *Macromolecules* **1996**, *29*, 3384-3389.

82) Allcock, H. R.; Sunderland, N. J.; Ravikiran, R.; Nelson, J. M. *Macromolecules* **1998**, *31*, 8026-8035.

83) Kerr, J.; Liu, G.; Curtiss, L. A.; Redfern, P. *Towards Room Temperature Performance for Lithium Metal-Polymer Batteries.*: Santa Fe, NM, 2002.

84) Gribble, G. W.; Jasinski, J. M.; Pellicone, J. T.; Panetta, J. A. *Synthesis* **1978**,

766-768.

85) Gribble, G. W.; Nutaitis, C. F. *Synthesis* **1987**, 709-711.

86) Ogawa, Y.; Ohta, M.; Sakakibara, M.; Matsuura, H.; Harada, I.; Shimanouchi, T. *Bull. Chem. Soc. Jpn.* **1977**, *50*, 650.

87) Matsuura, H.; Fukuhara, K. *Journal of Polymer Science: Part B: Polymer Physics* **1986**, *24*, 1383-1400.

88) Matsuura, H.; Fukuhara, K.; Tamaoki, H. *J. Mol. Struct.* **1987**, *156*, 293.

89) Matsui, Y.; Kubota, T.; Tadokoro, H.; Yoshihara, T. *J. Polym. Sci., A* **1965**, *3*, 2275.

90) Shimomura, M.; Tanabe, Y.; Watanabe, Y.; Kobayashi, M. *Polymer* **1990**, *31*, 1441.

91) Yoshihara, T.; Tadokora, H.; Murahashi, S. *J. Chem. Phys.* **1964**, *41*, 2902.

92) Frech, R.; Huang, W. *Macromolecules* **1995**, *28*, 1246-1251.

93) Painter, P. C.; Coleman, M. M. *Fundamentals of Polymer Science An Introductory Text*; Technomic Publishing CO., INC.: Lancaster, 1997.

Appendix of Spectra

Spectrum Number	Title	Page
A-1	^{1}H NMR Spectrum of poly(2-methyloxazoline)	127
A-2	^{1}H NMR Spectrum of branched poly(ethylenimine)	128
A-3	^{1}H NMR Spectrum of low molecular weight linear poly(ethylenimine)	129
A-4	^{13}C NMR Spectrum of low molecular weight linear poly(ethylenimine)	130
A-5	^{1}H NMR Spectrum of high molecular weight linear poly(ethylenimine)	131
A-6	^{13}C NMR Spectrum of high molecular weight linear poly(ethylenimine)	132
A-7	^{1}H NMR Spectrum of linear poly(*N*-methylethylenimine), Method 1	133
A-8	^{13}C NMR Spectrum of linear poly(*N*-methylethylenimine), Method 1	134
A-9	^{1}H NMR Spectrum of Reaction Mixture LPMEI Synthesis, Method 2	135
A-10	^{1}H NMR Spectrum of linear poly(*N*-methylethylenimine), Method 3, Good Batch	136
A-11	^{1}H NMR Spectrum of linear poly(*N*-methylethylenimine), Method 3, Bad Batch	137
A-12	^{1}H NMR Spectrum of branched poly(*N*-methylethylenimine)	138
A-13	^{1}H NMR Spectrum of linear poly(*N*-methoxyethylenethylenimine)	139
A-14	^{1}H NMR Spectrum of branched poly(*N*-methoxyethylenethylenimine)	140

A-15	^{13}C NMR Spectrum of linear poly(*N*-methoxyethylenethylenimine)	141
A-16	^{1}H NMR Spectrum of linear poly(*N*-(2-(2-methoxyethoxy)ethyl)ethylenimine)	142
A-17	^{13}C NMR Spectrum of linear poly(*N*-(2-(2-methoxyethoxy)ethyl)ethylenimine)	143
A-18	^{1}H NMR Spectrum of (3, 6-dioxaheptyl)diethylamine, DEA-G2	144
A-19	^{13}C NMR Spectrum of (3, 6-dioxaheptyl)diethylamine, DEA-G2	145
A-20	COESY NMR Spectrum of (3, 6-dioxaheptyl)diethylamine, DEA-G2	146
A-21	HMQC NMR Spectrum of (3, 6-dioxaheptyl)diethylamine, DEA-G2	147
A-22	^{1}H NMR Spectrum of linear poly(*N*-(2-(2-(2-methoxyethoxy)ethoxy)ethyl)ethylenimine)	148
A-23	IR Spectrum of poly(2-ethyloxazoline) in CH_2Cl_2	149
A-24	IR Spectrum of poly(*N*-methylethylenimine) in CH_2Cl_2	150

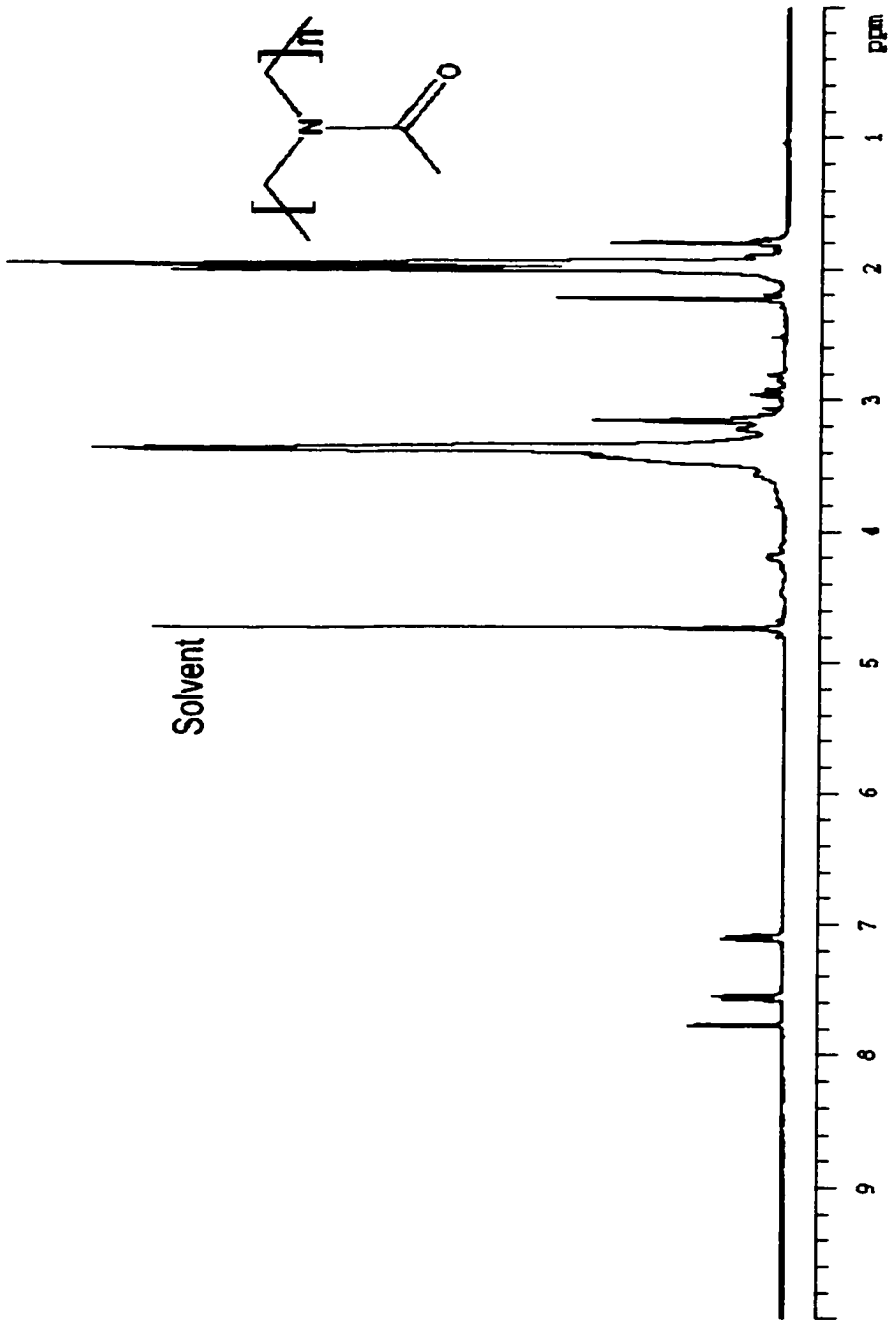

Figure A-1 ^{1}H NMR Spectrum of poly(2-methyloxazoline)

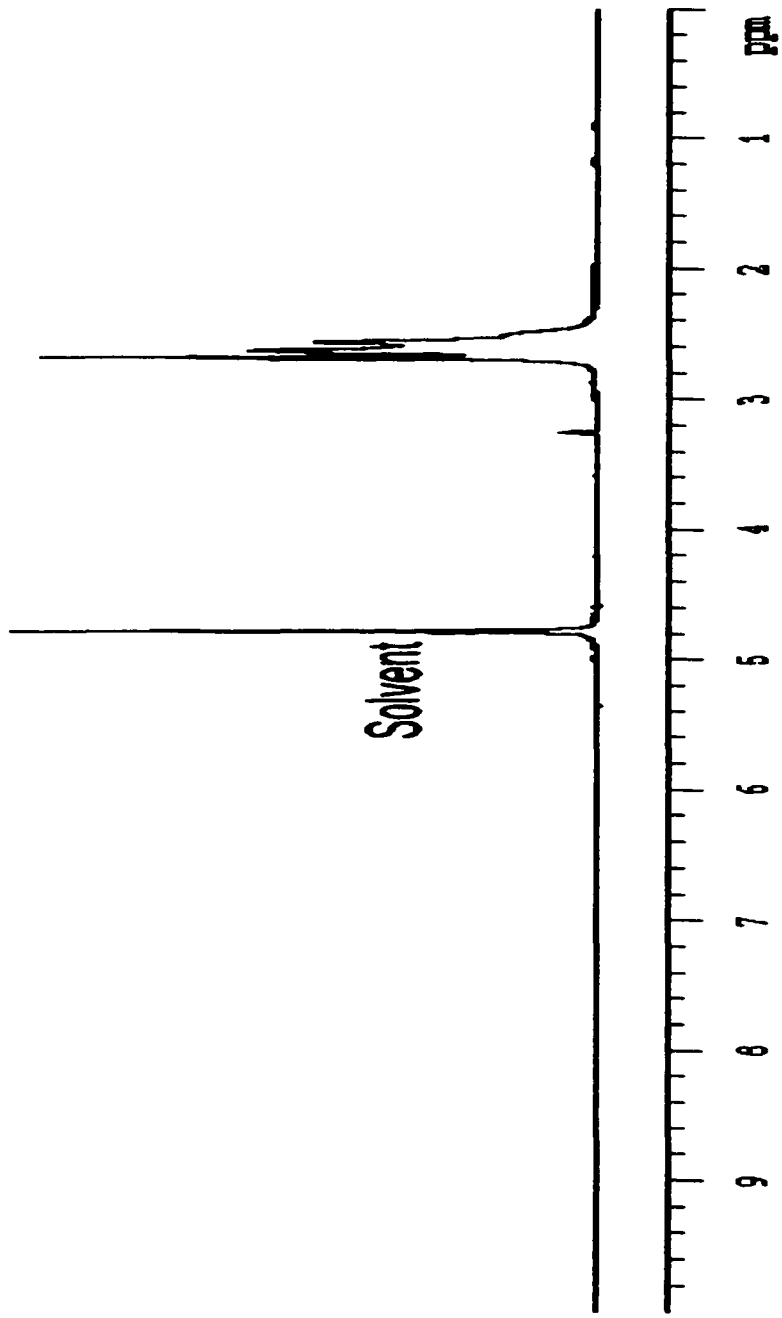

Figure A-2 ^{1}H NMR Spectrum of branched poly(ethylenimine)

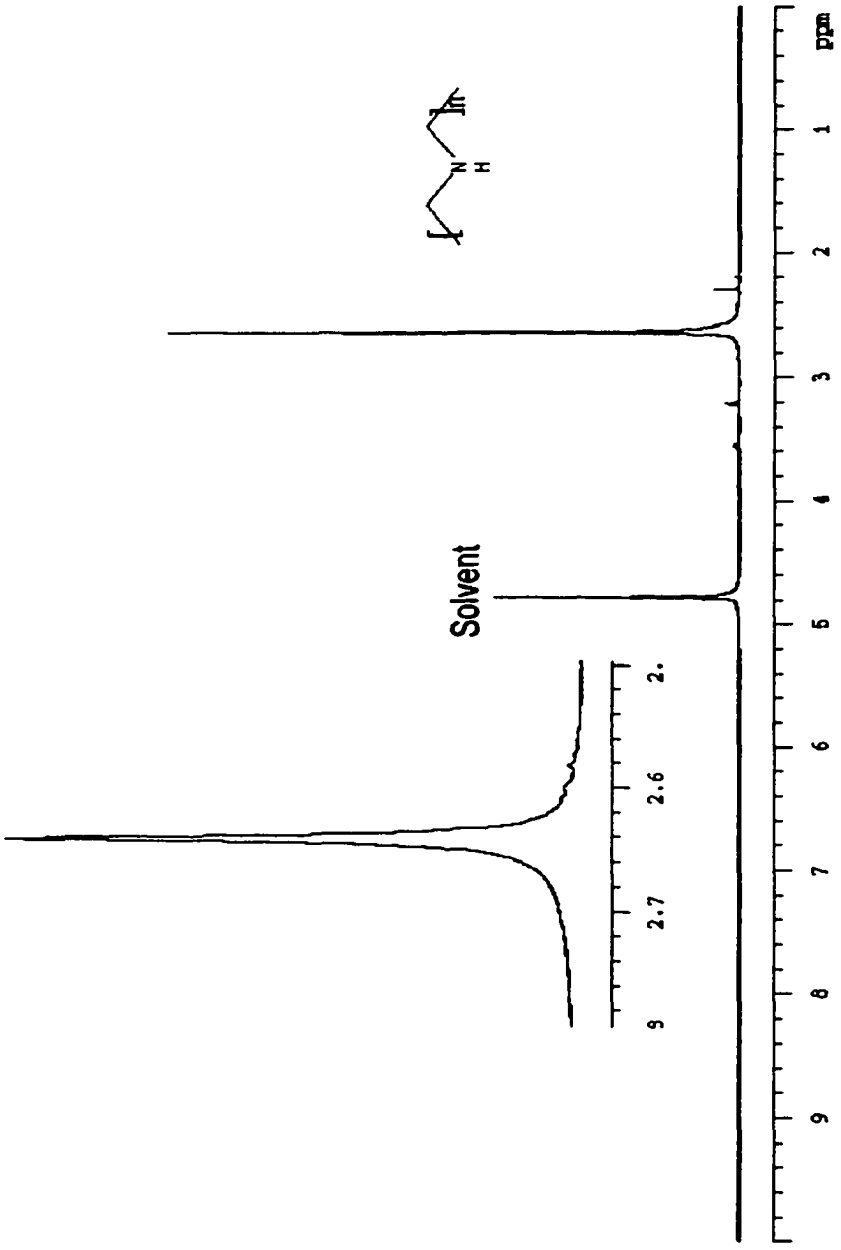

Figure A-3 ^{1}H NMR Spectrum of low molecular weight linear poly(ethylenimine)

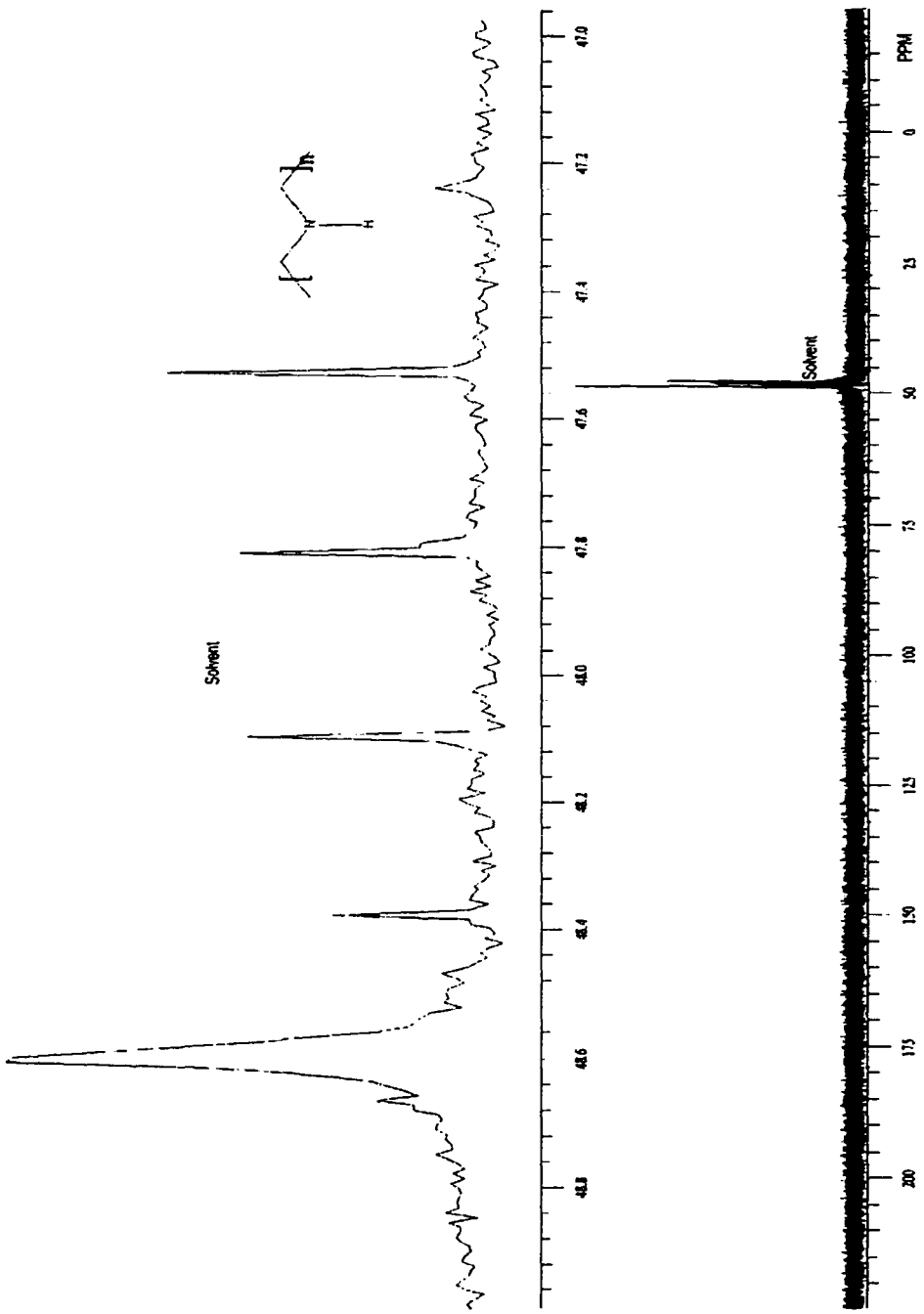

Figure A-4 ^{13}C NMR Spectrum of low molecular weight linear poly(ethylenimine)

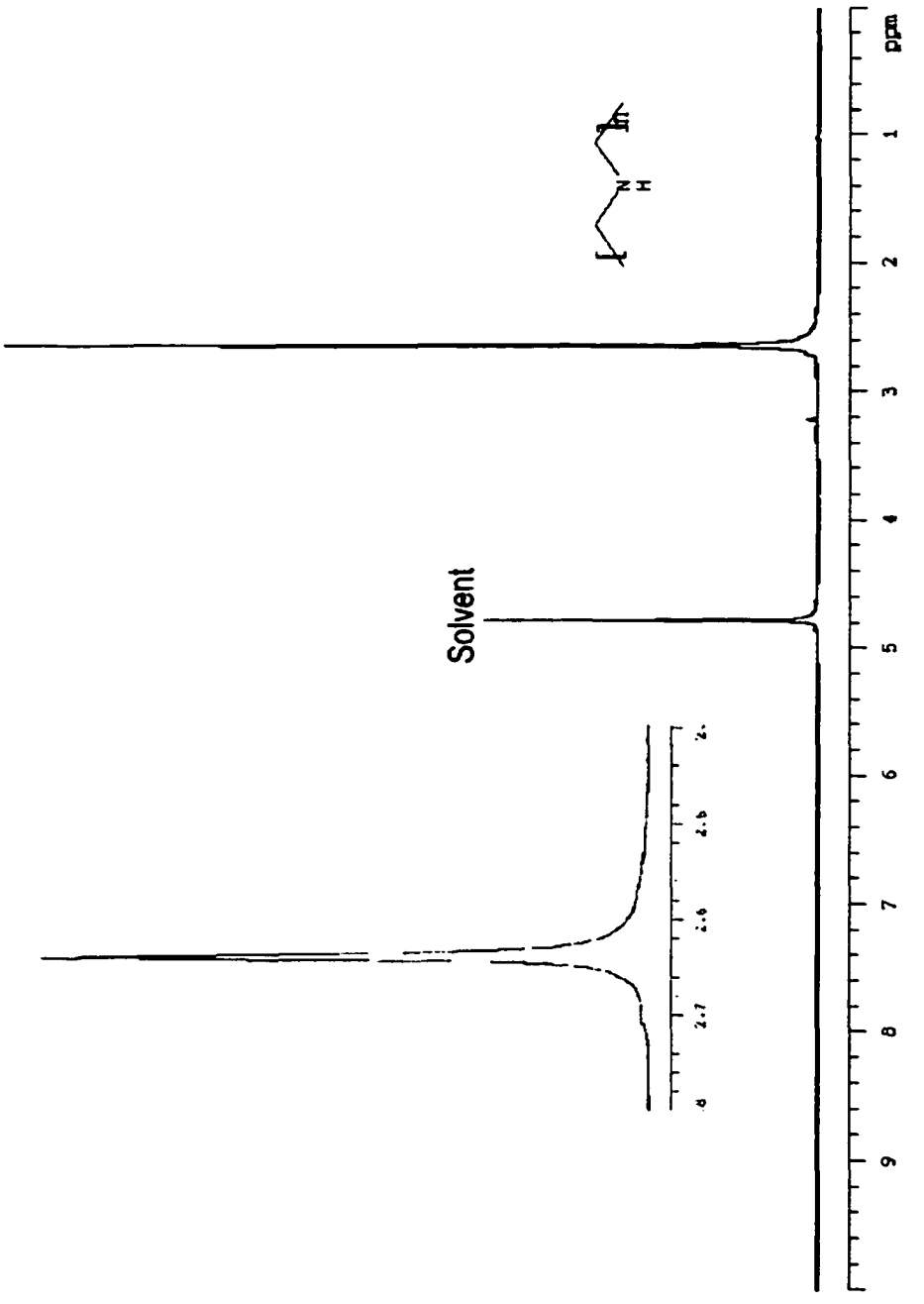

Figure A-5 ^{1}H NMR Spectrum of high molecular weight linear poly(ethylenimine)

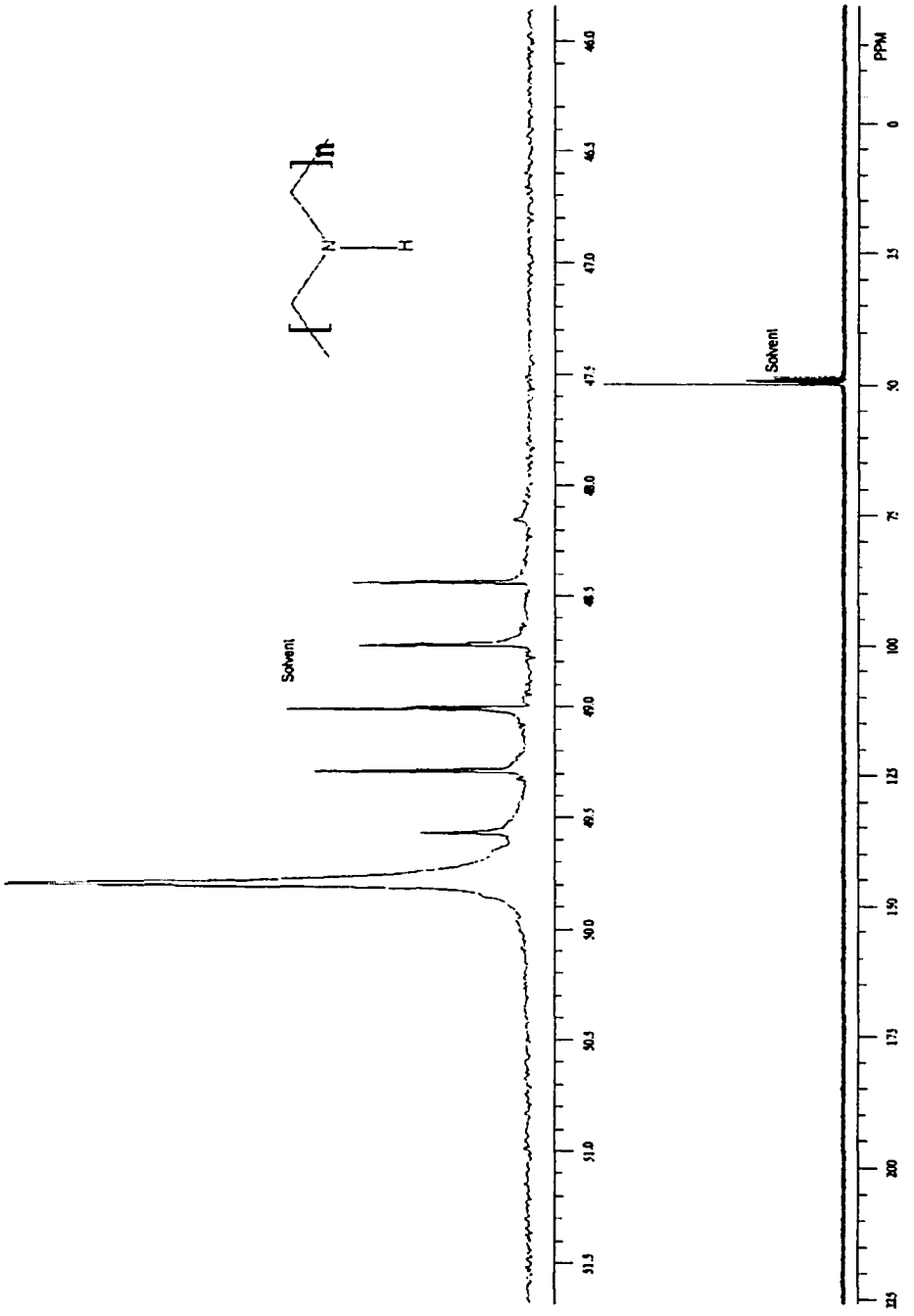

Figure A-6 ^{13}C NMR Spectrum of high molecular weight linear poly(ethylenimine)

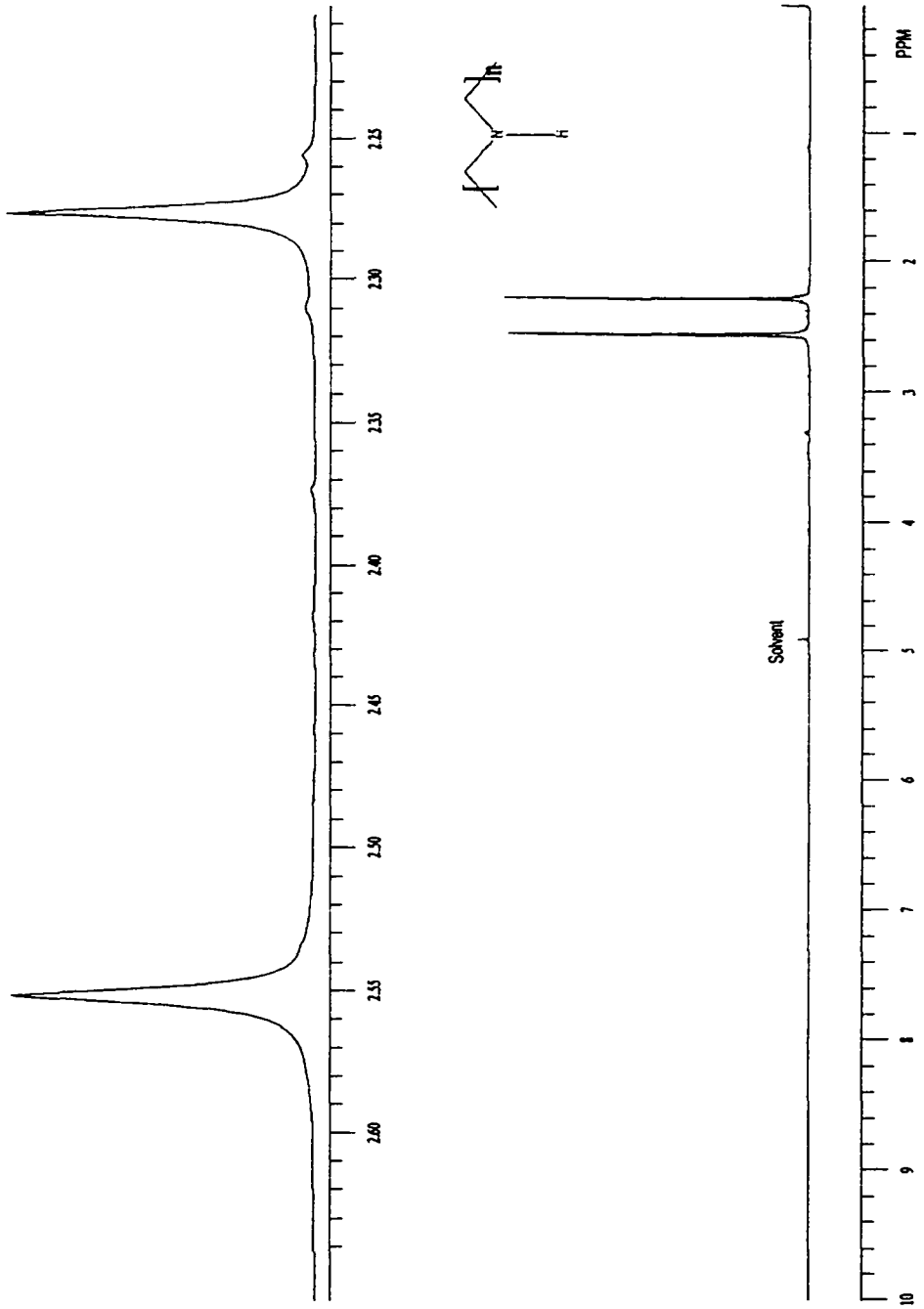

Figure A-7 ^{1}H NMR Spectrum of linear poly(*N*-methylethylenimine), Method 1

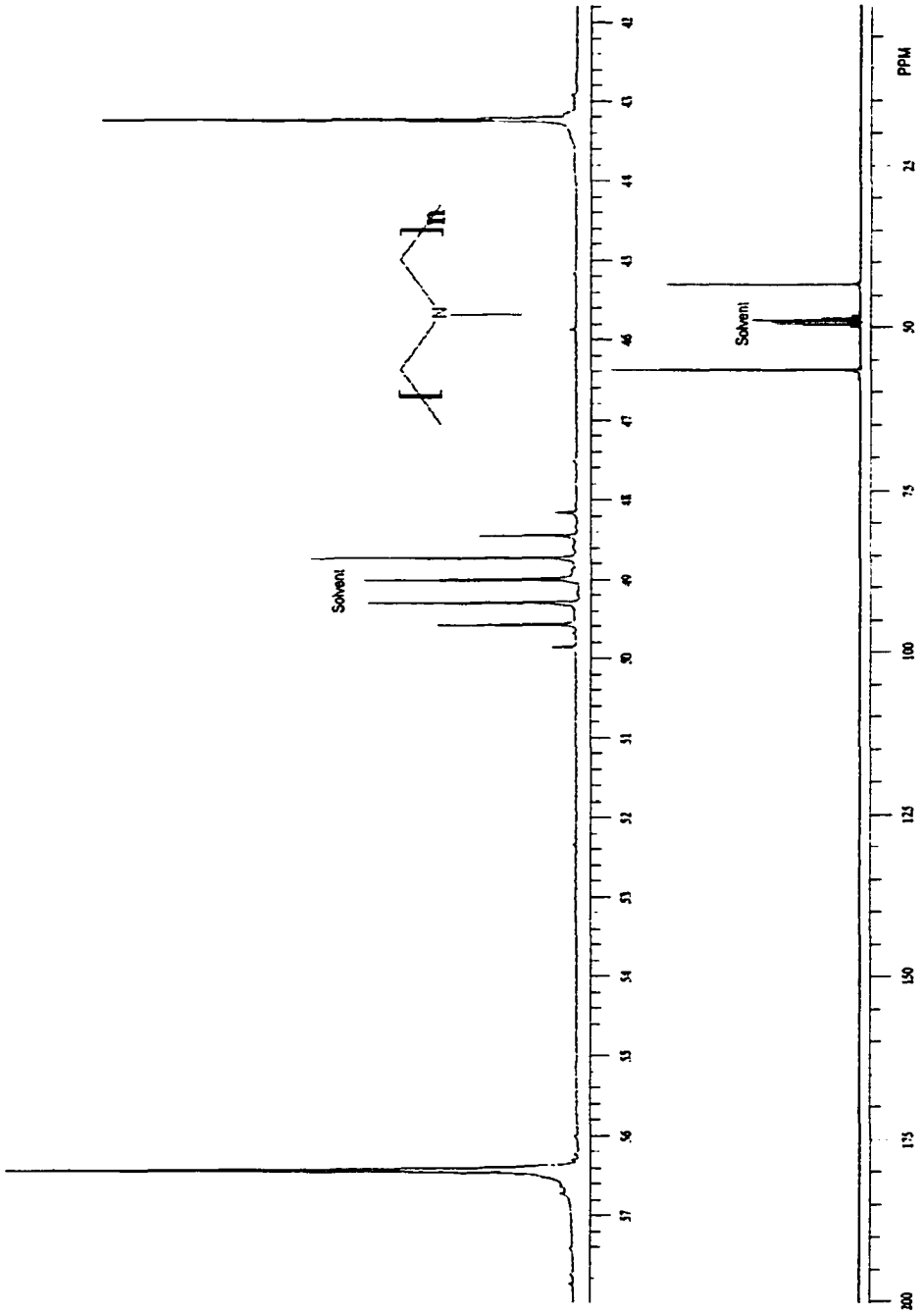

Figure A-8 ^{13}C NMR Spectrum of linear poly(*N*-methylethylenimine), Method 1

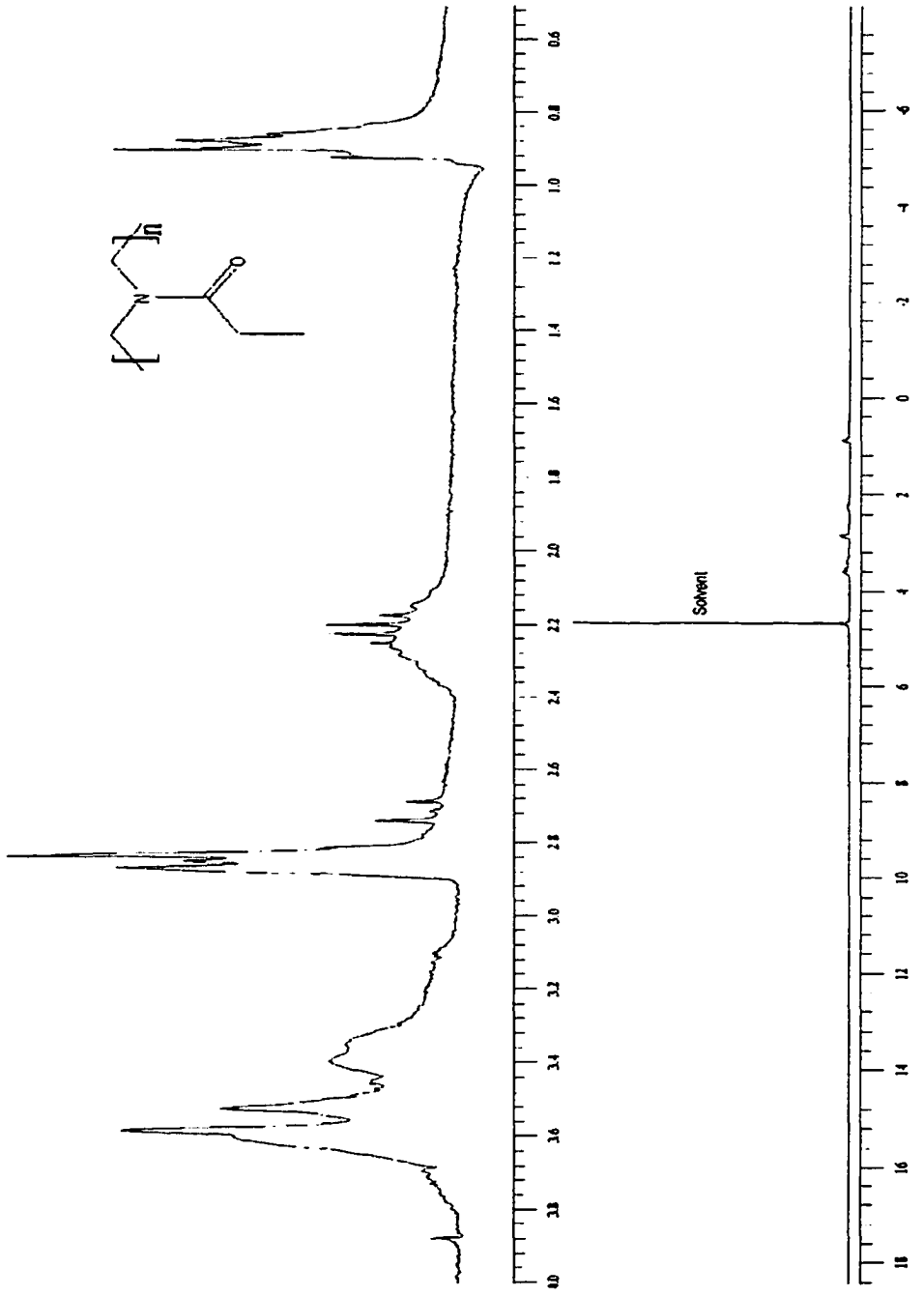

Figure A-9 ^{1}H NMR Spectrum of Reaction Mixture LPMEI Synthesis, Method 2

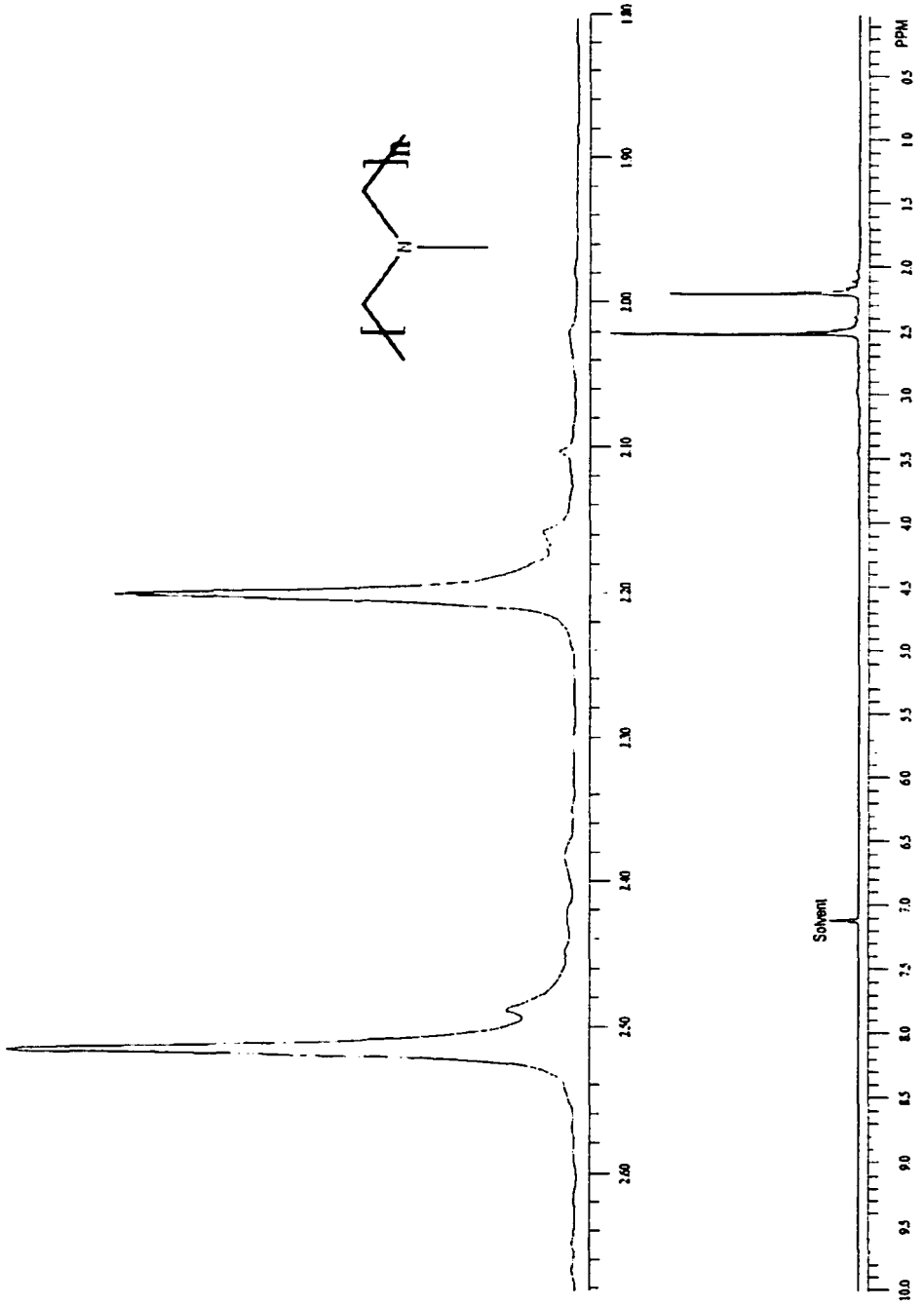

Figure A-10 ^{1}H NMR Spectrum of linear poly(*N*-methylethylenimine), Method 3, Good Batch

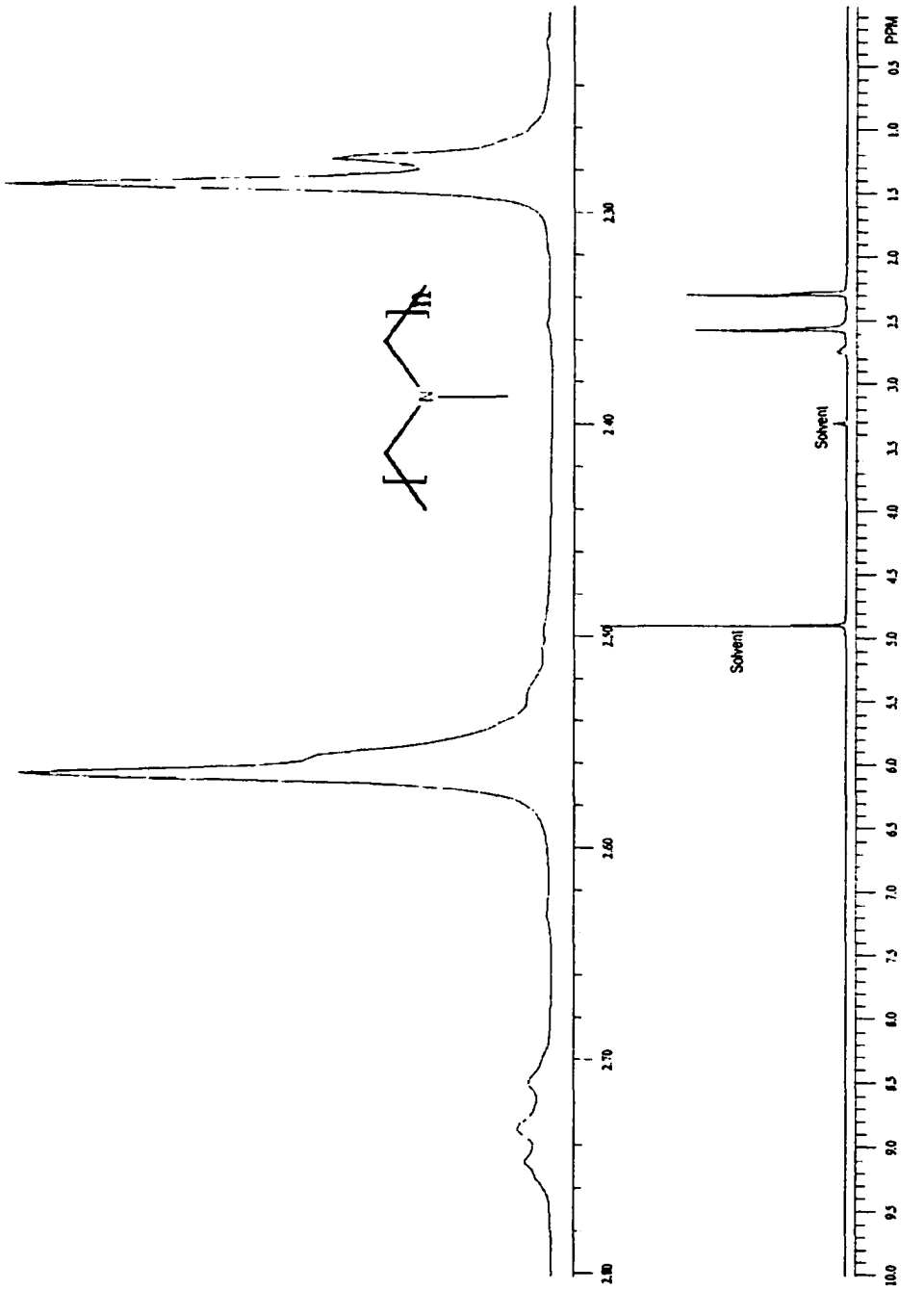

Figure A-11 ^{1}H NMR Spectrum of linear poly(*N*-methylethylenimine), Method 3, Bad Batch

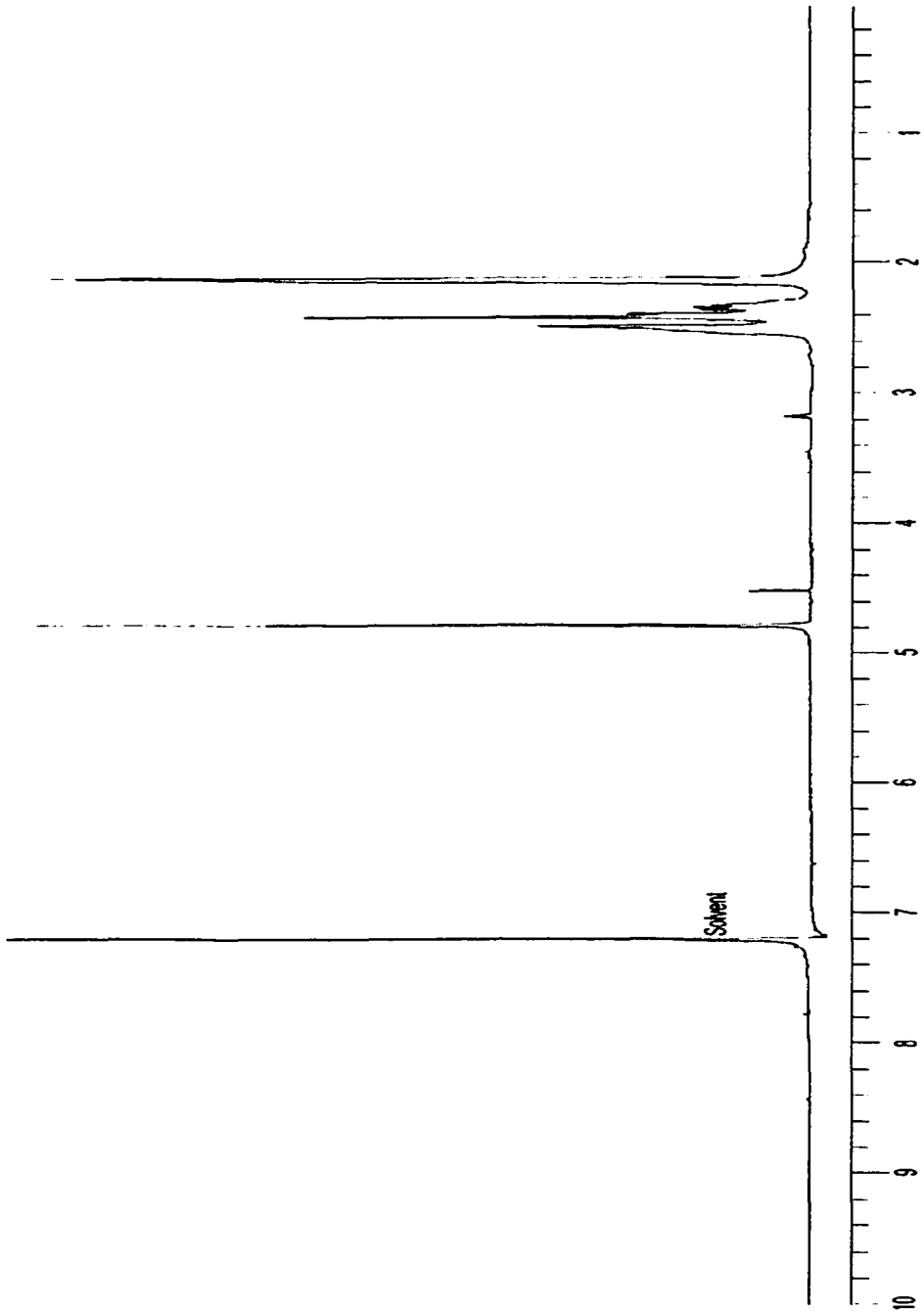

Figure A-12 ^{1}H NMR Spectrum of branched poly(*N*-methylethylenimine)

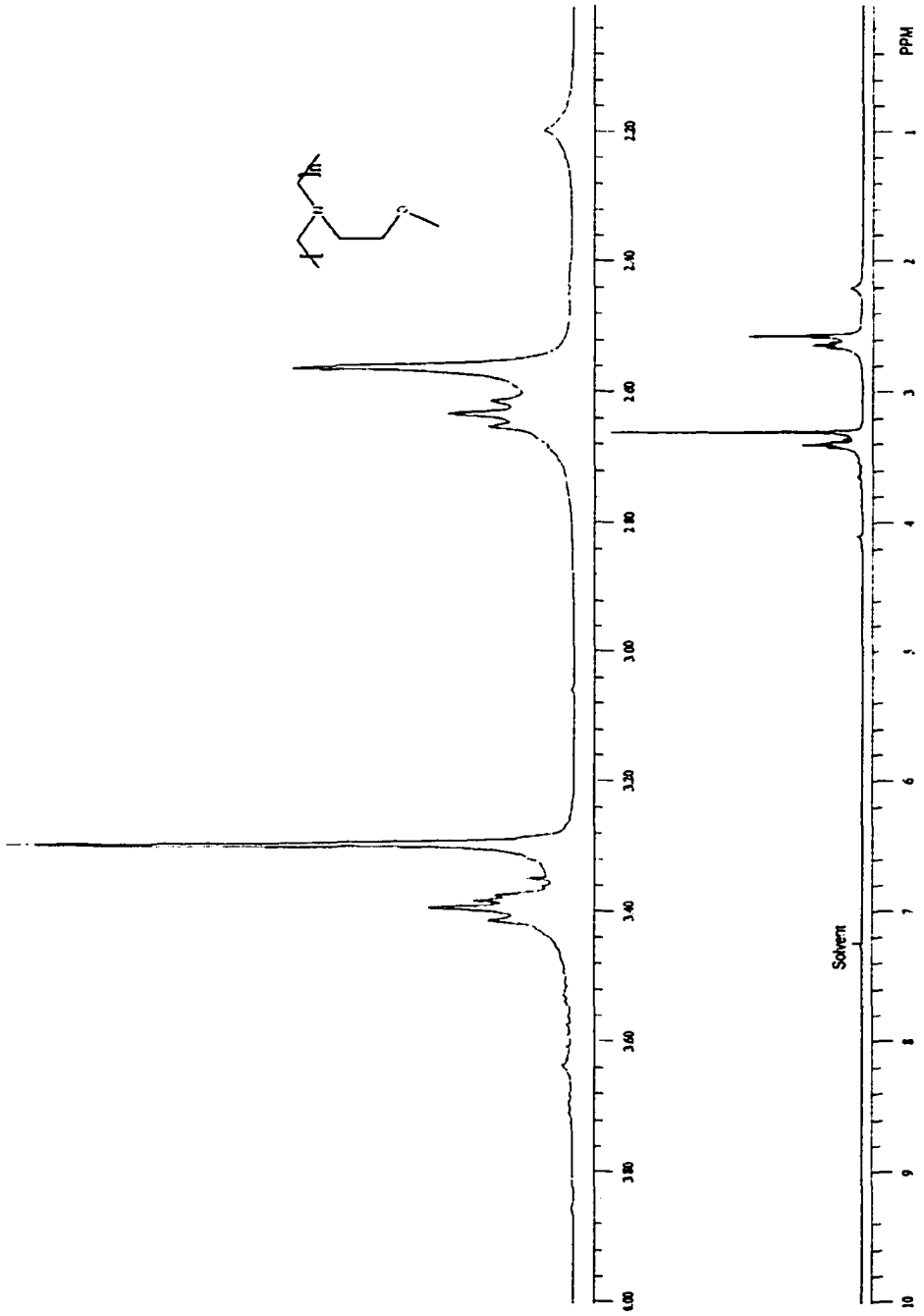

Figure A-13 ^{1}H NMR Spectrum of linear poly(*N*-(2-methoxyethyl)ethylenimine)

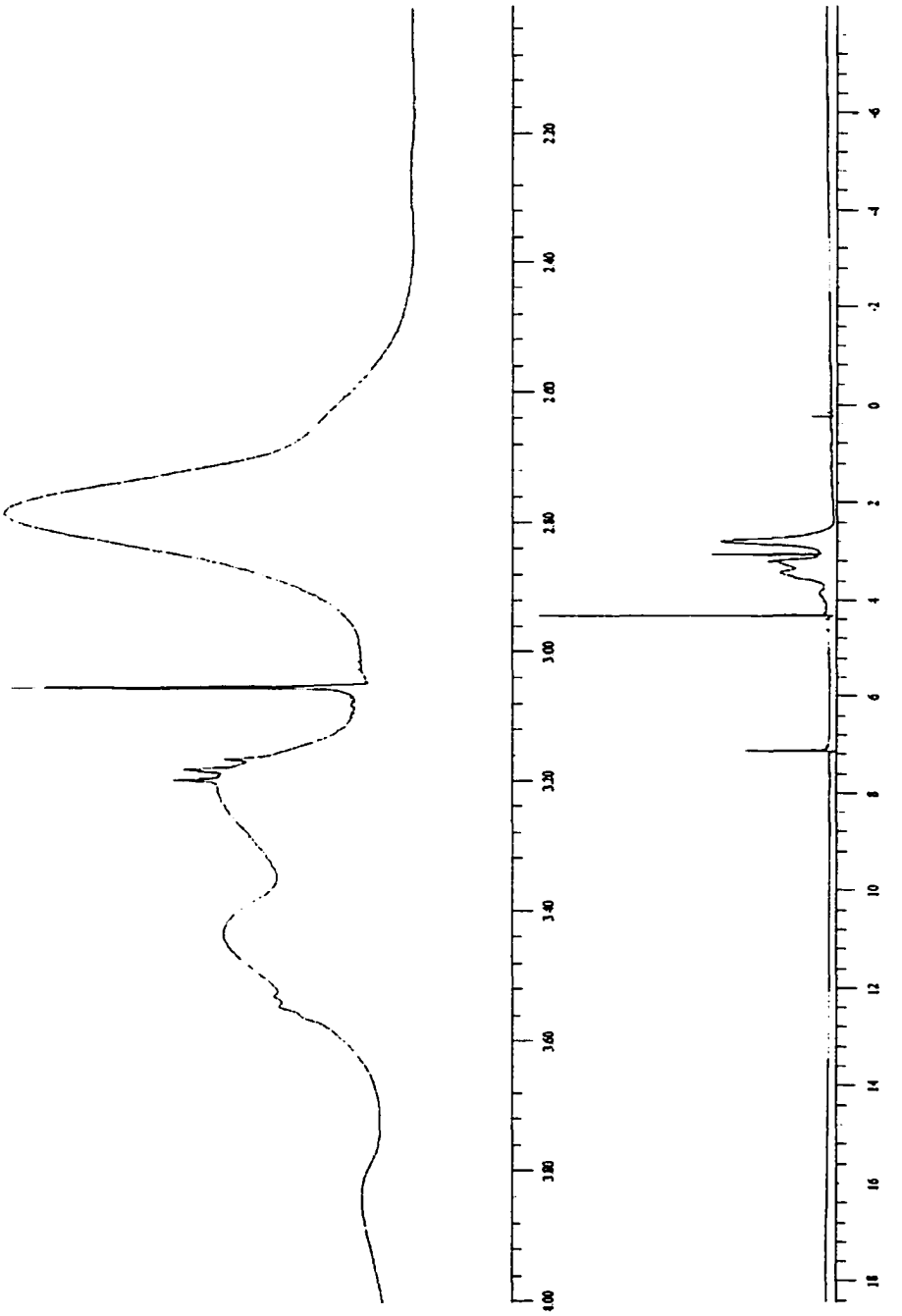

Figure A-14 ^{1}H NMR Spectrum of branched poly(*N*-(2-methoxyethyl)ethylenimine)

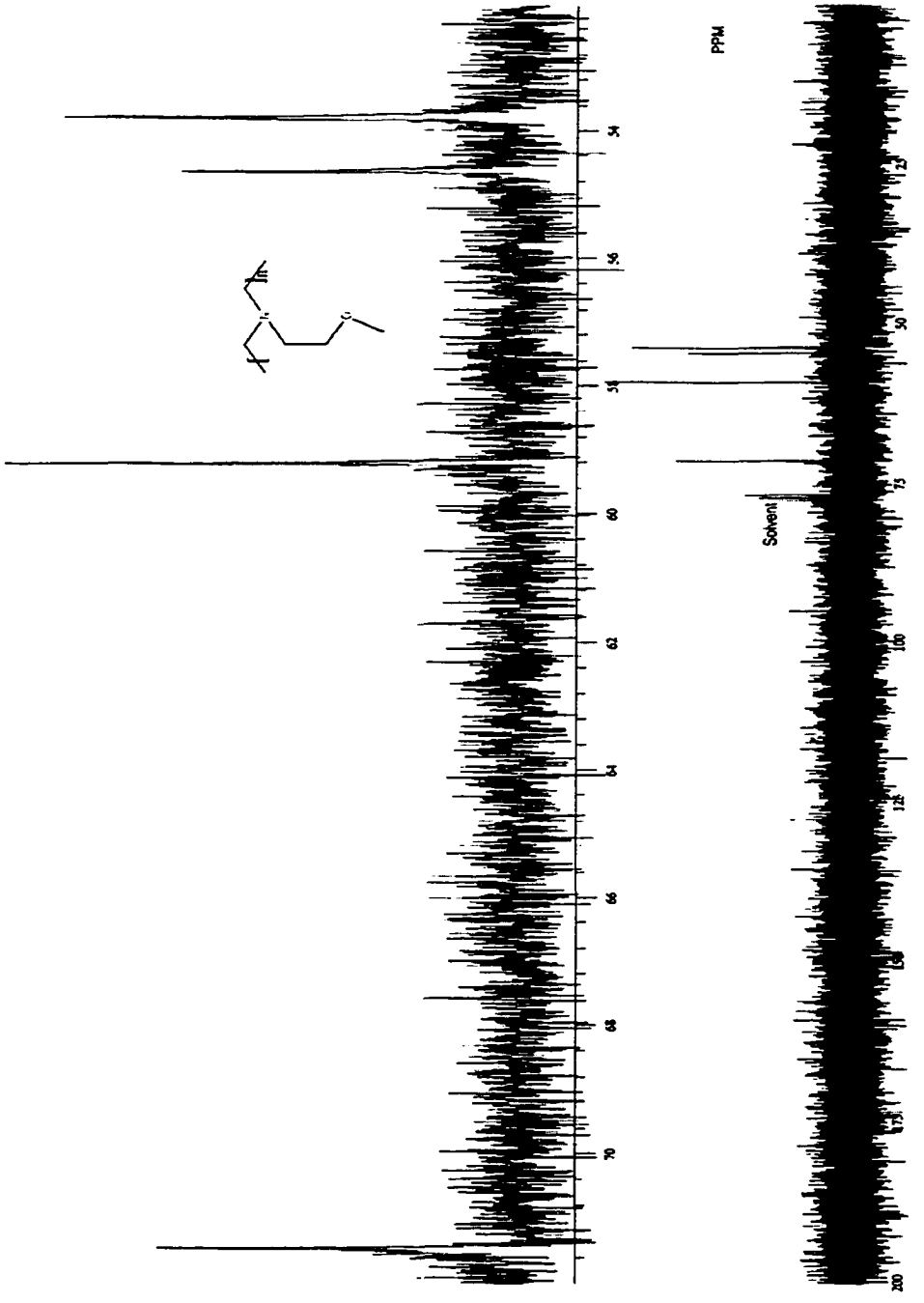

Figure A-15 ^{13}C NMR Spectrum of linear poly(*N*-(2-methoxyethyl)ethylenimine)

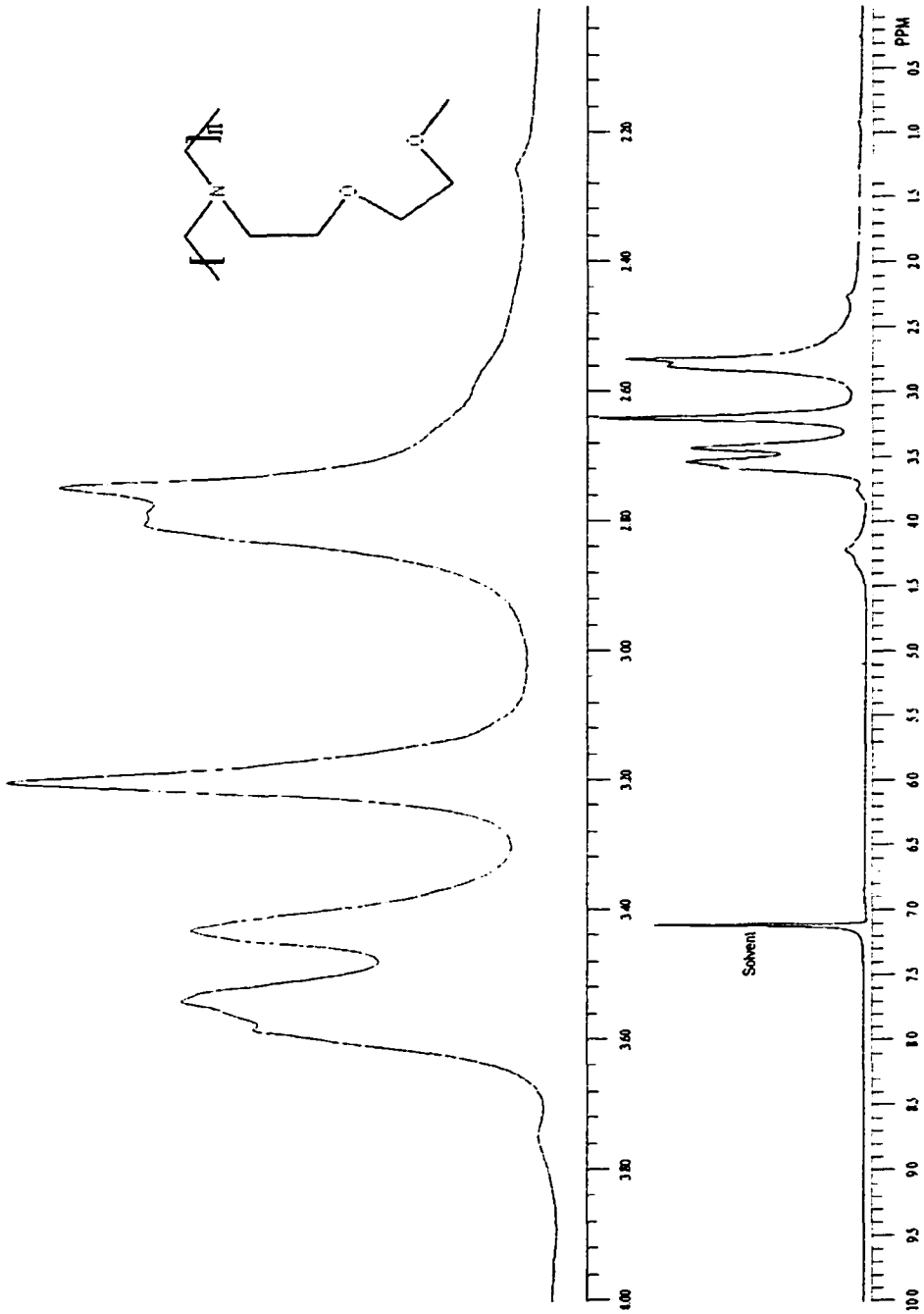

Figure A-16 ^{1}H NMR Spectrum of linear poly(*N*-(2-(2-methoxyethoxy)ethyl)ethylenimine)

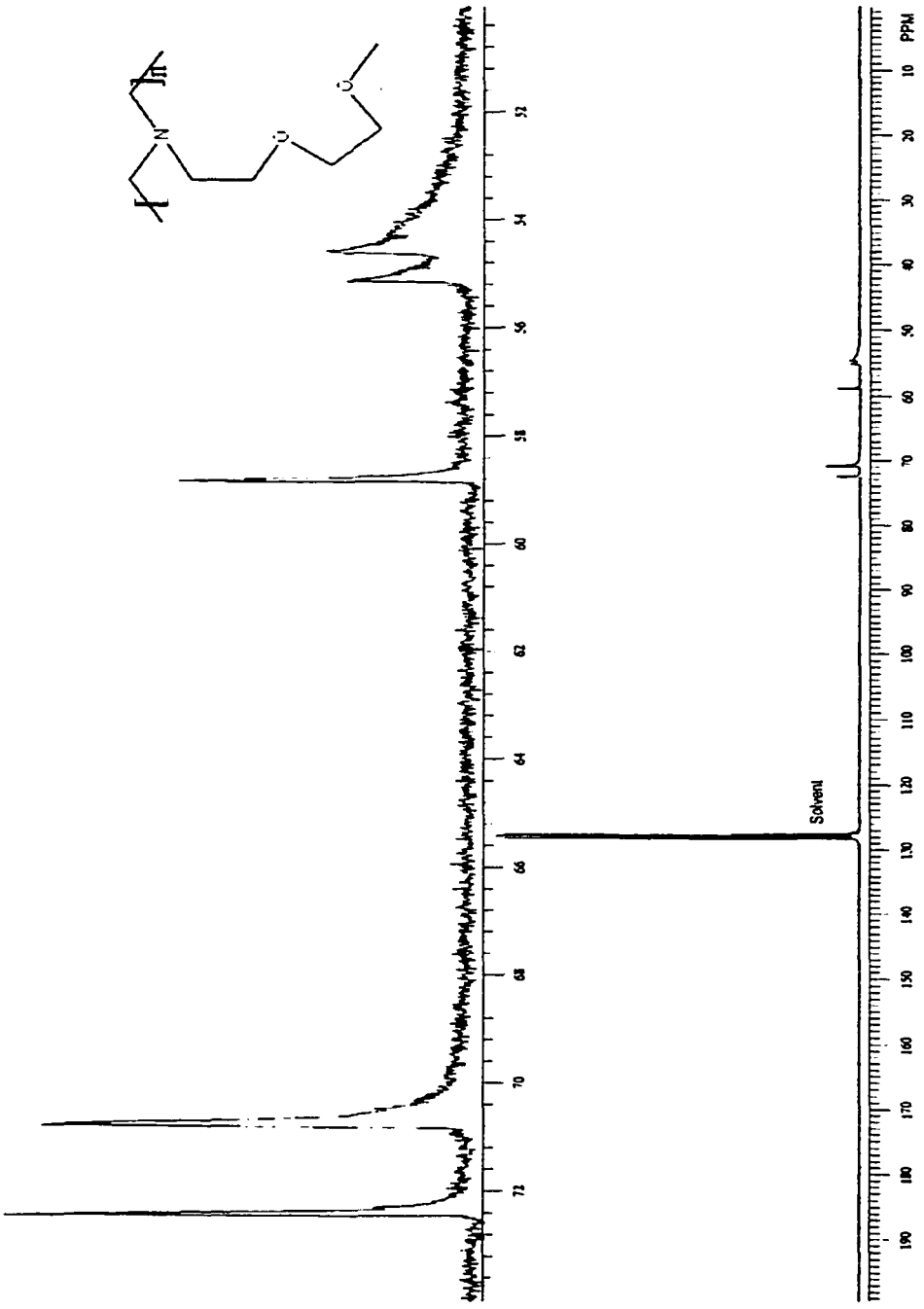

Figure A-17 ^{13}C NMR Spectrum of linear poly(*N*-(2-(2-methoxyethoxy)ethyl)ethylenimine)

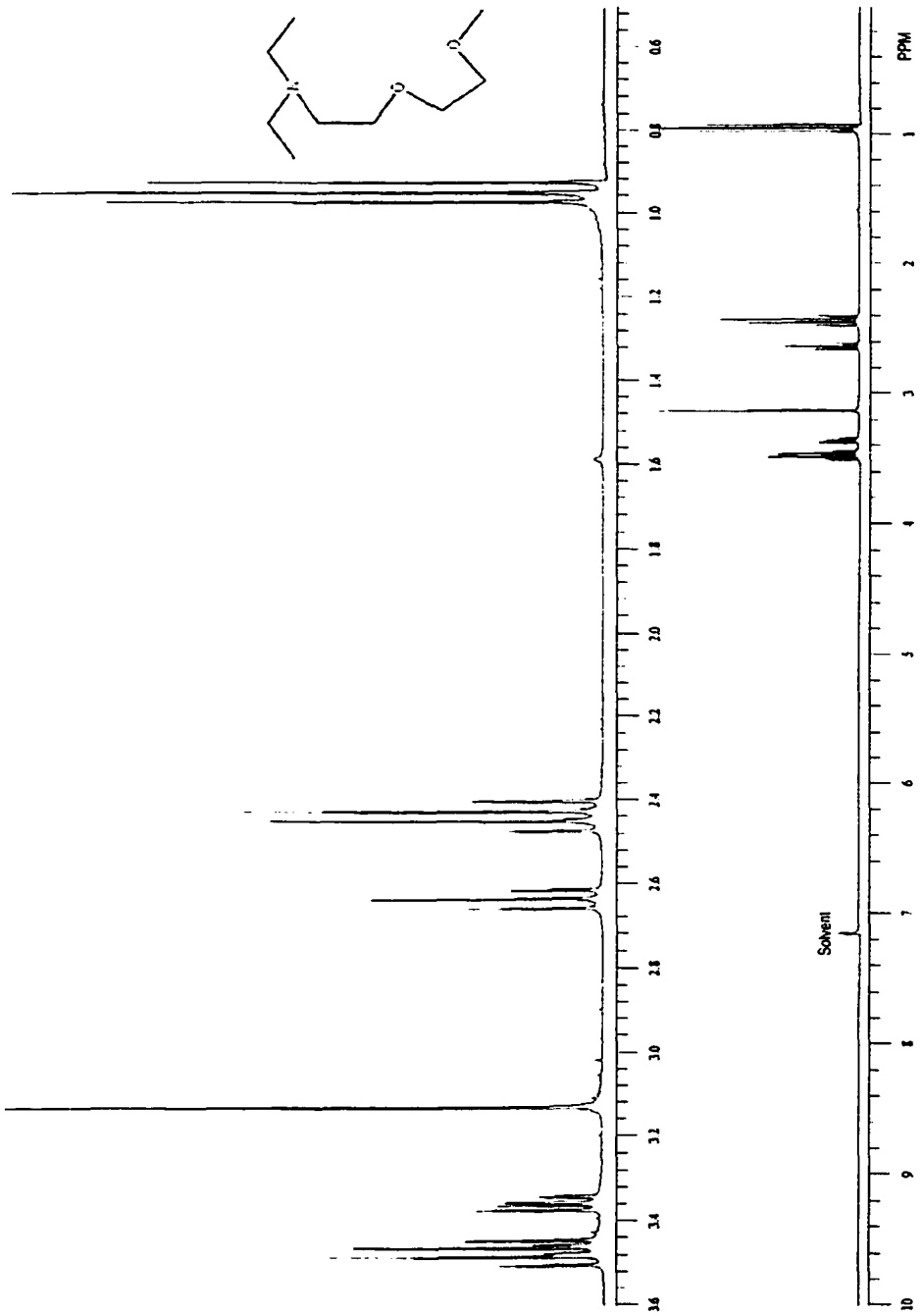

Figure A-18 ^{1}H NMR Spectrum of (3, 6-dioxaheptyl)diethylamine, DEA-G2

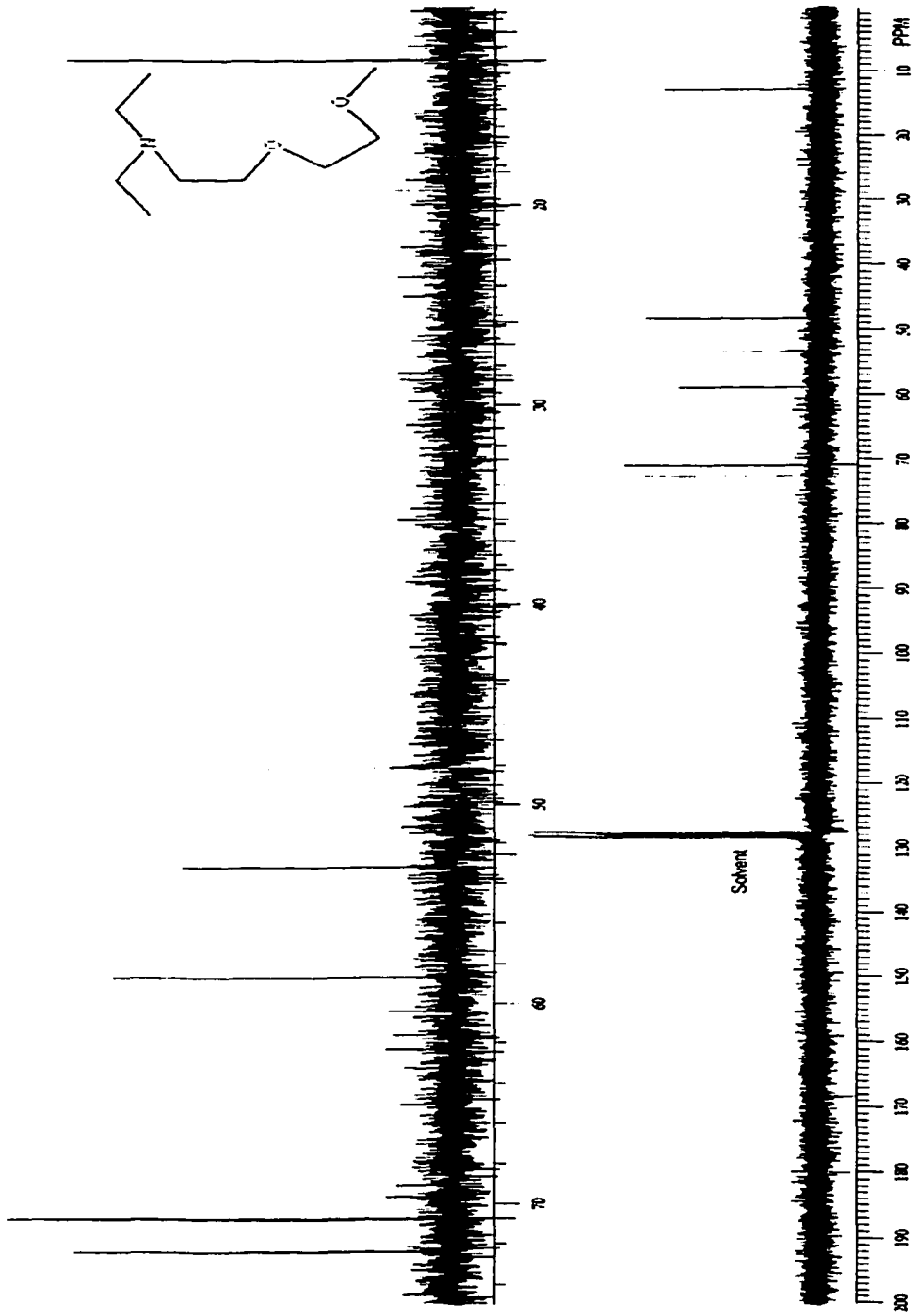

Figure A-19 ^{13}C NMR Spectrum of (3, 6-dioxaheptyl)diethylamine, DEA-G2

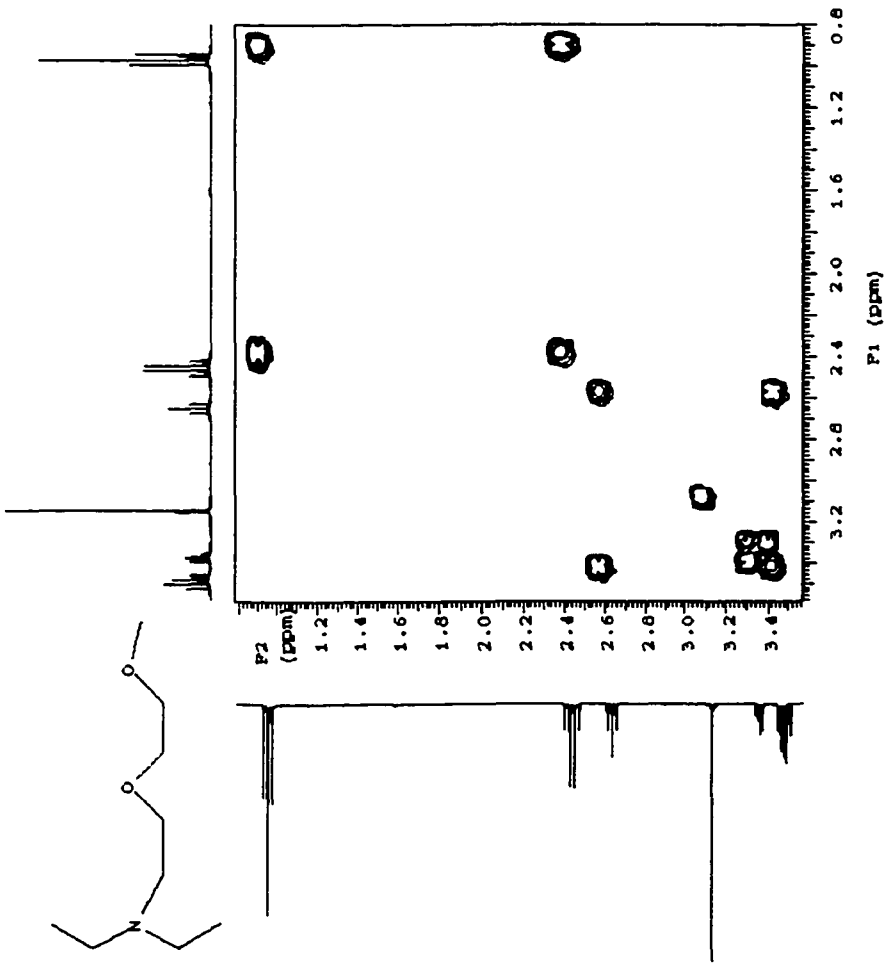

Figure A-20 gCOSY NMR Spectrum of (3, 6-dioxaheptyl)diethylamine, DEA-G2

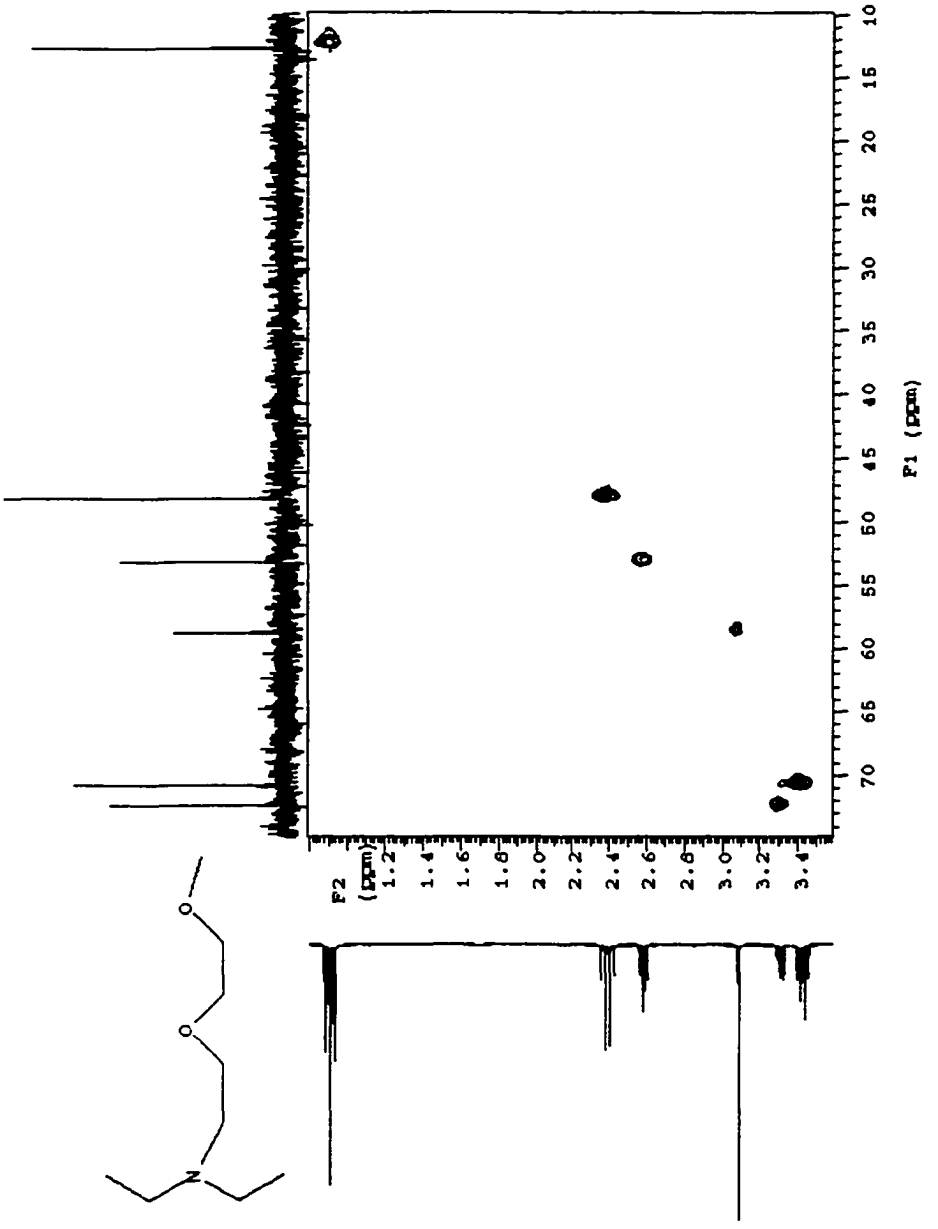

Figure A-21 gHMQC NMR Spectrum of (3, 6-dioxaheptyl)diethylamine, DEA-G2

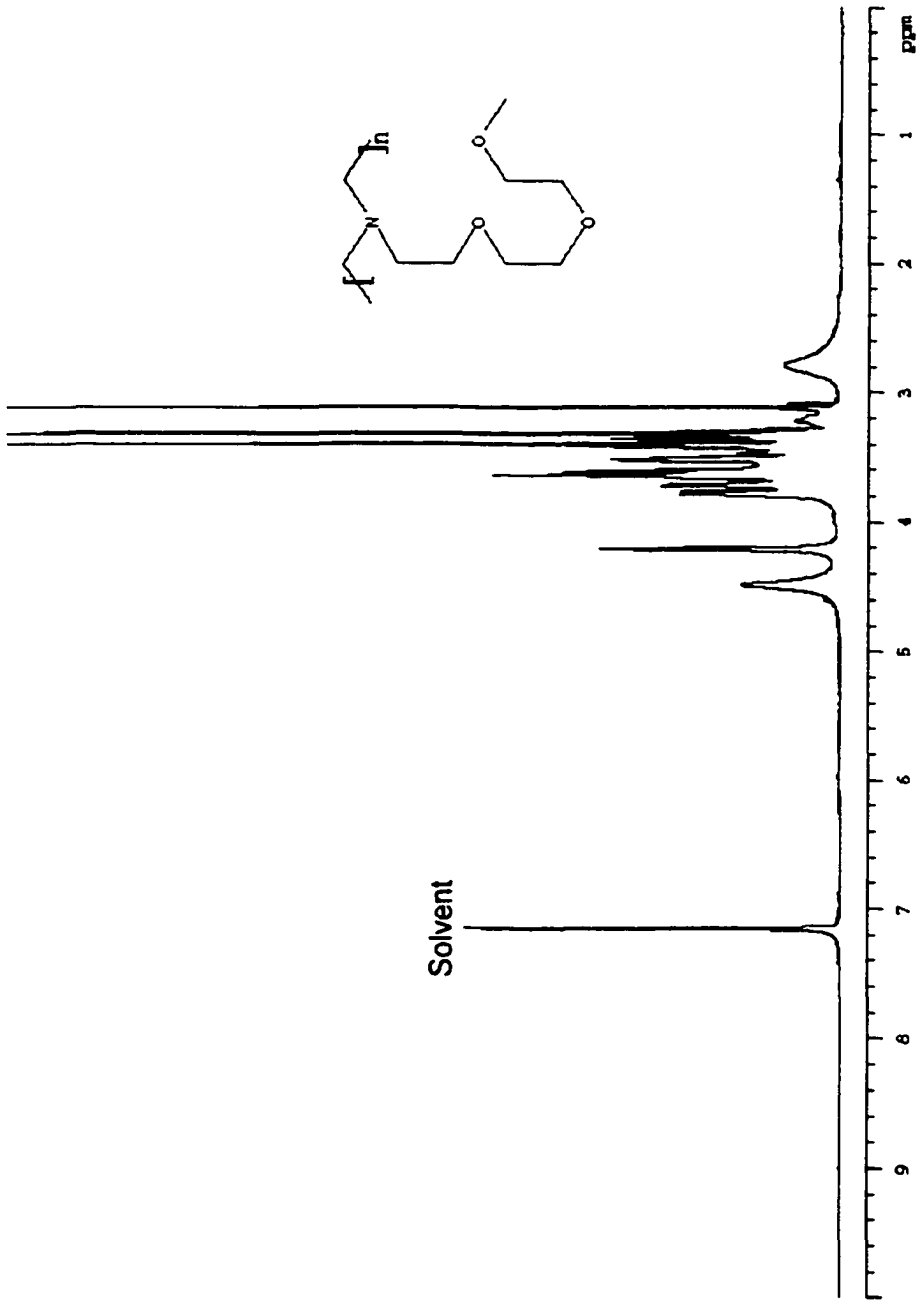

Figure A-22 ^{1}H NMR Spectrum of linear poly(*N*-(2-(2-(2-methoxyethoxy)ethoxy)ethyl)ethylenimine)

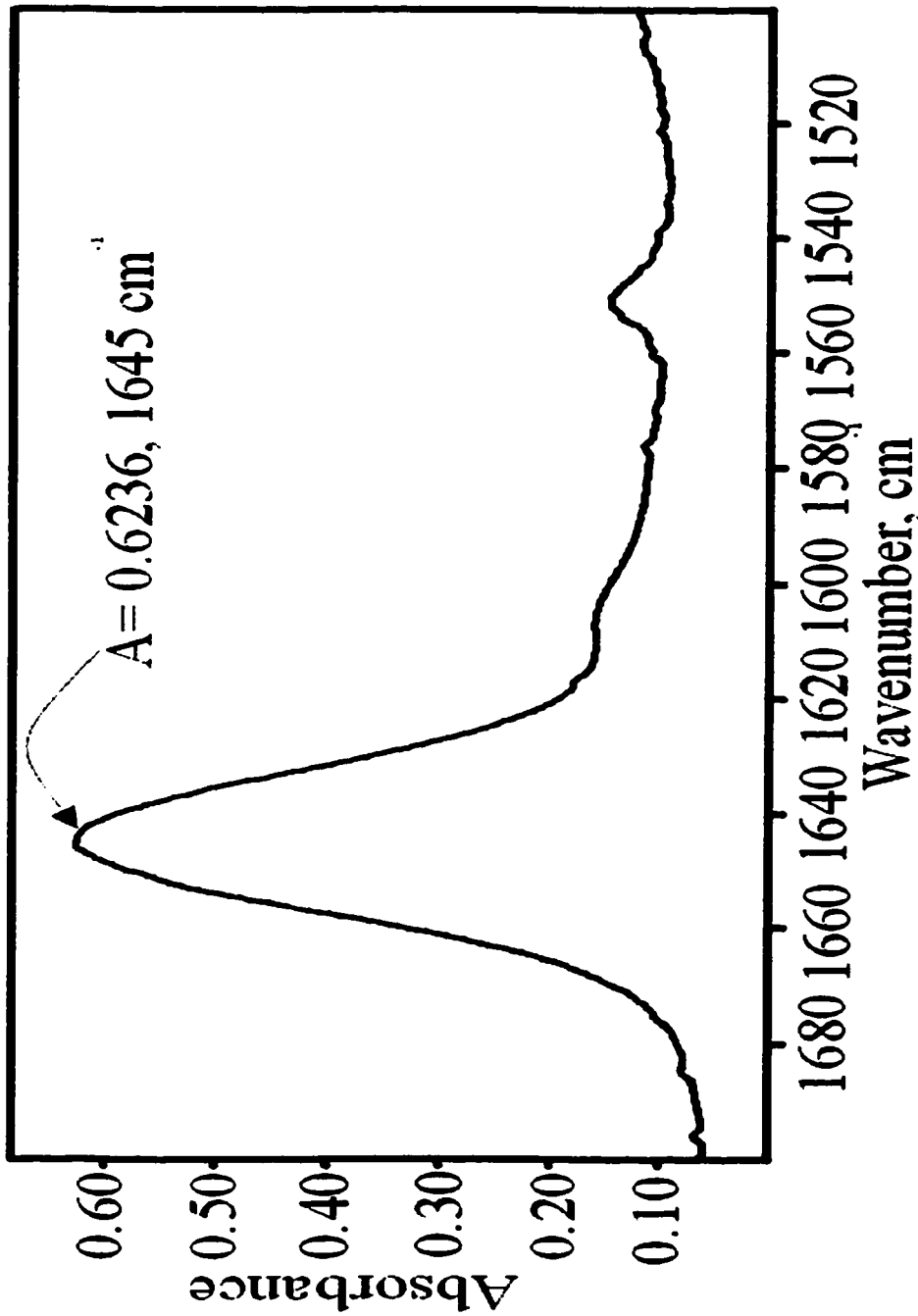

Figure A-23 IR Spectrum of poly(2-ethyloxazoline) in CH_2Cl_2

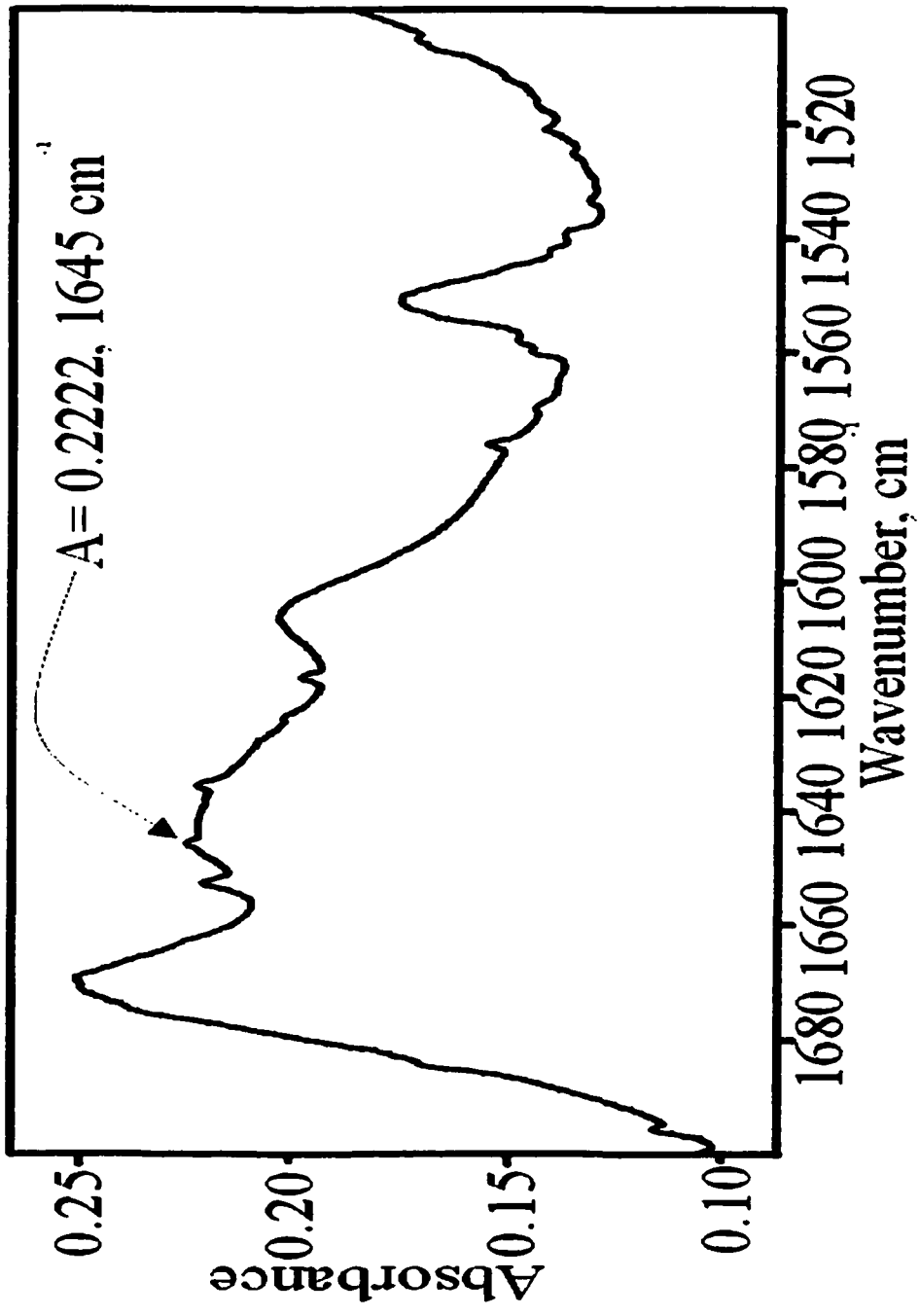

Figure A-24 IR Spectrum of poly(*N*-methylethylenimine) in CH_2Cl_2